



Andrés María
Roldán Aranda



David Aguilera
Jiménez

In this Masters Thesis the ground segment for the GranaSAT-I cubesat is presented. The ground segment is a key subsystem of the GranaSAT project, required for the tele-operation of the satellite from the Earth.

From the early design steps to the final deployment and implementation, all the tasks, configurations and problems arised in the process are described in detail in this Thesis.

"Ground segment design and
deployment for GranaSAT-I"

David Aguilera Jiménez



UNIVERSIDAD DE GRANADA

ESTUDIOS DE INGENIERÍA
DE TELECOMUNICACIÓN

PROYECTO FIN DE CARRERA

*"Ground segment design and
deployment for GranaSAT-I"*

David Aguilera Jiménez

Curso 2014/2015

Tutor: Andrés María Roldán Aranda





ESTUDIOS DE INGENIERÍA
DE TELECOMUNICACIÓN
PROYECTO FIN DE CARRERA

*“Ground segment design and deployment for
GranaSAT-I”*



CURSO: 2014/2015

David Aguilera Jiménez



ESTUDIOS DE INGENIERÍA DE TELECOMUNICACIÓN

*“Ground segment design and deployment for
GranaSAT-I”*

REALIZADO POR:

David Aguilera Jiménez

DIRIGIDO POR:

Andrés María Roldán Aranda

DEPARTAMENTO:

Electrónica y Tecnología de los Computadores



ugr

Universidad
de Granada

ESTUDIOS DE INGENIERÍA DE TELECOMUNICACIÓN

***“Ground segment design and deployment for
GranaSAT-I”***

REALIZADO POR: **David Aguilera Jiménez**

DIRIGIDO POR: **Andrés María Roldán Aranda**

EL TRIBUNAL CONSTITUIDO POR:

D/Dña _____

D/Dña _____

D/Dña _____

Ha resuelto asignarle la calificación de:

- [] Sobresaliente (9-10 puntos)
- [] Notable (7-8.9 puntos)
- [] Aprobado (5-6.9 puntos)
- [] Suspenso

Con la nota de: _____ puntos.

El Presidente

El Vocal

El Secretario

Presentado en Granada, a _____ de septiembre de 2015.
Evaluado en Granada, a _____ de septiembre de 2015.

D. Andrés María Roldán Aranda, Profesor del departamento de Electrónica y Tecnología de los Computadores de la Universidad de Granada, como director del Proyecto Fin de Carrera de D. David Aguilera Jiménez,

Informa:

que el presente trabajo, titulado:

“Ground segment design and deployment for GranaSAT-I”

ha sido realizado y redactado por el mencionado alumno bajo nuestra dirección, y con esta fecha autorizo a su presentación.

Granada, a de septiembre de 2015

Fdo. Andrés María Roldán Aranda

Los abajo firmantes autorizan a que la presente copia de Proyecto Fin de Carrera se ubique en la Biblioteca del Centro y/o departamento para ser libremente consultada por las personas que lo deseen.

Granada, a de septiembre de 2015

Fdo. David Aguilera Jiménez

Fdo. Andrés María Roldán Aranda

Ground segment design and deployment for GranaSAT-I

David Aguilera

KEYWORDS:

GranaSAT-I, ground segment, cubesat, microsatellite, link budget, ham radio, Software Defined Radio, radiolink, atmospheric attenuation, orbit mechanics, satellite tracking.

ABSTRACT:

This Thesis presents the design of a ground segment for the GranaSAT-I cubesat, a microsatellite in development process which will require of a system capable of receiving its telemetry and sending telecommands when it is launched. The project includes an analysis of all the physical phenomena and components involved in the transmission of the signal from an spacecraft in Low Earth Orbit to the station located in the Faculty of Sciences of the University of Granada. The deployment and testing processes were also carried out and are described in detail.

Dedicado a

Mis padres, Constanza y Salvador

Agradecimientos:

Me gustaría comenzar dando las gracias a mis padres por su apoyo incondicional. Ellos me han inculcado unos valores que me han permitido afrontar con entereza todas las situaciones y retos que se me han presentado hasta ahora, incluyendo este Proyecto de Fin de Carrera. Les estoy asimismo enormemente agradecido por el esfuerzo que han hecho para proporcionarme una educación y bienestar.

A mis hermanos y el resto de familiares me gustaría también agradecer expresamente su cariño y apoyo. Y a mis abuelas y abuelos, que son un modelo a seguir para mí.

También quiero agradecer a mis compañeras y compañeros de Ingeniería de Telecomunicación, con los que he compartido tantos buenos y malos momentos, y que son también responsables de que haya podido llegar hasta aquí.

Y finalmente quiero dar mi más sincero agradecimiento a mi director de proyecto, Andrés Roldán, por su excepcional entrega a su trabajo y alumnos. Personalmente, ha contribuido en mi formación más allá de lo meramente académico, ayudándome a ser un mejor profesional en el futuro.

Sin todos vosotros, no habría podido llegar hasta aquí.

CONTENTS

Cover	i
Read authorization	vii
Autorización Depósito Biblioteca	ix
Summary	xi
Dedication	xiii
Acknowledgments	xv
Contents	xvii
List of Figures	xxi
List of Tables	xxv
1 Introduction	1

1.1	Context	1
1.2	CubeSats	2
1.3	Frequency Spectrum and Amateur Radio	2
1.4	System testing	4
2	Theoretical Fundamentals	5
2.1	Satellite Orbits	5
2.1.1	Orbits classification	6
2.1.2	The Geometry of the Ellipse	6
2.1.3	Orbital Elements	7
2.1.4	Ground Track	10
2.2	Frequency bands and fundamental parameters of antennas review	14
2.2.1	Frequency bands	14
2.2.2	Fundamental parameters of antennas	14
2.2.3	Polarization	15
2.3	Radio wave propagation	17
2.3.1	Effects of the non-ionized atmosphere	17
2.3.2	Ionospheric effects	21
2.3.3	Doppler shift	23
2.4	Transmission lines	24
2.5	Digital communications in space	26
3	Downlink link budget	27
3.1	Free space loss	29
3.2	Atmospheric attenuation	31
3.3	Attenuation by polarization mismatch	32
3.4	Antenna pointing loss	32
3.5	System loss	34
3.5.1	Feeder, RF connector and cable loss	34

3.5.2	Miscellaneous losses	34
3.6	System gain	35
3.7	Spacecraft communications unit	35
3.8	Link budget results	36
4	Equipment Description	39
4.1	Antennas	41
4.1.1	Wimo X-Quad directional antennas	41
4.1.2	Diamond X-200N Antenna	43
4.1.3	70 cm / 2 m X-Quad circular pol. emphaser	45
4.1.4	Pre-amplifiers	45
4.1.5	Diamond MX-72D Diplexer	47
4.2	Rotor	48
4.2.1	Rotor External Control	50
4.3	Transceivers	52
4.3.1	Keenwood TM-241 and TM-441	52
4.4	TNC	54
4.5	Antenna switcher	55
4.6	Diamond SX600 Dual-Band SWR/Power meter	56
4.7	USB receivers	57
4.8	Software	58
4.8.1	Satellite tracking software	58
4.8.2	SDR programs	59
4.8.3	Multi-functionality programs	59
4.8.4	FUNcube Telemetry Dashboard	61
5	Software Defined Radio	63
5.1	FUNcube Dongle Pro+	67
5.2	Realtek RTL2832U based DVB-T receivers	68

5.2.1	RTL-TCP	69
6	Ground station deployment	71
6.1	Antennas deployment	71
6.2	Control room deployment	79
6.2.1	Rotor control	79
6.2.2	Transceivers	85
6.3	Reparation after deployment	87
7	System performance and conclusion	91
7.1	Evaluation of system performance	91
7.1.1	FUNcube	91
7.1.2	ISS contact	92
7.1.3	NOAA APT	93
7.2	Conclusion	97
7.2.1	Future work	97
	Appendices	99
A	Project budget	101
A.1	Project budget	101
A.1.1	Material cost	101
A.1.2	Human resources costs	101
A.1.3	Final project budget	102
B	Gantt Diagram	103
	Acronyms	105
	Glossary	107
	Bibliography	109

LIST OF FIGURES

1.1	ITU and IARU Regions [9]	3
2.1	Elliptical geometry [41]	6
2.2	Geometry of the orbital ellipse [29]	7
2.3	Inclination tilt [29]	7
2.4	Vernal equinox [29]	8
2.5	Right ascension of the Ascending Node [29]	8
2.6	Argument of Perigee [29]	9
2.7	Two Line Element [5]	9
2.8	Location of the ground segment marked on a map [7]	10
2.9	Coordinates of Washington DC in ECEF coordinate system [41]	11
2.10	Satellite coverage [41]	12
2.11	Cross-section of satellite-coverage cone [41]	12
2.12	Satellite elevation determination [41]	13
2.13	Back view of the antenna with the two crossed antennas (vertical and horizontal) [23]	17

2.14	Total, dry air and water-vapour zenith attenuation due to atmospheric gases from sea level [30]	18
2.15	Variations of rain specific attenuation vs. frequency and rain intensity [44] .	19
2.16	An estimate of loss due to the additional spreading of a beam and standard deviation about the average [28]	20
2.17	Amplitude scintillations predicted from the ITU-R tropospheric scintillation model [47]	21
2.18	S_4 index measured in Toulouse (France) on 03/04/2015 [15]	22
2.19	Ionospheric reflection for flat Earth [40]	23
2.20	Basic transmission line circuit, showing voltage and current waves initiated by closing switch S1 [59]	24
2.21	Voltage wave reflection from a complex load impedance [59]	25
2.22	Typical protocol stack in a CubeSat ground segment [55]	26
3.1	Generic diagram of attenuation in radio transmissions [52]	28
3.2	Slant ranges for LEO orbits	29
3.3	FSL for 160 km altitude orbits in VHF and UHF amateur bands	30
3.4	FSL for 1600 km altitude orbits in VHF and UHF amateur bands	31
3.5	Antenna misalignment in satellite links [44]	33
4.1	Diagram of hardware devices and their connections	40
4.2	X-Quad radiation patterns [23]	42
4.3	X-Quad antennas mounted on the rotor	43
4.4	Diamond X-200N antenna	44
4.5	2 m X-Quad circular pol. emphaser	45
4.6	Mini 2 preamplifier	46
4.7	Diagram of a diplexer operation [13]	47
4.8	Yaesu G-5500 rotor controller unit	48
4.9	Rotor controller unit buttons and functions [24]	48
4.10	Rotor mounted on the mast	50

4.11	LVB connection diagram [42]	51
4.12	Back view of the rotor controller unit [24]	51
4.13	Keenwood TM-241 and TM-441 transceivers	52
4.14	Functional block diagram of a typical TNC [27]	54
4.15	TNC-URE	55
4.16	MFJ-1704 Antenna switcher [10]	56
4.17	SX600 Dual-Band SWR/Power Meter [16]	57
4.18	Screenshot of the main screen of GPredict tracking program	59
4.19	Screenshot of the main screen of SDR#	60
4.20	Screenshot of the main screen of GNURadio	61
4.21	Screenshot of FUNcube Telemetry Dashboard	62
5.1	Simple SDR receiver diagram [46]	64
5.2	FUNCube Dongle Pro+ [34]	68
5.3	RTL2832U based devices: EzTV 668 [58]	68
5.4	Rtl-test command output	69
5.5	Sample configuration of rtl-tcp	70
5.6	Configuration of SDR# for rtl-tcp reception	70
6.1	Base of the mast	72
6.2	Diamond X-200N two-band vertical antenna	72
6.3	Mast of the X-Quad antennas	73
6.4	Attachment of the cords to the floor	74
6.5	X-Quad antennas mounted on the rotor	74
6.6	N-Connector preparation	75
6.7	Self-amalgamating tape covering the two connectors of the 70 cm antenna	75
6.8	Parallel connection of the RCA and DIN connectors	76
6.9	Detailed diagram of X-Quad antennas interconnection	77
6.10	Connection scheme of rotor supply [24]	77

6.11	Satellite view of the Faculty of Science [7]	78
6.12	Mast uprising	79
6.13	Back view of the rotor controller unit	80
6.14	Calibration warning of the rotor	80
6.15	Screenshot with the response message of LVB after calibration	82
6.16	Sample screenshot of the rotor addition in GPredict	85
6.17	SWR meter connection scheme	86
6.18	Equipment on the control room	87
6.19	Ripped cable on the side of the rotor	88
6.20	Front view of the Keysight E5071C vectorial network analyzer[35]	88
6.21	Scattering parameters diagram [36]	89
6.22	Measurement of the S_{11} parameter over the VHF circular emphaser connected to the 2 m antenna	89
6.23	Measurement of the S_{11} parameter over the UHF circular emphaser connected to the 70 cm antenna	90
7.1	Telemetry data from FUNcube-1 displayed in its dashboard	92
7.2	Diagram of the NOAA APT reception process	93
7.3	Real time FFT of NOAA's APT signal in SDR#	94
7.4	Image received from NOAA-18 on January 2 nd 2015	95
7.5	Image received from NOAA-18 on January 2 nd 2015, rotated and with <i>MCIR map color IR</i> enhancement	96
7.6	Image received from NOAA-18 on January 2 nd 2015, rotated and with <i>NO colour IR</i> enhancement	96
7.7	Panoramic photo of the rooftop of the Faculty of Sciences	97

LIST OF TABLES

2.1	Orbits classification by altitude [29]	6
2.2	Frequency bands [40]	14
2.3	Empirical conversion table for scintillation indices [31]	22
3.1	Distance between the ground segment and the spacecraft for LEO orbits at maximum and minimum elevation angle	30
3.2	FSL for shortest and longest slant ranges in LEO orbits	31
3.3	Atmospheric attenuation values for the GranaSAT ground segment	32
3.4	Antenna pointing loss	33
3.5	Connection loss	34
3.6	Insertion loss by other devices	35
3.7	System gain	35
3.8	VHF study case [33]	36
3.9	UHF study case [33]	36
3.10	Downlink link budget analysis for the VHF band	37
3.11	Downlink link budget analysis for the UHF band	38

4.1	Wimo X-Quad technical specifications [23]	41
4.2	Diamond X-200N technical specifications [22]	44
4.3	Pre-amplifiers technical specifications [11] [12]	46
4.4	Diamond MX-72D Diplexer technical specifications [13]	47
4.5	Yaesu G-5500 technical specifications [24]	49
4.6	LVB external port pins [24]	51
4.7	Keenwood TM-241 and TM-441 general technical specifications [17] [18]	53
4.8	Keenwood TM-241 and TM-441 transmitter technical specifications [17] [18]	53
4.9	Keenwood TM-241 and TM-441 receiver technical specifications [17] [18]	53
4.10	MFJ-1704 antenna switcher technical specifications [10]	56
4.11	SX600 Dual-Band SWR/Power meter technical specifications [16]	57
5.1	SDR Sampling hardware	66
5.2	FUNCube Dongle Pro+ technical specifications [34]	68
5.3	Comparison of FUNCube Dongle Pro+ and Realtek RTL2832U	69
A.1	Project budget	102
B.1	Gantt diagram	104

CHAPTER

1

INTRODUCTION

1.1 Context

The [GranaSAT-I](#) project was conceived in 2013 as the first university pico-satellite in Granada and Andalusia. The primary aim of the project is to encourage students to develop their interest in electronics and its applications in the aerospace industry. They work together in a multidisciplinary team in the design and implementation of each of the subsystems of the satellite.

The laboratories and the equipment are located in the Science Faculty of the University of Granada. The project is held by The Electronics and Computers Architecture Department (Departamento de Electrónica y Tecnología de Computadores) and supervised by Dr. Andrés Roldán –academic head of the [GranaSAT-I](#) project–.

[Telemetry](#) and [telecommand](#) play a crucial role in order to be able to carry out the programmed experiments in outer space and retrieve their results. A system for establishing a communication link between the satellite was therefore an essential element that had to be developed for the [GranaSAT-I](#) project. This Master’s Thesis covers the design and deployment of the ground segment, while the satellite elements will be developed by other students.

Although not all the specifications –such as required bandwidth, transmission frequency, modulation, etc.– were defined by the time of the writing of this thesis, it was possible to define the characteristics of the ground system to address the typical requirements of a pico-satellite. For this purpose a *link budget* analysis was carried out, presented in chapter [3](#).

In addition, the plentiful literature and information reported by other similar projects was taken as a reference. Even if the experiment to be carried out may differ greatly from one to another, the telecommunications systems are very similar for this kind of budget limited, long distance transmission links.

1

1.2 CubeSats

The [CubeSat](#) concept had its origin in 1999, when Prof Jordi Puig-Suari (California Polytechnic State University), San Luis Obispo and Prof. Bob Twiggs (Stanford University's Space System Development Laboratory) defined a standard for reduced cost and fast design of pico-satellites [3].

In general terms, a [CubeSat](#) is defined as a 10 cm cube with a mass of up to 1.33 kg. The standard contemplates bigger and weightier satellites as well, being this case achieved by adding together the dimensions and weight of several [CubeSats](#). 1U (1.33 kg), 1.5U (2 kg), 2U (2.66 kg), 3U (4 kg) and 3U+ (4 kg and extra volume) [CubeSats](#) are defined according to this scheme [3].

2005 can be considered as the beginning of the [CubeSats](#) era due to the explosion of the number of projects[56]. The standard gave the possibility to many universities and organizations to develop experiments in space and launch their own satellite, which together with the scientific interest, has also a potentially big positive impact on the education and training of many students interested in electronics, astrophysics, mechanical engineering, etc.

1.3 Frequency Spectrum and Amateur Radio

Amateur Radio (also known as *ham radio*) is a popular hobby and service in which licensed Amateur Radio operators ([hams](#)) operate communications equipment on radio frequencies known as the "Amateur Bands" [20].

While each State regulates its own telecommunications, including the division of the frequency spectrum, the International Telecommunications Regulations was signed by 89 countries with the purpose of promoting the development of telecommunication services and their most efficient operation while harmonizing the development of facilities for worldwide telecommunications [21].

This is specially relevant for cases like the one covered by this thesis, where the involved parties may belong to different, very distant regions and one of the communication endpoints is orbiting around the world.

In order to leave as much volume and weight as possible free for the rest of the equipment in the satellite, the main constraints for the communications system with the Earth are imposed by the [CubeSat](#) part. This includes a light and small system capable of transmitting at an adequate frequency to propagate through the terrestrial atmosphere and which provides

enough bandwidth as to operate remotely the rest of the systems and retrieve data obtained by sensors.

Additionally, as it was introduced in the previous sections, the reduction of costs was always present when choosing among different solutions. For the case of the frequency, amateur bands are an interesting option due to their only requirement of an inexpensive amateur radio license for the operator to transmit.

The [International Amateur Radio Union \(IARU\)](http://www.iaru.org/) (<http://www.iaru.org/>) defines 3 regions, organized to broadly mirror the structure of the [International Telecommunication Union \(ITU\)](http://www.itu.int) (<http://www.itu.int>) and its related regional telecommunications organizations. Spain and most countries from Europe, Africa, Middle East and Northern Asia belong to Region 1, as it can be seen in figure 1.1.

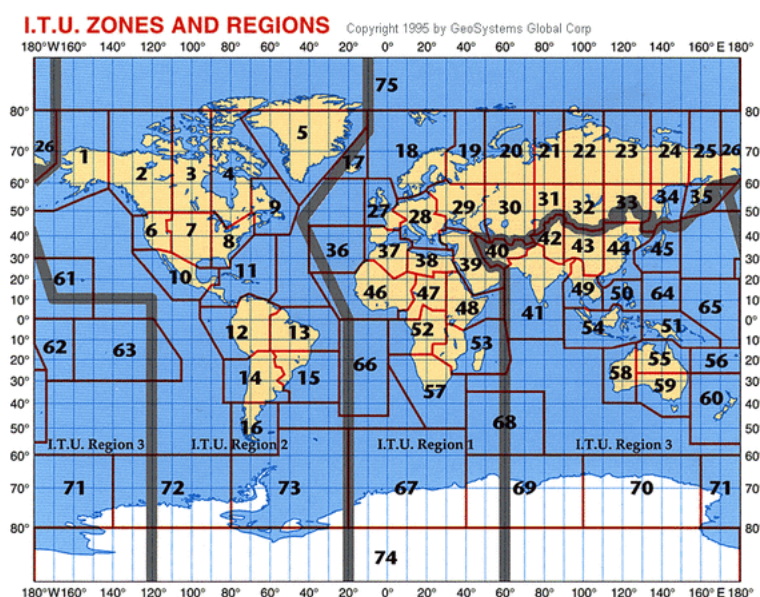


Figure 1.1 – ITU and IARU Regions [9]

Communication with satellites in the amateur frequency bands are very often established in the **Very High Frequency (VHF)** and **Ultra High Frequency (UHF)** ranges. VHF/UHF frequencies assigned for amateur purposes in Region 1 are the [144 – 146] MHz and [430 – 440] MHz sub-bands, respectively [49]. The suitability of these bands to be used for space links will be discussed in section 2. Additionally, the high availability of hardware and big amount of on going projects make them a good choice for the GranaSAT's ground segment too. This will also make possible the testing of the system in reception with real space links, prior to the conclusion and launch of **GranaSAT-I**.

1.4 System testing

The development of a [CubeSat](#) usually takes several years. Since the deployment of the ground station started at the beginning of the [GranaSAT-I](#) project and its development cycle is much shorter, it was not possible by the time of the writing of this Thesis to present results with successful communication between this satellite and the ground segment.

However, the chosen design is indeed widely extended and compatible for communication with other [CubeSats](#) and satellites, notably the [International Space Station \(ISS\)](#) and its [Amateur Radio on the ISS \(ARISS\)](#) (<http://www.ariss.org/>) programme. Thanks to them, it was possible to perform several tests to verify the correct operation of the system. They will be presented in chapter 7.

It should also be remarked that the experience and documentation reported by many other [CubeSats](#) was a big support for this project and it is one of the aims of this Thesis to contribute to the development of other projects by sharing the acquired experience as well.

CHAPTER

2

THEORETICAL FUNDAMENTALS

The design of a ground station is supported by theoretical fundamentals of a wide variety of fields which include electronics and [Radio Frequency \(RF\)](#) electronics, antennas and electromagnetic field theory or astrophysics. In this chapter a summary of the most relevant theoretical results will be discussed.

2.1 Satellite Orbits

The most basic concepts and expressions for the understanding of the movement of the planets were first deduced by Johannes Kepler and Isaac Newton. In the 17th century Kepler discovered certain properties of the planetary motion that are nowadays known as *Kepler's laws* [41].

- Each planet moves around the Sun in an ellipse, with the Sun in one focus (motion lies in a plane).
- The line from the Sun to planet (radius vector, r) sweeps across equal areas in equal interval of time.
- The ratio of the square of the period (T) to the cube of the semi-major axis (a) is the same for all the planets in our Solar System. (T^2/a^3) is a constant.

With his **Universal Law of Gravitation**, Isaac Newton gave a more detailed solution to the know as *two-body problem*. It states that every mass (m_1) attracts every other mass

(m_2) separated a distance (r) with a force directed along the line joining the two masses and having a magnitude F given by [57]:

$$F = \frac{Gm_1m_2}{r^2} \quad (2.1.1)$$

where G is the Universal Gravitational Constant.

2.1.1 Orbits classification

There are several classifications for satellite orbits depending on which parameter is evaluated. A common one is made attending to their altitude above the sea level, as given by table 2.1.

Orbit	Altitude	Denomination
LEO	160 – 1600 km	Low Earth Orbit
MEO	1 600 – 19300 km	Medium Earth Orbit
GEO	35786 km	Geostationary Earth Orbit
HEO	1060 – 38624 km	Highly Elliptical Orbit

Table 2.1 – *Orbits classification by altitude [29]*

2.1.2 The Geometry of the Ellipse

The orbit of a satellite around the Earth has the shape of a geometric ellipse, with the Earth on the focus. An ellipse is the curve traced out by a point which moves in such a manner that its distance from a given point is in a constant ratio of less inequality to its distance from a given straight line [38].

An allipse and its main parameters are represented in figure 2.1.

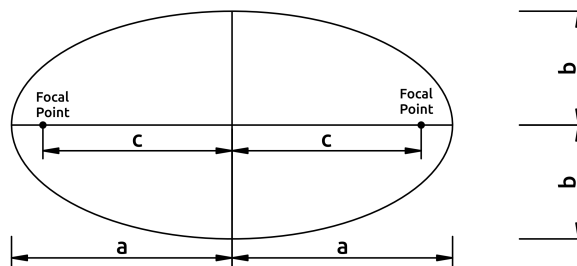


Figure 2.1 – *Elliptical geometry [41]*

a = semi-major axis b = semi-minor axis

The **eccentricity** e is an extended parameter to describe the geometry of the ellipse and is defined as the ratio between the minor axis and the major axis

$$c = ae \quad (2.1.2)$$

During the periodic motion of a satellite, the distance that the focus (for the case of the Earth, the geocenter) goes through a minimum and a maximum is referred to as **perigee** r_p and **apogee** r_a , respectively, as shown in figure 2.2 [39].

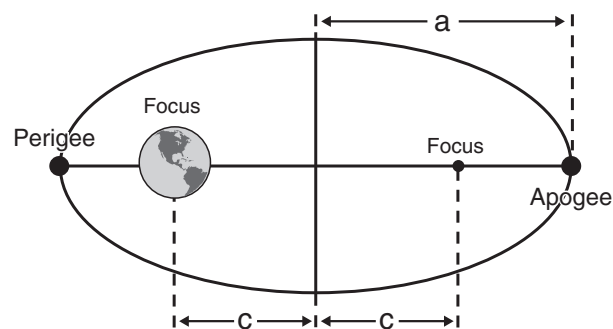


Figure 2.2 – Geometry of the orbital ellipse [29]

2.1.3 Orbital Elements

The intersection of the surface of the Earth and any plane containing the geocenter is called a **great circle**. The **inclination**, i , is the angle between the line joining the geocenter and North Pole and the line through the geocenter perpendicular to the orbital plane [41]. It is measured counter clockwise at the point at which an object crosses the equatorial plane travelling north in its orbit (the **ascending node**) [29]. These parameters are shown graphically in figure 2.3.

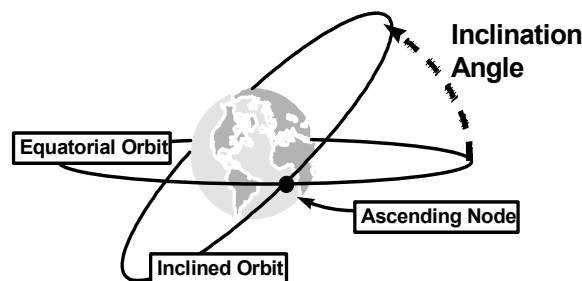


Figure 2.3 – Inclination tilt [29]

The First Point of Aries is a fixed point in space. The Vernal Equinox is defined as the first day of spring (in the northern hemisphere). The **right ascension** or **longitude of the ascending node** Ω is the angle, measured eastward, from the Vernal Equinox to the ascending node [29]. This can be seen in figures 2.4 and 2.5

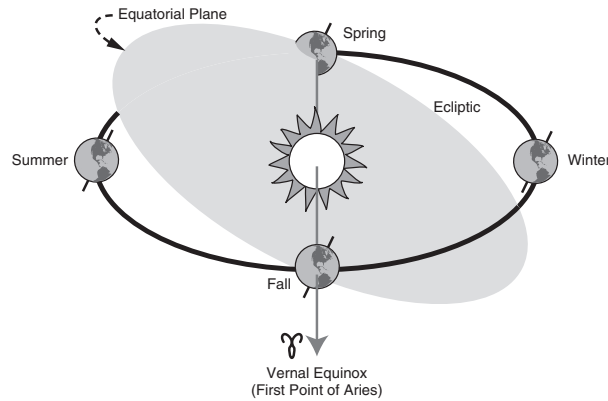


Figure 2.4 – Vernal equinox [29]

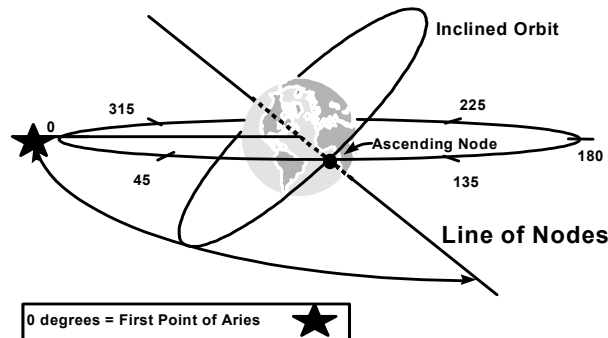


Figure 2.5 – Right ascension of the Ascending Node [29]

The **argument of perigee** or **argument of periapsis** is the angle, measured in the direction of satellite motion from the ascending node to perigee, as shown in figure 2.6 [29].

The **mean anomaly** is the angle, in degrees, measured from perigee of the satellite location in the orbit referenced to a circular orbit with the radius equal to the semi major axis [29].

Five independent quantities are sufficient to completely describe the size, shape and orientation of an orbit. To determine the exact position of a satellite at a particular time, an additional parameter is also required [53]. These six parameters are referred to as **orbital elements** or Keplerian elements.

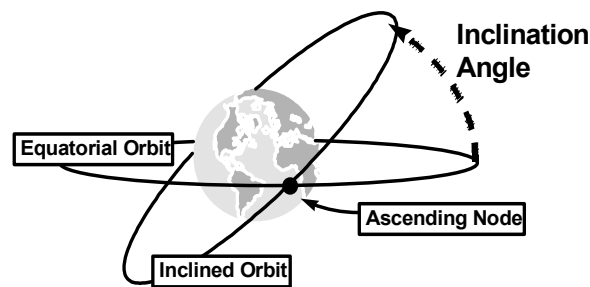


Figure 2.6 – *Argument of Perigee* [29]

- a , semi-major axis
- e , eccentricity
- i , inclination
- Ω , longitude of the ascending node
- ω , argument of periapsis
- M , Mean anomaly

The orbital information of many satellites is usually accessible through the **Two-Line Element (TLE)** set. It is indeed a three-line file which contains the Keplerian elements and some more data of a certain satellite, such as its international designator, satellite number, etc. [5]. A sample Two-Line Element set is shown in figure 2.7.

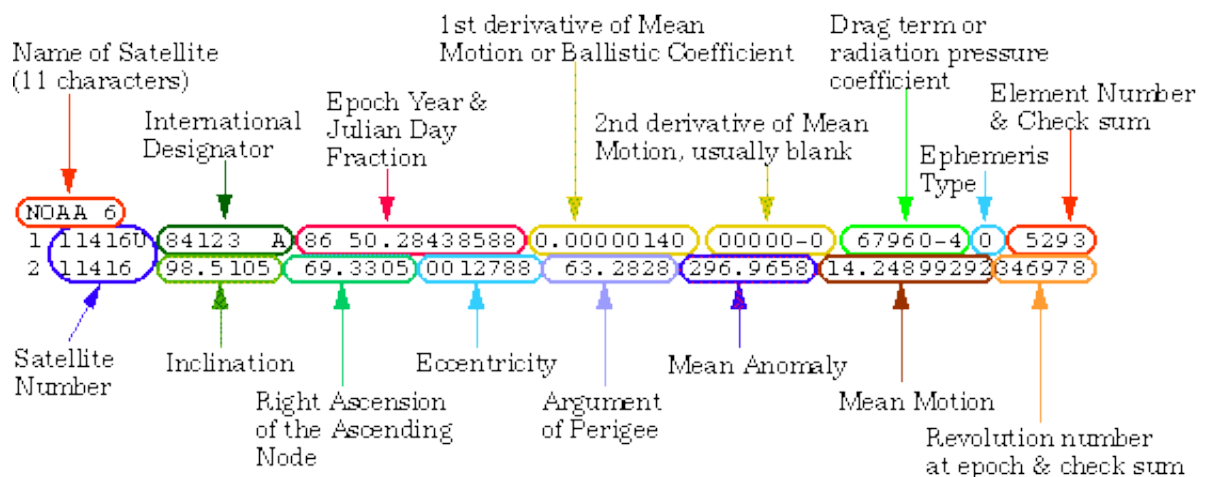


Figure 2.7 – *Two Line Element* [5]

These files can be publicly accessed from www.celestrak.com and they are used by most tracking software to calculate the position of satellites.

2.1.4 Ground Track

The previous definitions, used to determine the location of a satellite, take the Earth as reference. For tracking purposes, the relative motion of the satellite with respect to the the location of the observation is also to be considered. A common way to do this is referencing the location of the observation using a Geographical Coordinate System. A convenient coordinate system for this purpose is the Earth-Centred Earth-Fixed (ECEF) coordinate system, also known as Conventional Terrestrial System (CTS) [45]. For instance, the coordinates of ground segment, marked in a map in figure 2.8 are given in the following format:

$$37^{\circ}10'41''N \quad 3^{\circ}36'3''W \quad (2.1.3)$$



Figure 2.8 – Location of the ground segment marked on a map [7]

In this example, the location of the city of Granada is defined by these coordinates. The three first figures correspond to the latitude, the angle in degrees, minutes and seconds measured from the equator plane. The other three indicate longitude, the angle from a reference or *prime* meridian (the original site of the Royal Greenwich Observatory in England is used). The first letter (N or S) indicates whether the position is in the North or the South Pole, and the second (E or W) indicates whether the angle is taken east or west of the prime meridian. These parameters can be seen in figure 2.9.

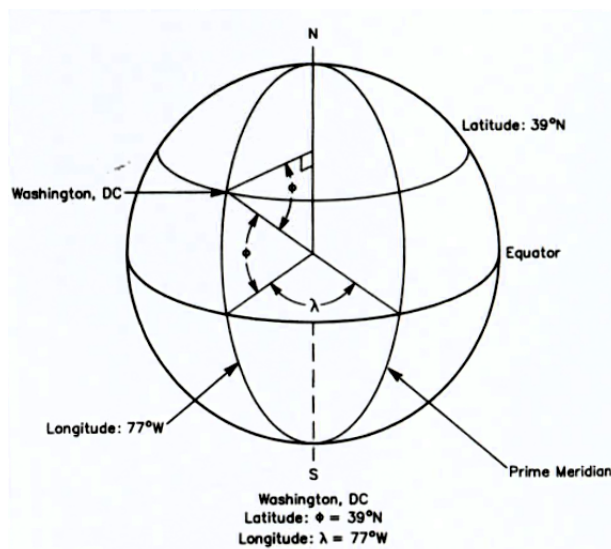


Figure 2.9 – Coordinates of Washington DC in ECEF coordinate system [41]

Without considering other propagation modes than direct propagation, a ground station will only be able to establish communication with a satellite at a certain time when the latter is in an unobstructed **line-of-sight (LOS)** with the antennas on the Earth. Within the scope of this Thesis, the ultimate purpose of calculating the position of a satellite determining when will it be in the **line-of-sight** of the ground station and how must the antennas be aimed towards it so that a good quality link can be established.

The surface of the Earth in **line-of-sight** with the satellite defines the *coverage circle*. Its centre is also the closest point from the surface of the Earth to the aircraft and is referred to as **Sub-Satellite Point (SSP)** [41]. The coverage circle and the **SSP** are graphically shown in figure 2.10.

To study the satellite coverage at a particular time all lines radiating from the satellite and tangent to the Earth are to be considered [41]. The problem can be geometrically evaluated as shown in figure 2.11.

The maximum angle β (central angle) between the **SSP** and the ground station which allows that they are in **line-of-sight** can be obtained using trigonometry on triangle AOC, formed by the satellite, the geocenter and the ground station [41]. It is given by expression 2.1.5, where R represents the radius of the Earth and h the altitude of the satellite above the surface of the Earth.

$$\cos(\beta) = \frac{R}{R+h} \quad (2.1.4)$$

$$\beta = \arccos\left(\frac{R}{R+h}\right) \quad (2.1.5)$$

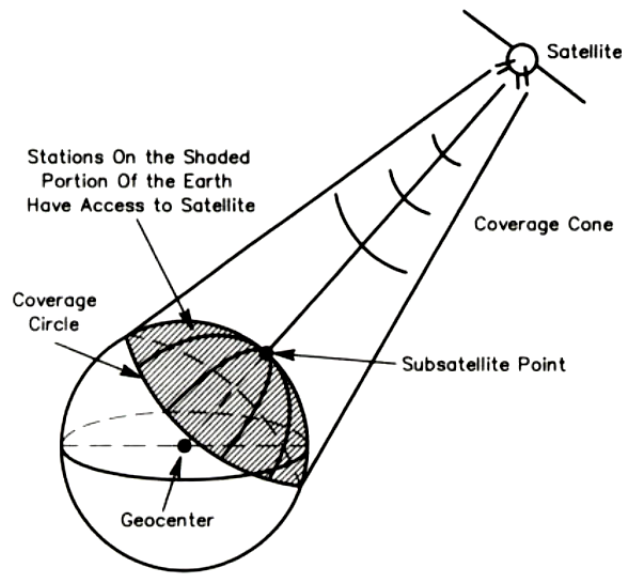


Figure 2.10 – Satellite coverage [41]

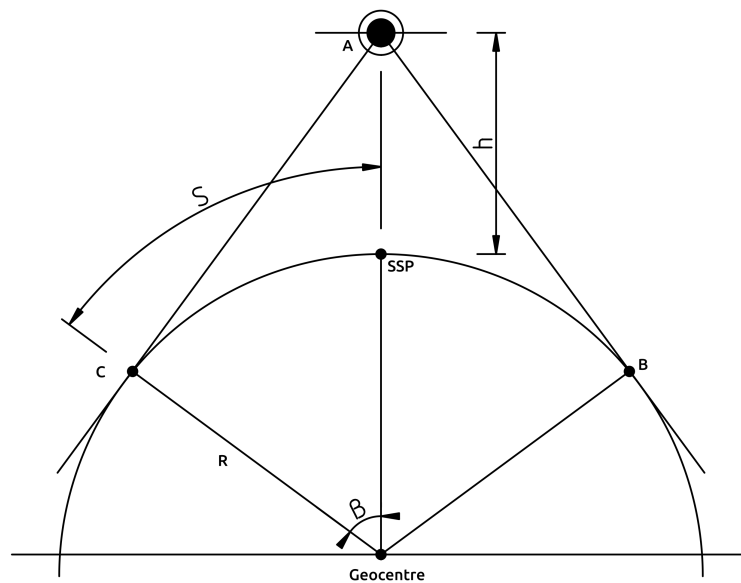


Figure 2.11 – Cross-section of satellite-coverage cone [41]

The maximum access distance, S_O , is obtained as in expression 2.1.6 [41].

$$S_O = R\beta = R \arccos\left(\frac{R}{R+h}\right) \quad (2.1.6)$$

When the ground station is in the coverage circle, the bearing of the antennas has to be calculated –the **azimuth** and **elevation** angles–. The elevation angle, represented in figure 2.12 as ϵ , is given by expression 2.1.7 [41].

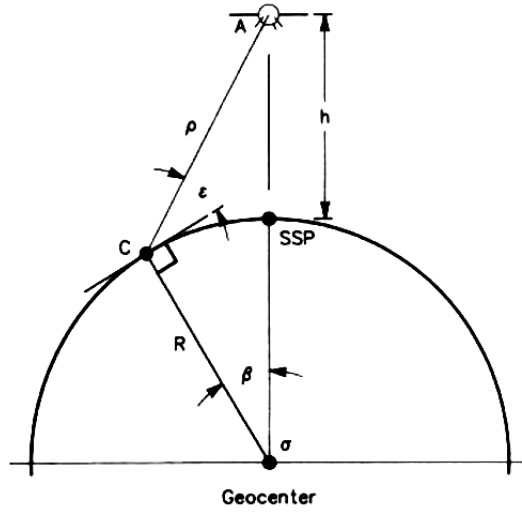


Figure 2.12 – Satellite elevation determination [41]

$$\varepsilon = \arctan \left[\frac{(R + h) \cos(\beta) - R}{(R + h) \sin(\beta)} \right] \quad (2.1.7)$$

Expression 2.1.8 gives the azimuth angle of the satellite as seen from the ground station –in this case, the spacecraft and the ground segment–, not at the same level relative to a specific datum. In practice, it is useful to determine the **slant range** in function of the elevation angle of the antennas [43], as given by expression 2.1.9.

$$Az = \arccos \left[\frac{\sin \phi_2 - \sin \phi_1 \cos \beta}{\cos \phi_1 \sin \beta} \right] \quad (2.1.8)$$

To conclude, the **slant range** is defined as the **line-of-sight** distance between two points –in this case, the spacecraft and the ground segment–, not at the same level relative to a specific datum. In practice, it is useful to determine the **slant range** in function of the elevation angle of the antennas [43], as given by expression 2.1.9.

$$s(\varepsilon) = \sqrt{(R_E \sin(\varepsilon))^2 + 2R_E h + h^2} - R_E \sin(\varepsilon) \quad (2.1.9)$$

Alternatively, expression 2.1.10 states the **slant range** as a function of time [26] [25]. This will specially useful in section 2.3, where the **Doppler shift** on the frequency of the received signal will be characterized by taking into account the relative speed of the aircraft with respect to the ground segment.

$$s(t) = \sqrt{a^2 + R_E^2 - 2aR_E \cos(\varphi(t))} \quad (2.1.10)$$

2.2 Frequency bands and fundamental parameters of antennas review

Communication between the spacecraft and the ground segment can only be guaranteed when the received power meets the dynamic range of the receiver, that is, the power of the received signal is between its minimum and maximum admitted levels. Specifically, in satellite communications the determining factor will be inferior margin due to the long distance between transceivers and consequent high attenuation. In order to ensure the suitability of the equipment and minimize the attenuation produced by the installation, the design of the ground segment must necessarily take antennas and wave propagation theory into account.

The main concepts and expressions to be considered for the system design will be discussed in this section.

2.2.1 Frequency bands

Frequency bands are the result of dividing the frequency spectrum into smaller ranges as shown in table 2.2.

Band	Frequency	Denomination
ELF	<3 kHz	Extremely Low Frequency
VLF	3–30 kHz	Very Low Frequency
LF	30–300 kHz	Low Frequency
MF	0.3–3 MHz	Medium Frequency
HF	3–30 MHz	High Frequency
VHF	30–300 MHz	Very High Frequency
UHF	0.3–3 GHz	Ultra High Frequency
SHF	3–30 GHz	Super High Frequency
EHF	30–300 GHz	Extremely High Frequency

Table 2.2 – *Frequency bands [40]*

As it was introduced in chapter 1, the bands of interest for this project are **VHF** and **UHF**. The reasons for this election will be presented in section 2.3.

2.2.2 Fundamental parameters of antennas

Antennas are part of a system that can be seen as a circuit. At the input of the antenna, the **input impedance** Z_i , composed of a real part R_i and an imaginary part X_i , can be defined. When Z_i has no frequency reactive part, the antenna is said to be **resonant** [40].

In order to have maximum power transference, the impedance of the antenna $Z_i = R_i + jX_i$ and the impedance of the transmission line or generator to which it is connected $Z_L = R_L + jX_L$ must be complex conjugates $Z_L = Z_i^*$ [40]. This is referred to as matched network. For the case of this project, antennas with an input real impedance of 50Ω were chosen, so the transmission lines and transceivers had to have an impedance of 50Ω as well.

A **directional antenna** is one having the property of radiating or receiving electromagnetic waves more efficiently in some directions than in others. An **omnidirectional antenna** is one which essentially has a non directional pattern in a given plane and a directional pattern in any orthogonal plane [37]. The ground station will be provided with one omnidirectional antenna and two directional antennas. Since the satellite is in constant motion, the directional antennas cannot aim to a fixed point, but have to be placed on a rotor which gives them the possibility to *track* the aircraft in its movement on the sky.

2.2.3 Polarization

The **polarization** of a radiated wave is defined as its property to describe the time varying direction and relative magnitude of the electric-field vector, as observed along the direction of propagation. An antenna is also said to have a polarization, which corresponds to the polarization of the wave it radiates [37].

Electromagnetic waves can be classified depending on their polarization in three categories: linearly polarized, circularly polarized and elliptically polarized waves.

Linear polarization is achieved when the field vector (electric or magnetic) possesses only one component or two orthogonal components that are in phase or 180° out of phase, as given by 2.2.1, where ρ_w is the unit vector (polarization vector) of the wave and θ and ϕ are the polar and azimuth components in a spherical coordinates system.

$$\hat{\rho}_w = \hat{\theta}; \quad \hat{\rho}_w = \hat{\phi}; \quad \hat{\rho}_w = \cos \alpha \hat{\theta} + \sin \alpha \hat{\phi} \quad (2.2.1)$$

Circular polarization is accomplished when the field vector possesses two orthogonal linear components with the same magnitude and they have a time-phase difference of odd multiples of 90° . In this case, there is an extra distinction between **right-hand** and **left-hand** circular polarization, as given by expressions 2.2.2 and 2.2.3.

$$\hat{\rho}_w = \frac{1}{\sqrt{2}} (\hat{\theta} + j\hat{\phi}) \quad (\text{right-hand}) \quad (2.2.2)$$

$$\hat{\rho}_w = \frac{1}{\sqrt{2}} (\hat{\theta} - j\hat{\phi}) \quad (\text{left-hand}) \quad (2.2.3)$$

A wave is elliptically polarized if it is not linearly or circularly polarized.

$$\hat{\rho}_w = \frac{1}{\sqrt{a^2 + b^2}} (a\hat{\theta} + be^{j\alpha}\hat{\phi}) \quad (2.2.4)$$

$$a, b > 0, \quad 0 < \alpha < \pi \quad (\text{right-hand})$$

$$a, b > 0, \quad 0 < \alpha < -\pi \quad (\text{left-hand})$$

In reception, the polarization of the antenna might not be the same of the incident wave, what is referred to as **polarization mismatch** [37]. This concept is mathematically expressed by the **polarization loss factor (PLF)** as given by 2.2.5, where ρ_a is the unit vector of the antenna and ψ_p is the angle between the two unit vectors.

$$PLF = |\hat{\rho}_w \cdot \hat{\rho}_a|^2 = |\cos \psi_p|^2 \quad (\text{dimensionless}) \quad (2.2.5)$$

Polarization is thus a determining factor for the design of the ground segment and a wrong choice may lead to a poor signal reception. For satellite links, where one of the communication endpoints is in constant movement linear polarization is a bad option, since the angle between unit vectors of the incident wave and the antenna will be in general different to zero, producing a polarization loss factor. In particular, if the direction of polarization is opposite, their unit vectors will be orthogonal the PLF will be zero ($-\infty$ dB) and there will not be reception.

Elliptical polarization would avoid this problem. However, due to the shape-changing nature of its wave front along the propagation direction, a certain PLF would be likely to happen as well.

The optimal election for the ground station is a circular polarization, which would theoretically ensure a 0 dB PLF as long as the direction of the polarization –right-hand or left-hand– is the same in the transmitter and the receiver. The big majority of **CubeSats** have right-hand circular polarization antennas. Since the verification of the correct operation of the system will be based on the reception of their signals and there are no further advantages with a left-hand polarization, this was the choice for the **GranaSAT-I** ground segment too.

There are several ways to obtain a circularly polarized antenna. Some antennas, notably the helix antenna, directly radiate in circular polarization. However, a commercial Yagi-Uda type antenna is also able to produce circular polarization by using two crossed antennas $\pi/2$ out of phase between them. With this configuration, an electric vector like in 2.2.2 is achieved and a circularly polarized wave is radiated or received with 0 dB PLF.

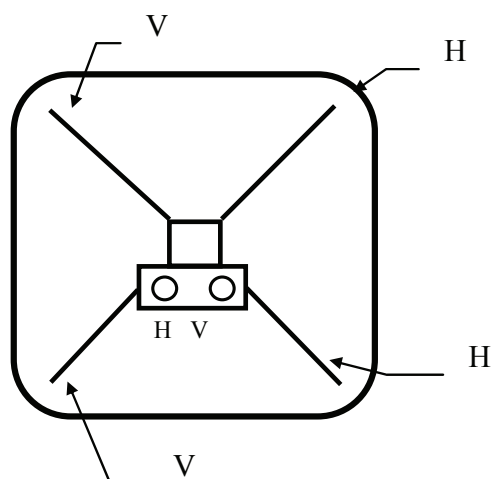


Figure 2.13 – Back view of the antenna with the two crossed antennas (vertical and horizontal) [23]

2.3 Radio wave propagation

As a consequence of its propagation along a certain path, an electromagnetic wave will undergo certain changes from its transmission to its reception. In order to predict the characteristics of the received wave, the effects on propagation must be identified and taken into account.

The **Free-Space path Loss (FSL or L_0)** represents the ratio between the received power and the transmitted power of a signal with wavelength λ by two antennas separated a distance r [40].

$$L_0 = 20 \log \left(\frac{P_R}{P_T} \right) = 20 \log \left(\left(\frac{\lambda}{4\pi r} \right)^2 D_T D_R \right) [dB] \quad (2.3.1)$$

This expression does not symbolize a real loss of power but a decrease of the power density with the distance. Hence, the directivity of the transmitting and receiving antennas D_T and D_R , representing their beam width, have a direct effect on this ratio.

2.3.1 Effects of the non-ionized atmosphere

In addition to the **FSL** the received signal will suffer a higher attenuation due to the propagation loss, which in an Earth-space link can be determined as sum of the contributions of [32]:

- Attenuation by atmospheric gases
- Attenuation by rain, other precipitations and clouds

- Focusing and defocusing
- Decrease in antenna gain due to wave-front incoherence
- Scintillation and multipath effects
- Attenuation by sand and dust storms

2

Atmospheric attenuation is mainly caused by the molecular absorption and the attenuation by precipitation and clouds. Figure 2.14 presents the specific zenith (in the vertical path) attenuation due to atmospheric gases. As is can be observed, for the frequency bands within the scope of this Thesis this value can be neglected.

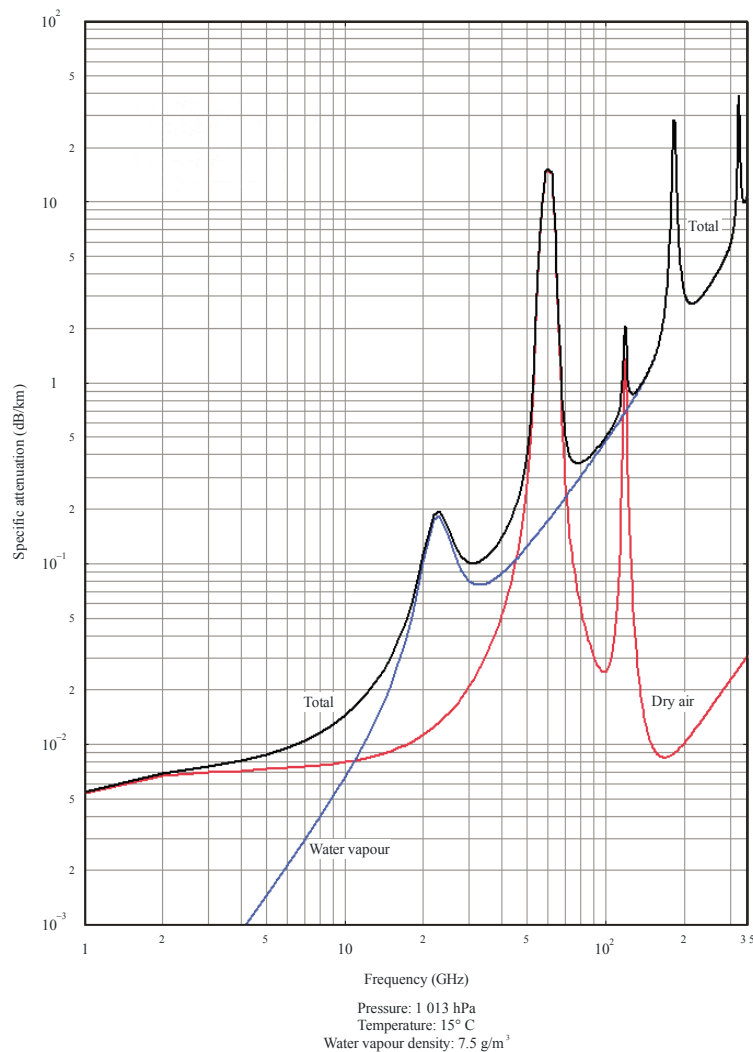


Figure 2.14 – Total, dry air and water-vapour zenith attenuation due to atmospheric gases from sea level [30]

Similarly, the rain specific attenuation can be neglected for the current used frequency bands, as it can be seen in figure 2.15. A more complex study should be carried out if higher frequencies were used.

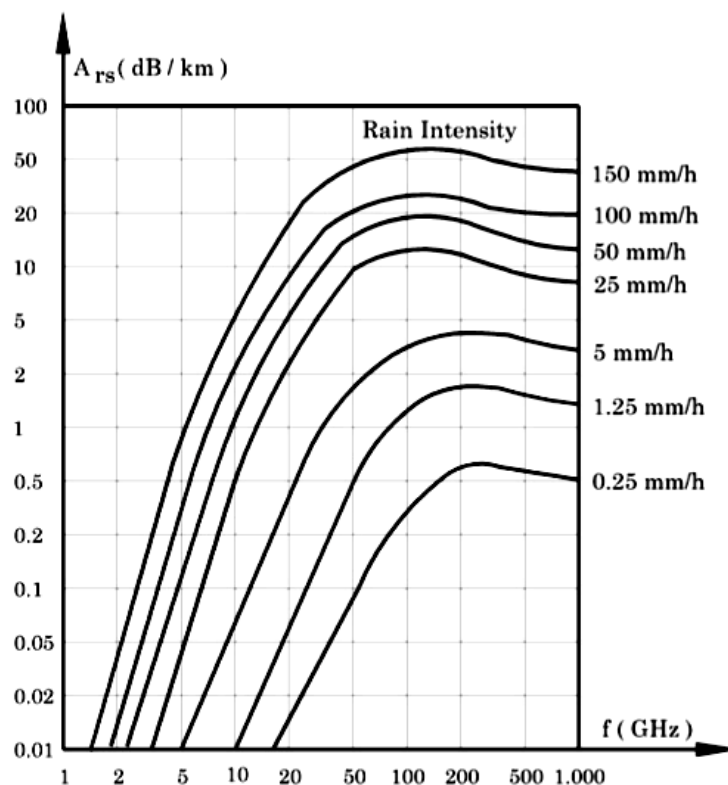


Figure 2.15 – Variations of rain specific attenuation vs. frequency and rain intensity [44]

The loss due to defocusing effect, also known as beam spreading loss, is caused by ray-bending at low elevation angles due to the regular decrease of refractive index with the height. In figure 2.16 an estimate of the losses through the total atmosphere due to atmospheric refraction effects is presented. The loss due to beam spreading in regular refractive conditions can be ignored at elevation angles above about 3° at latitudes less than 53° , as it is the case of Granada [32].

Incoherence of the wave-front of a wave incident on a receiving antenna is caused by small-scale irregularities in the refractive index structure of the atmosphere. Although not explicitly accounted for in the refraction model presented above, this effect is negligible in comparison with it [32].

Tropospheric scintillation is produced by fluctuation in the refractive index in the first kilometres of the atmosphere and is caused by high humidity gradients and temperature inversion layers. Amplitude scintillations increase with frequency and with the path length, are seasonally dependent, vary day-to-day, and with the local climate [47] [32].

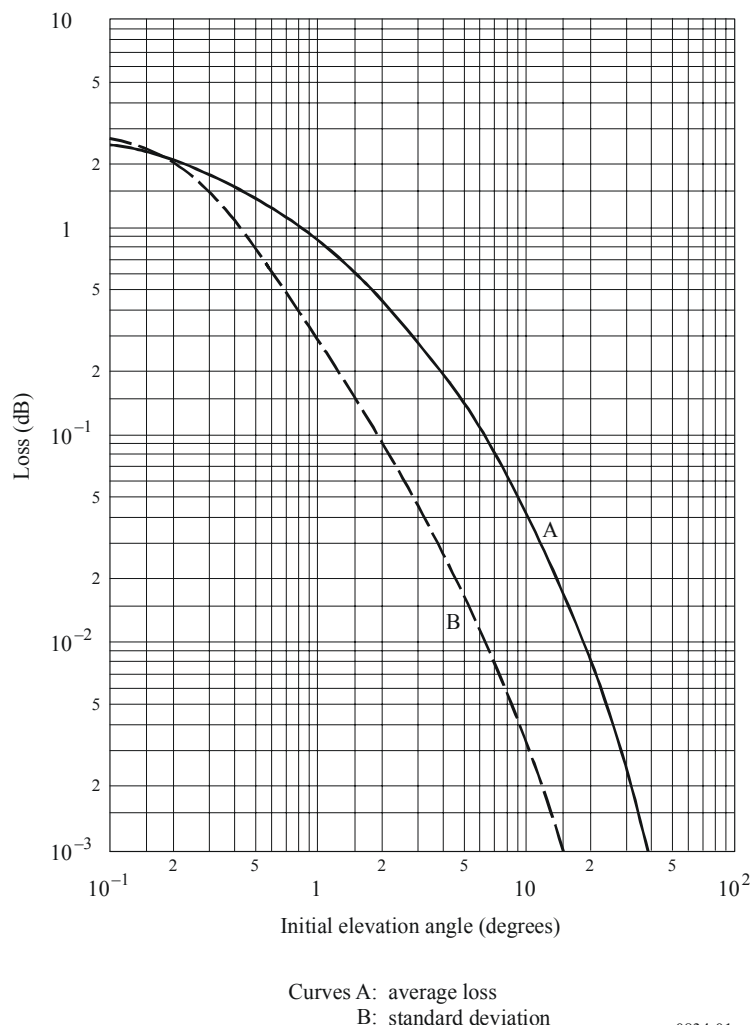


Figure 2.16 – An estimate of loss due to the additional spreading of a beam and standard deviation about the average [28]

It was not possible to find in the literature specific information of the effects of tropospheric scintillation for the frequency bands of interest. For instance, the fading prediction method proposed by the [ITU Radiocommunication Sector \(ITU-R\)](#) [32] is recommended for higher frequencies. However, observing the tendency to a less severe fading with lower frequencies, the model can be taken as a reference, giving the results shown in figure 2.17. For a frequency of 1 GHz and elevation angles higher than 10 degrees the amplitude fluctuation does not exceed to 0.1 dB.

Due to the location of Granada, in a region relatively far away from big deserts or sand deposits, and the high particle concentrations or high moisture contents required to produce significant propagation effects, the effect of sand and dust storms should not be of great impact for the link [32].

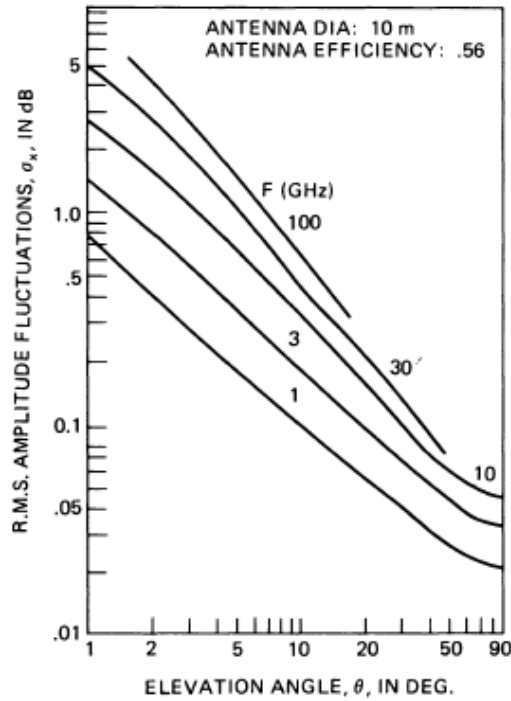


Figure 2.17 – Amplitude scintillations predicted from the ITU-R tropospheric scintillation model [47]

2.3.2 Ionospheric effects

Ionospheric scintillation makes reference to amplitude fluctuations due to inhomogeneities of electron density in the ionosphere causing refractive focusing or defocusing of radio waves [32]. These fluctuations decrease with increasing frequency and depend upon path geometry, location, season, solar activity and local time. The effects are maximum near the geomagnetic equator and smallest in the mid-latitude regions. The most commonly used parameter characterizing the intensity fluctuations is the scintillation index S_4 , defined by Equation 2.3.2 [31].

$$S_4 = \left(\frac{\langle I^2 \rangle - \langle I \rangle^2}{\langle I \rangle^2} \right)^{1/2} \quad (2.3.2)$$

where I is the intensity of the signal and $\langle \rangle$ denotes averaging.

Table 2.3 gives a conversion between the scintillation index S_4 and peak-to-peak fluctuations P_{fluc} (dB) based on empirical measurements.

The station closest to the latitude of Granada providing open access to S_4 data is located in Toulouse (France), with coordinates 43.57N, 1.47E. As a reference, S_4 index measured on April 3rd 2015 is shown in figure 2.18.

S_4	P_{fluc} (dB)
0.1	1.5
0.2	3.5
0.3	6
0.4	8.5
0.5	11
0.6	14
0.7	17
0.8	20
0.9	24
1.0	27.5

Table 2.3 – Empirical conversion table for scintillation indices [31]

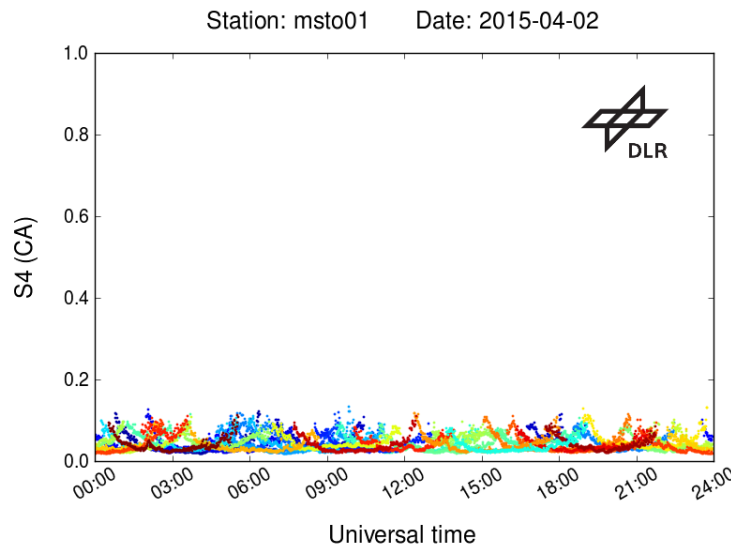


Figure 2.18 – S_4 index measured in Toulouse (France) on 03/04/2015 [15]

The terrestrial magnetic field has an effect on the polarization of the wave as well. This is known as the **Faraday Effect**, and it consists on the arbitrary rotation of the polarization vector [40]. It does not affect circular polarization, but for a linear polarization it may produce considerable PLF in the **VHF** and **UHF** bands, so this becomes another important reason to use circular polarization instead of linear polarization for this link.

A further ionospheric effect to consider is the **ionospheric reflection**. For frequencies under a certain limit, the propagating wave is refracted (although the effect is called ionospheric reflection, the physic phenomenon is indeed a refraction) and comes back to to the surface of the Earth, as shown in figure 2.19 [40].

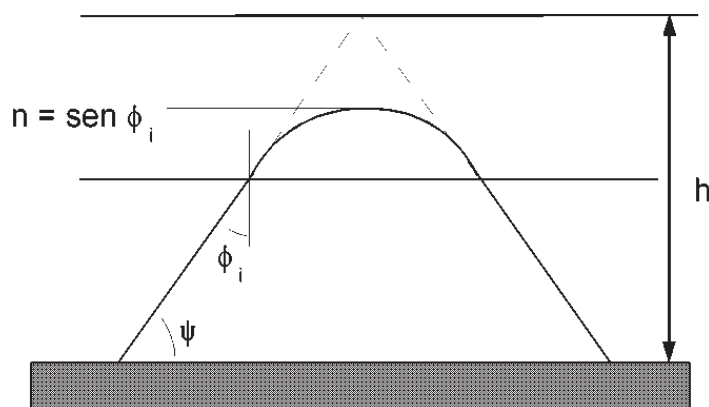


Figure 2.19 – Ionospheric reflection for flat Earth [40]

This effect is very useful for some terrestrial communications, but it defines a lower limit for the frequencies that can be used for space links, which is the MF band. Therefore this restriction does not apply to VHF and UHF bands.

2.3.3 Doppler shift

Lastly, the **Doppler shift** is to be considered in satellite communications. It is caused by the relative motion of the transmitter (Tx) and the receiver (Rx) units, and produces an offset between the transmitted frequency and received frequency. The time variations related to this phenomenon depend on the velocity of the Rx unit designated as v , radio frequency designated as f_0 (with wavelength of λ), and the angle between the direction of motion and the direction of radio wave propagation [44].

A compensation of this frequency shift must be performed so that the tuned frequency corresponds with the signal frequency during the transmission. Two groups of methods for compensation can be established:

- The first is based on a direct compensation by the receiver. In an analog device, a phase-lock loop can track the carrier frequency along its shift, while in a digital device an algorithm can be implemented in software to perform the same task.
- If the position and relative speed of the aircraft to the ground segment is known, an analytical expression given in 2.3.3 can be used to determine the frequency offset, where c represents the speed of light in vacuum.

$$f_d = v \frac{f_0}{c} \quad (2.3.3)$$

This is the approach used by the tracking software GPredict, which determines the

Doppler shift for a 100MHz transmission frequency with expression, where v represents the range-rate of the satellite –rate that the satellite moves towards or away from the ground station–, f_d the transmission frequency (100MHz), and c the speed of light.

2.4 Transmission lines

The transmission of a signal with a high frequency cannot be described with distributed circuit analysis methods. In particular, when the wave length is comparable to the dimensions of the transmission medium, the time delay suffered by the wave along its propagation in the medium results in phase differences in different points in the transmission line.

In the circuit shown in figure 2.20, the wave front is represented in blue. On reaching the far end after a certain time, if the switch S_2 is closed, all or a fraction of the wave voltage and current will reflect, depending on the load to which the line is attached. The wave will also be completely reflected if the switch S_2 is open [59].

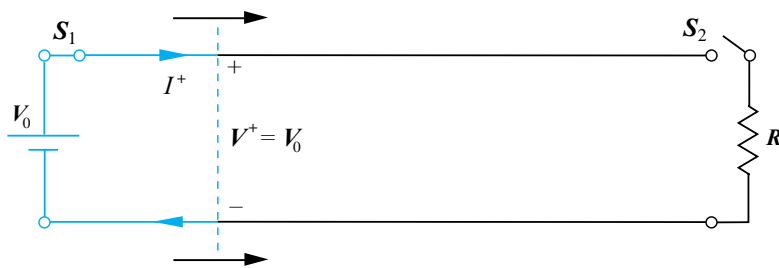


Figure 2.20 – Basic transmission line circuit, showing voltage and current waves initiated by closing switch S_1 [59]

The equation describing the wave along its propagation in a lossy medium is given by 2.4.1, where V_0^+ and V_0^- represent the voltage of the transmitted and reflected wave, respectively, α the attenuation coefficient, β the phase constant, and 'z' the distance from the source. For convenience, coordinates are assigned such that the load is at location $z = 0$. Therefore, the line occupies the region $z < 0$.

$$V_s = V_0^+ e^{-\alpha z} e^{-j\beta z} + V_0^- e^{\alpha z} e^{j\beta z} \tag{2.4.1}$$

The characteristic impedance must be introduced before the next concepts are presented. The **characteristic impedance** Z_0 of the line is the ratio of positively travelling voltage wave V_0^+ to current wave I_0^+ at any point on the line [54].

$$Z_0 = \frac{V_0^+}{I_0^+} \tag{2.4.2}$$

The basic reflection problem is illustrated in figure 2.21. On it, a transmission line of characteristic impedance Z_0 is terminated by a load having complex impedance, $Z_L = R_L + jX_L$. If the line is lossy, Z_0 will be complex as well [59].

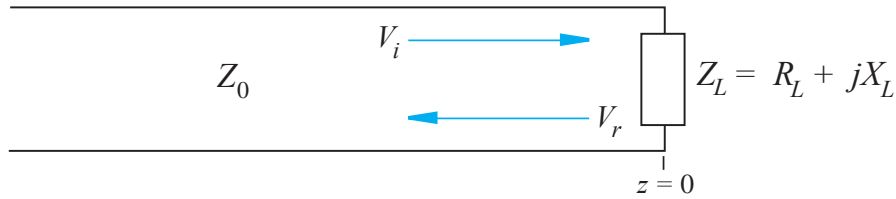


Figure 2.21 – Voltage wave reflection from a complex load impedance [59]

An important parameter in the analysis of transmission lines is the **reflection coefficient**, given in Equation 2.4.3 and defined as the ratio between the incident and the reflected voltages of the wave [59].

$$\Gamma = \frac{V_0^+}{V_0^-} = \frac{Z_0 - Z_L}{Z_0 + Z_L} \quad (2.4.3)$$

$$0 < \Gamma < 1$$

A low reflection coefficient, which is achieved when $Z_0 \approx Z_L$, indicates that the power of the undesired reflected wave is low in comparison with the power of the transmitted wave. Therefore in the process of design of the network the elements must be chosen carefully in order to satisfy that the values of the characteristic impedance and the load impedances are as similar as possible.

Another parameter commonly used in engineering is the **standing wave ratio (SWR)**, defined as the ratio of the maximum voltage V_{max} to the minimum V_{min} , or equivalently the ratio of the maximum current intensity I_{max} to the minimum current intensity I_{min} [54].

$$SWR = \frac{V_{max}}{V_{min}} = \frac{I_{max}}{I_{min}} = \frac{1 + |\Gamma|}{1 - |\Gamma|} \quad (2.4.4)$$

$$1 < SWR$$

By analysing Equation 2.4.4 it can be concluded that a SWR close to 1 indicates a low reflection in the load.

2.5 Digital communications in space

The final goal of a ground segment is to be capable of receiving **telemetry** from and sending **telecommands** to the spacecraft. Therefore, the capability to send and receive digital data must be taken into account for the design of the ground segment.

In **CubeSat** projects **AX.25** is usually adopted as digital transmission protocol for the data link layer of the ISO model [51]. The modulation and demodulation of packets into **AX.25** is done by a **Terminal Node Controller (TNC)**, which connects to a terminal (i.e. a PC) and a transceiver. The computer sends and receives packets from the **TNC** using the physical layer protocols **KISS** or **6pack**, and the transceiver sends and receives FM modulated audio signals from the **TNC**. On top of it, **IP** and **TCP** operate on the network and transport layers as support for a certain application being executed on the endpoints of the link.

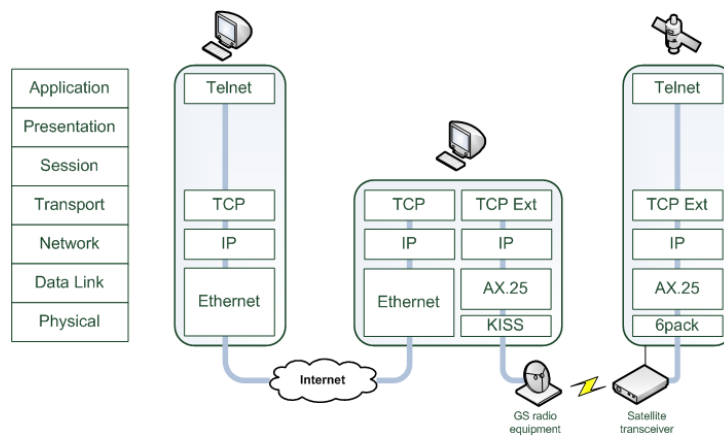


Figure 2.22 – Typical protocol stack in a *CubeSat* ground segment [55]

The **TNC** physical device can be substituted for a software running directly on the terminal, also known as **soundmodem**.

CHAPTER

3

DOWNLINK LINK BUDGET

A [link budget](#) analysis was carried out in order to ensure an efficient design of the ground segment. Having it as a reference not only helps to select equipment capable for communications with [CubeSats](#), but also not to exceed the required performance, which would unnecessarily increase the cost.

The [link budget](#) calculates the level of a signal upon its arrival to the receiver, taking into account the amplification and attenuation that it suffers along its path from transmission to reception. The level of the signal –usually expressed as E field or voltage– is computed as the lineal contribution of the effects produced by each element taking part in the communication process. The effects taken into account have an atmospheric origin or due to wave propagation in free space and transmission lines, as it was discussed in chapter 2. Additionally, they can be produced by the active elements in the receiving system. The [link budget](#) analysis can therefore only be concluded after the inclusion of specific hardware, which will be presented in detail chapter 4. An illustrative diagram is given in figure 3.1.

In spite of the transmitting capability of the transceivers considered, the lack of a power amplifier impedes the possibility of sending signals to the space with enough power as to be detectable by satellites. For that reason, only a downlink [link budget](#), from space to the ground segment, was calculated.

The basic expression giving the signal level upon reception is given by Equation 3.0.1 [44].

$$\begin{aligned} P_r &= G_t - L_t \text{ [dB]} \\ L_t &= (FSL + L_f + L_a + L_{pf} + L_{pv} + L_m) \end{aligned} \tag{3.0.1}$$

Where each term stands for:

- P_r : Received power
- G_t : Total gain
- L_f : Total loss
- **FSL**: Free space loss
- L_f : feeder, RF connector and cable loss
- L_a : losses related to the antenna misalignment
- L_{pf} : losses due to the absorbents of clear sky
- L_{pv} : atmospheric variable path losses
- L_m : miscellaneous losses specific to each link. Insertion loss produced by hardware devices will be included in this point.

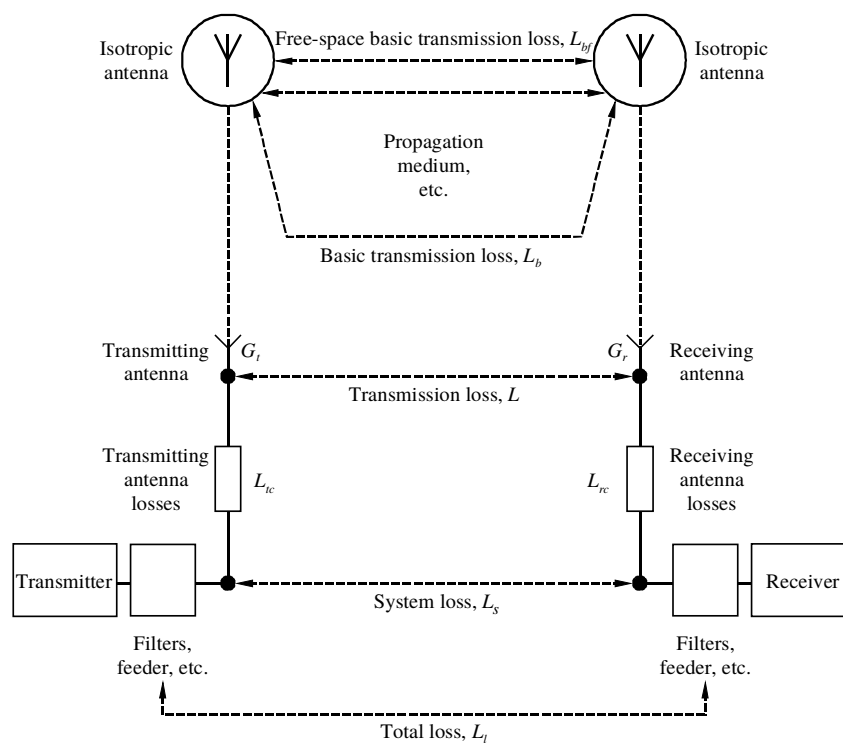


Figure 3.1 – Generic diagram of attenuation in radio transmissions [52]

As a consequence of the geographical placement of the ground segment and its intended use, the following assumptions were made:

- The minimum elevation angle considered was 10 degrees. Transmission and reception with lower angles present a much higher attenuation of the signal not only due to atmospheric effects, but also to the surrounding buildings, which obstruct the direct view between the aircraft and the antennas.
- The scientific and mainly educational purpose of the [GranaSAT-I](#) mission makes unnecessary a 100% up time of the link or its disposal in critical situations. Therefore a less demanding performance of the system is required, with a consequent reduction of its cost but at the expense of possible loss of communication in certain conditions like severe weather conditions. Particularly, atmospheric variable path losses L_{pv} was not considered.

3.1 Free space loss

The distance between the ground segment and the spacecraft is minimum when the [SSP](#) is directly above the antennas and maximum when the spacecraft is at the horizon. However, due to the 10° minimum elevation restriction, the maximum distance of the link is achieved when the antennas are aimed at this angle. Considering a typical [CubeSat](#) scenario, with a [Low Earth Orbit \(LEO\)](#) orbit between 160 km and 1600 km, figure 3.2 shows the [slant range](#) for elevation angles between 10° and 90° , as calculated from expression 2.1.9.

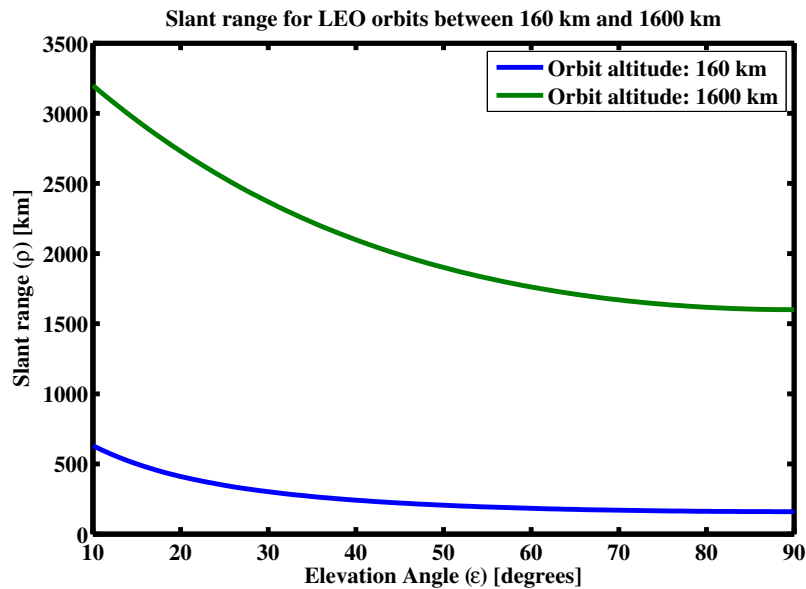


Figure 3.2 – *Slant ranges for LEO orbits*

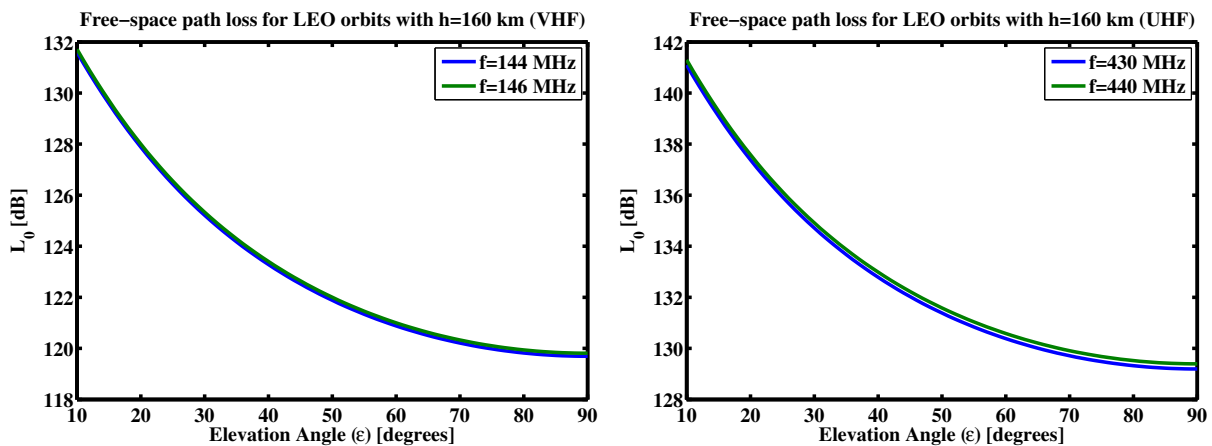
Table 3.1 summarizes the minimum and maximum [slant rangess](#) for typical [LEO](#) orbits

between 160 km and 1600 km. When the SSP is directly above the antennas, the slant range equals the spacecraft altitude.

Orbit distance	Slant range at $\varepsilon=90^\circ$	Slant range at $\varepsilon=10^\circ$
160 km	160 km	630.1 km
1600 km	1600 km	3198.4 km

Table 3.1 – Distance between the ground segment and the spacecraft for LEO orbits at maximum and minimum elevation angle

Once the distance between the satellite and the ground segment has been calculated, the FSL can be obtained using expression 2.3.1. The results for 160 km and 1600 km altitude orbits are plotted in figures 3.3 and 3.3. For favourable and adverse cases consideration, the top of and bottom of the VHF and UHF amateur bands were calculated.



(a) VHF band

(b) UHF Band

Figure 3.3 – FSL for 160 km altitude orbits in VHF and UHF amateur bands

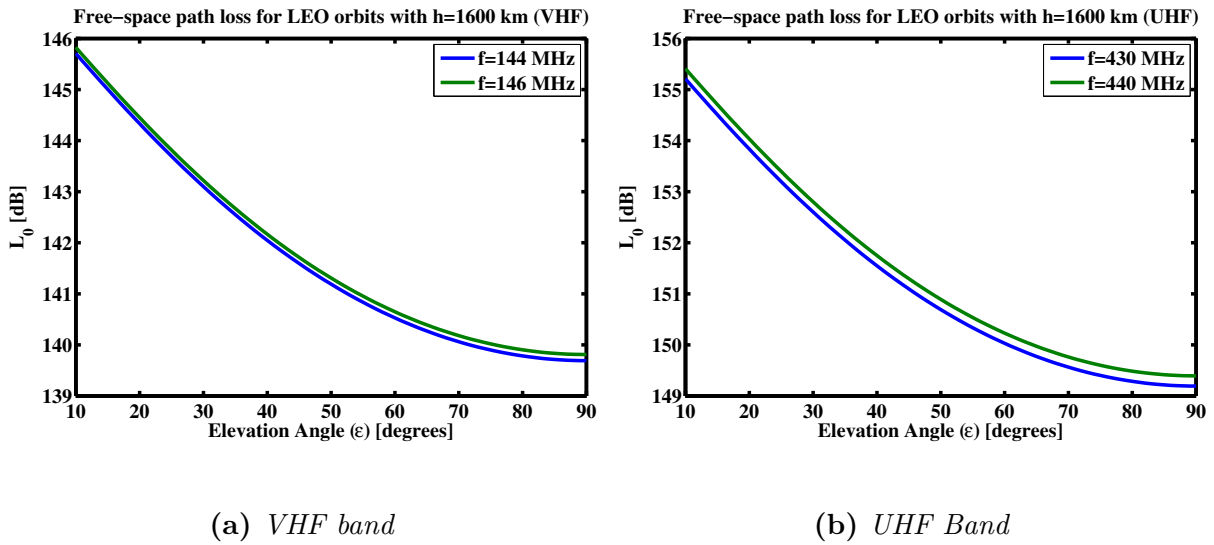


Figure 3.4 – FSL for 1600 km altitude orbits in VHF and UHF amateur bands

Table 3.2 shows a summary of the results for the FSL in VHF and UHF for the maximum and minimum slant ranges in LEO orbits. Although in the final budget calculations the top and bottom of the bands are considered, for convenience only the results for the centre frequencies are given in this table.

Slant Range [km]	L_0 (145 MHz) [dB]	L_0 (435 MHz) [dB]
160 km	119.75	129.29
3198.4 km	145.77	155.31

Table 3.2 – FSL for shortest and longest slant ranges in LEO orbits

3.2 Atmospheric attenuation

As it was discussed in sections 2.3.1 and 2.3.2, different atmospheric effects result in an attenuation of the signal along its propagation. For the frequency bands of interest and considering the assumptions made at the beginning of this chapter, some of those effects are limited and the attenuation they produce can be neglected.

For the case of the ionospheric scintillation, no analytical or empirical expressions could be found in the literature for the exact bands of interest. However, using as reference figure 2.16 and the conversion values given in table 2.3 an upper bound could be established.

Atmospheric effect	Attenuation (145 MHz) [dB]	Attenuation (435 MHz) [dB]
Attenuation by atmospheric gases	0	0
Attenuation by rain, other precipitations and clouds	0	0
Focusing and defocusing	0	0
Decrease in antenna gain due to wave-front incoherence	0	0
Tropospheric scintillation and multipath effects	< 0.1	< 0.1
Attenuation by sand and dust storms	0	0
Ionospheric scintillation	< 1.5	< 1.5
Total atmospheric loss	1.6	1.6

Table 3.3 – *Atmospheric attenuation values for the GranaSAT ground segment*

3.3 Attenuation by polarization mismatch

Using Equation 2.2.5, it can be determined that the PLF for the right-hand circular polarization chosen for the ground segment, provided that the spacecraft radiates with the same type and direction of polarization, will be 0dB.

3.4 Antenna pointing loss

A further difficulty in the [link budget](#) calculations is related to the [antenna pointing loss](#), which is produced by an offset between the direction of the main lobe of the antennas in ground segment and the direct vision line with the satellite, as it can be seen graphically in figure 3.5. The lack of specialized measuring equipment make it troublesome to determine the exact [antenna pointing loss](#), but an upper limit was determined in order to be used in the final [link budget](#) calculations.

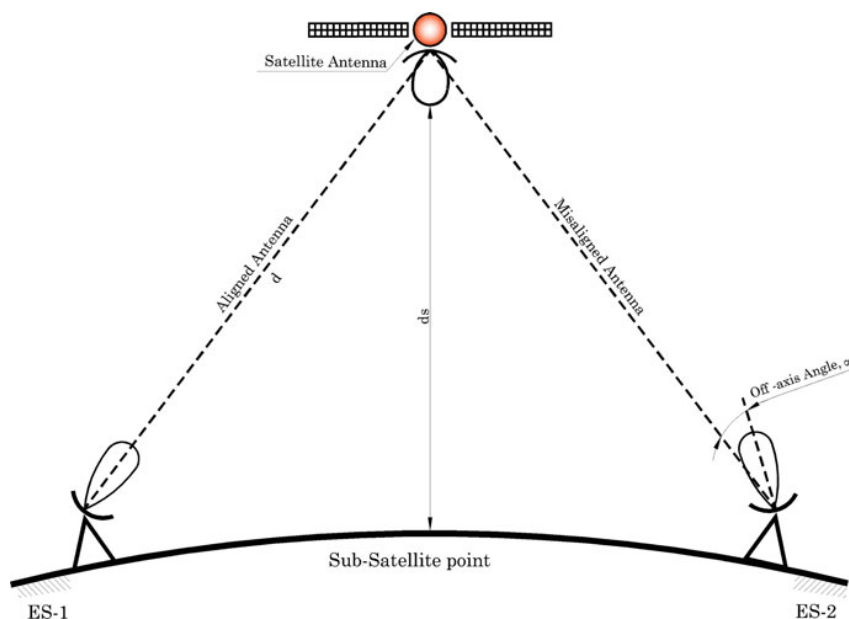


Figure 3.5 – Antenna misalignment in satellite links [44]

The [antenna pointing loss](#) can be calculated with Equation 3.4.1 as a function of the depointing angle α and the half power beamwidth θ_{3dB} [50].

$$L_T = 12 \left(\frac{\alpha}{\theta_{3dB}} \right)^2 [dB] \quad (3.4.1)$$

The estimation of the depointing angle is derived from the method used to deploy the antennas, described in detail in section 6.1, and based on the coincidence of the geographical North with a visible landmark, in this case a hospital. It will be therefore estimated that the depointing angle can be as high as the angle difference between the North and any other point of the façade, as shown in figure 6.11.

The half power beamwidth is characteristic of each antenna and thus the result of the [antenna pointing loss](#) cannot be determined without considering specific hardware. The complete equipment description, including the beamwidth for each of the antennas is given in chapter 4, which for the case of the 70 cm antenna is 36° and for the 2 m antenna is 47° .

Depointing angle α [deg]	L_T (145 MHz) [dB]	L_T (435 MHz) [dB]
< 6.5	0.23	0.39

Table 3.4 – Antenna pointing loss

3.5 System loss

The equipment in the ground station, formed by the antennas, connectors, transmission lines and transceivers will be responsible for an additional loss, the system loss.

3.5.1 Feeder, RF connector and cable loss

The connector type used for the directional antennas lines was type-N, which in most catalogues has a typical insertion loss of < 0.15 dB at GHz frequencies, and smaller at MHz frequencies. The total number of connectors from one antenna to one transceiver is 9.

The coaxial cable used for signal transmission was RG-11, which has a typical attenuation of 2.5 dB/100 feet (30.5 m) in the 145 MHz band and 4.8 dB/100 feet in the 435 MHz band. The exact distance of the cable could not be determined, since it was deployed by the university technicians prior to the beginning of this Thesis. However, known the mast height (10 m) and the number of floors between the rooftop and the control room (4), an approximate cable distance of 30 m can be assumed, including some extra meters in the control room and rolled on the antennas boom.

	L_C (145 MHz) [dB]	L_C (435 MHz) [dB]
Feeder and RF connector loss	1.35	1.35
Cable loss	2.46	4.72

Table 3.5 – *Connection loss*

3.5.2 Miscellaneous losses

Additionally to the cable and connectors loss, a number of devices placed in the transmission path between the antennas and the transceivers also produce an insertion loss which is accounted for in this section. Tables 4.3 and 4.11, as given by their vendors, directly provide an insertion loss value of the pre-amplifiers and the SWR meter.

As to the antenna switcher, the VSWR values given in table 4.10 cannot be converted to insertion loss without additional information. Similarly, the circular polarization emphasers do not provide that value. For that reason and taking into account that they are passive elements, the loss produced by both elements will be considered the same as the produced by two N-connectors, one for the input and one for the output.

Device	L_D (145 MHz) [dB]	L_D (435 MHz) [dB]
Pre-amplifier	0.2	0.5
SWR-Meter	0.2	0.3
Diplexer	0.15	0.2
Circular pol. emphaser	0.3	0.3
Antenna switcher	0.3	0.3

Table 3.6 – *Insertion loss by other devices*

3.6 System gain

Not only is the system on the ground segment responsible for the attenuation of the signal, but some of its elements produce an increase in its power level, namely the antennas –as a direct consequence of their directional radiation pattern– and the pre-amplifiers.

Device	Gain (145 MHz) [dB]	Gain (435 MHz) [dB]
Wimo X-Quad antennas	10.5	12.8
Pre-amplifiers	10 – 20	22 – 26

Table 3.7 – *System gain*

3.7 Spacecraft communications unit

The analysis performed by this downlink [link budget](#) can only be completed if a particular **Tx** unit is considered, with a certain transmission power and eventually an antenna gain as well.

To fulfil this requirement with a not yet designed communications unit for [GranaSAT-I](#), a survey on [CubeSat](#) communication systems was used: the **TUB Small Satellite Database** (https://www.raumfahrttechnik.tu-berlin.de/menue/publikationen/small_satellite_database/parameter/en/), part of the REPIN project of the Technical University of Berlin, is a very complete catalogue of [CubeSats](#) in which information of their on-board **Tx** system can be found [33]. Therefore, the **Tx** power and, if any, the antenna gain of these satellites was used as reference.

Among the big variety of missions listed in the database, [CubeSats](#) with downlink in the [VHF](#) and [UHF](#) bands were filtered and a favourable and adverse case was extracted for the [link budget](#) by taking the combined highest and lowest **Tx** power and antenna gain, respectively.

In the **VHF** band, satellites *UKUBE-I* and *InnoSat* were dismissed as favourable cases, since their 2500 W and 150 W transmission power seem to be misprints or, in any case, they cannot be considered typical **CubeSat** cases. Therefore, the *CanX-6 (NTS)* was taken as the favourable case with an EIRP of 33.98 dBm and *PW-Sat 1* was taken as adverse case with an EIRP of 23.01 dBm.

For the **UHF** band several satellites had an identical EIRP of 40 dBm and 20 dBm for the favourable and adverse cases, respectively. For instance, *AprizeSat 2 (LatinSat-D)* in the favourable group and *We Wish* in the adverse group.

CubeSat	Tx power [dBm]	Antenna Gain [dBi]	EIRP [dBm]
CanX-6 (NTS)	33.98	0.00	33.98
PW-Sat 1	23.01	0.00	23.01

Table 3.8 – *VHF study case [33]*

CubeSat	Tx power [dBm]	Antenna Gain [dBi]	EIRP [dBm]
AprizeSat 2 (LatinSat-D)	40.00	0.00	40.00
We Wish	20.00	0.00	20.00

Table 3.9 – *UHF study case [33]*

3.8 Link budget results

To conclude the **link budget** analysis, the previous results are summarized and presented in tables 3.10 and 3.11. The adverse and favourable values are the upper and lower limits when a range has been obtained. The nominal value was determined as the arithmetic mean of the adverse and favourable values.

Observing the results, it can be remarked that the link margin in the adverse case is reduced both in **VHF** and **UHF** bands, but still above the threshold of the transceiver. On the other hand, in optimum conditions the favourable case gives a high margin above the threshold also in both bands. Therefore it can be concluded that, while not exceeding greatly and unnecessarily the required performance, the designed system should be capable for communications with a **CubeSat** in a **LEO** orbit.

STATION : Granada
VHF Downlink

37°10 41 N 3°36 3 W

	Nominal	Adverse	Favourable	Unit
S/C Tx power	28.49	23.01	33.98	dBm
S/C antenna gain	0.00	0.00	0.00	dB
S/C EIRP	28.49	23.01	33.98	dBm
Frequency	145000000.0	146000000.0	144000000.0	Hz
Distance	1679.2	3198.4	160.0	km
Free Space Loss	132.76	145.83	119.69	dB
Attenuation by atmospheric Gases	0.00	0.00	0.00	dB
Attenuation by rain, Other precipitations and clouds	0.00	0.00	0.00	dB
Focusing and defocusing	0.00	0.00	0.00	dB
Decrease in antenna gain due to wave-front incoherence	0.00	0.00	0.00	dB
Tropospheric scintillation and multipath effects	0.10	0.10	0.10	dB
Attenuation by sand and dust storms	0.00	0.00	0.00	dB
Ionospheric scintillation	1.50	1.50	1.50	dB
Total atmospheric loss	1.60	1.60	1.60	dB
Antenna HPBW	47.00			deg
Antenna depointing angle	3.25	6.50	0.00	deg
Antenna pointing loss	0.06	0.23	0.00	dB
RF cable length	30.00			m
Cable loss per meter	0.08	0.08	0.08	dB/m
Total cable loss	2.46	2.46	2.46	dB
Number of feeders and RF connectors	9.00			
Loss per feeder and RF connector	0.15	0.15	0.15	dB
Total feeder and RF connector loss	1.35	1.35	1.35	dB
Pre-amplifier NF	0.20	0.20	0.20	dB
SWR-Meter NF	0.20	0.20	0.20	dB
Diplexer NF	0.15	0.15	0.15	dB
Circular pol. Emphaser NF	0.30	0.30	0.30	dB
Antenna switcher loss	0.30	0.30	0.30	dB
Total circuit loss	4.96	4.96	4.96	dB
Antenna gain	10.50	10.50	10.50	dB
Pre-amplifier	15.00	10.00	20.00	dB
Station total gain	25.50	20.50	30.50	dB
Receiver sensitivity	2.20	2.20	2.20	uV
Receiver sensitivity (dBm)	-120.14	-120.14	-120.14	dBm
Rx power margin	34.76	11.04	58.37	dBm

Table 3.10 – Downlink link budget analysis for the VHF band

STATION : Granada
UHF Downlink

37°10 41 N 3°36 3 W

	Nominal	Adverse	Favourable	Unit
S/C Tx power	30.00	20.00	40.00	dBm
S/C antenna gain	0.00	0.00	0.00	dBi
S/C EIRP	30.00	20.00	40.00	dBm
Frequency	435000000.0	440000000.0	430000000.0	Hz
Distance	1679.2	3198.4	160.0	km
Free Space Loss	142.30	155.41	129.19	dB
Attenuation by atmospheric Gases	0.00	0.00	0.00	dB
Attenuation by rain, Other precipitations and clouds	0.00	0.00	0.00	dB
Focusing and defocusing	0.00	0.00	0.00	dB
Decrease in antenna gain due to wave-front incoherence	0.00	0.00	0.00	dB
Tropospheric scintillation and multipath effects	0.10	0.10	0.10	dB
Attenuation by sand and dust storms	0.00	0.00	0.00	dB
Ionospheric scintillation	1.50	1.50	1.50	dB
Total atmospheric loss	1.60	1.60	1.60	dB
Antenna HPBW	36.00			deg
Antenna depointing angle	3.25	6.50	0.00	deg
Antenna pointing loss	0.10	0.39	0.00	dB
RF cable length	30.00			m
Cable loss per meter	0.16	0.16	0.16	dB/m
Total cable loss	4.72	4.72	4.72	dB
Number of feeders and RF connectors	9.00			
Loss per feeder and RF connector	0.15	0.15	0.15	dB
Total feeder and RF connector loss	1.35	1.35	1.35	dB
Pre-amplifier IL	0.50	0.50	0.50	dB
SWR-Meter IL	0.30	0.30	0.30	dB
Diplexer NF	0.15	0.15	0.15	dB
Circular pol. Emphaser NF	0.30	0.30	0.30	dB
Antenna switcher loss	0.30	0.30	0.30	dB
Total circuit loss	7.62	7.62	7.62	dB
Antenna gain	12.80	12.80	12.80	dB
Pre-amplifier	24.00	22.00	26.00	dB
Station total gain	36.80	34.80	38.80	dB
Receiver sensitivity	2.20	2.20	2.20	uV
Receiver sensitivity (dBm)	-120.14	-120.14	-120.14	dBm
Rx power margin	35.32	9.92	60.53	dBm

Table 3.11 – Downlink link budget analysis for the UHF band

CHAPTER

4

EQUIPMENT DESCRIPTION

In this chapter, a detailed description of the equipment employed for the deployment of the ground station will be presented.

The design was made in accordance to the topics discussed in chapter 2 and the recommendations of the [ARISS](#) [1], the international working group which regulates amateur contacts with the [ISS](#). Contacts are established with the crew of the [ISS](#) and give the opportunity to primary and high school pupils to directly speak to them and learn about life on board the [ISS](#).

The installation requirements for a *direct contact* involve a duplicated system with one prime station and one backup station. A diagram of the system can be seen in figure 4.1.

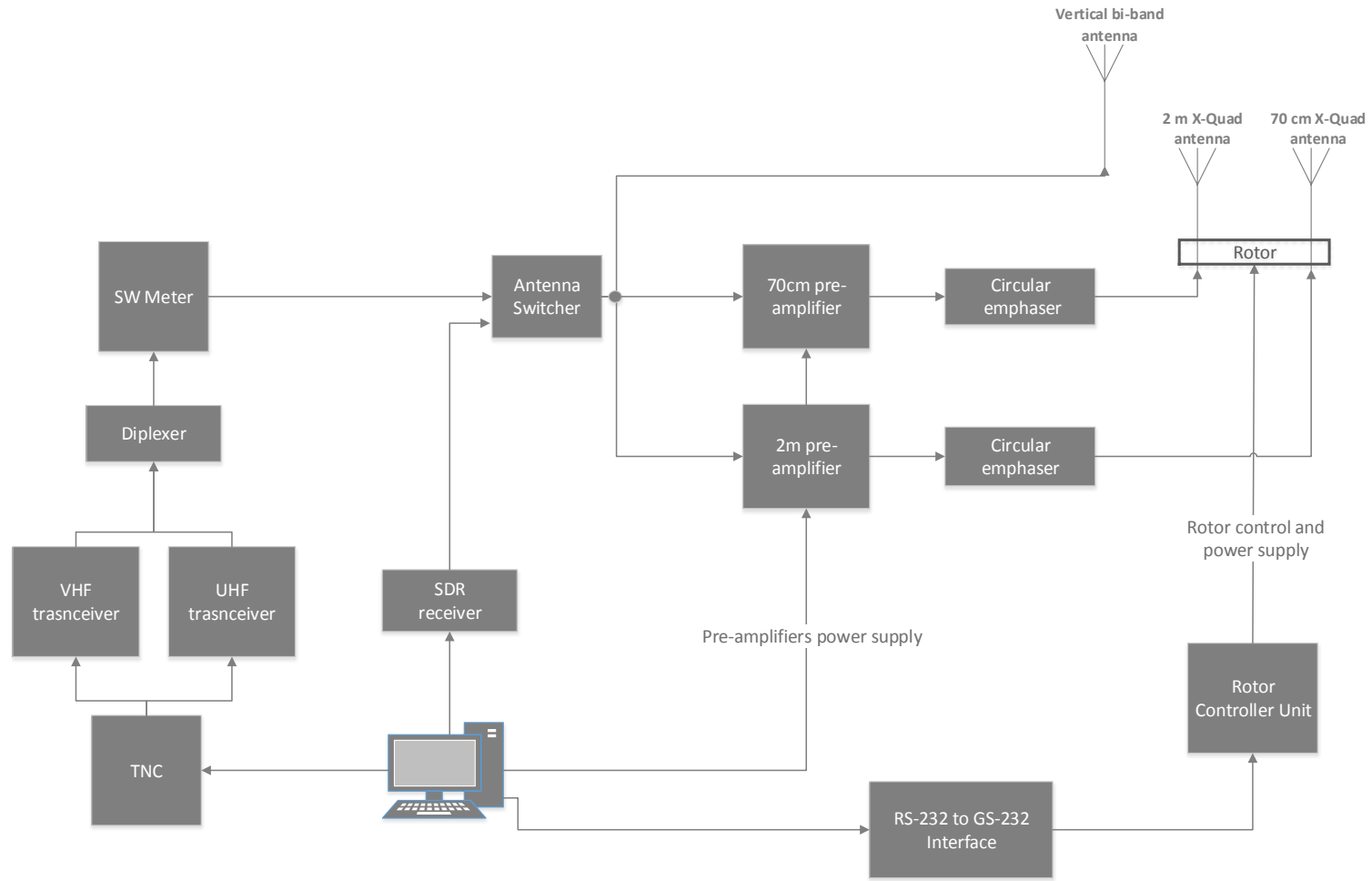


Figure 4.1 – *Diagram of hardware devices and their connections*

4.1 Antennas

4.1.1 Wimo X-Quad directional antennas

The main **VHF** and **UHF** antennas are two Wimo **X-Quad**. They are 2 m (**VHF**) and 70 cm (**UHF**) highly directional antennas, whose main characteristics are summarized in table 4.1. The radiation pattern is also provided in the technical documentation and can be seen in table 4.2.

	2m X-Quad	70cm X-Quad	
Elements per plane	12	18	
Gain	10.5	12.8	dBd
3dB bandwidth horiz. (E)	47	36	degrees
3dB bandwidth vert. (H)	47	36	degrees
F/B ratio	19	21	dB
Max. power	1500	1000	Watt
Length	1460	1270	mm
Height	730	220	mm
Weight	2.3	1.6	kg
Wind load @ 160km/h (100mph)	74	48	N
Connector	2xN-jack	2xN-jack	
Stacking distance	2.82	1.1	m
Phasing harness for RHCP or LHCP	18047	18049	
Part no.	18010	18011	

Table 4.1 – *Wimo X-Quad technical specifications [23]*

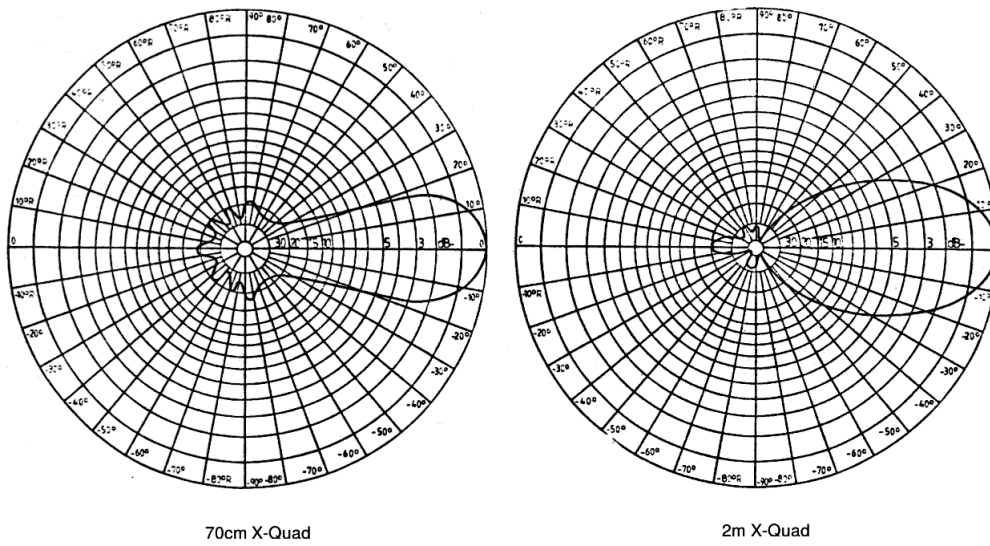


Figure 4.2 – *X-Quad radiation patterns [23]*

Each **X-Quad** consists in two antennas, both linearly polarized and $\pi/2$ out of phase between them thanks to the circular polarization emphaser. This configuration allows the transmission and reception of circularly polarized waves, as described in section 2.2.3. The desired sense of polarization is chosen in accordance with the connection to the two N-type inputs that they have. Figure 4.3 shows of both antennas mounted on the boom.



Figure 4.3 – *X-Quad antennas mounted on the rotor*

4.1.2 Diamond X-200N Antenna

The Diamond X-200N is a vertical antenna with coverage on both 2 m and 70 cm bands. Although it is not specified in the technical documentation, the geometry of the antenna suggest an omnidirectional radiation pattern. That means that, in a given plane, they radiate with the same power in all directions and hence their performance for space communications is lower than the [X-Quad](#) antennas. However, the main advantages over the latter is that it does not need to be mounted on a rotor to aim the main lobe to the satellite –being thus more immune to mechanical failure–, and both frequency bands are available simultaneously in the same antenna. These characteristics make the Diamond X-200N suitable as a backup antenna. Its technical specifications are given in [table 4.2](#).

Frequency	430–440 144–146	MHz
Gain 2m	6.0	dB
Gain 70cm	8.0	dB
Max. power rating	200	W
Max. wind resistance	50	m/sec
Impedance	50	Ω
V.SWR	less than 1.5:1	
Mast diameter accepted	30 – 62	mm
Length	2.5	m
Weight	1.2	kg
Connector	N	
Type	5/8 wave two element (2 m) 5/8 wave four element (70 cm)	

Table 4.2 – *Diamond X-200N technical specifications [22]*

The interior of the antenna out of the outer shell can be seen in figure 4.4.



Figure 4.4 – *Diamond X-200N antenna*

4.1.3 70 cm / 2 m X-Quad circular pol. emphaser

In addition to the crossed linear polarization achieved by the antenna geometry itself, the $\pi/2$ phase shift necessary to obtain circular polarization is accomplished with two emphasers, one in each X-Quad antenna.

The phase shift is achieved with two transmission lines of $\lambda/4$ and $\lambda/2$, respectively, one connected to the horizontal antenna feeder and the other to the vertical antenna, as shown in figure 4.5. Right hand polarization is obtained when the longer line is connected to the horizontal feeder and left hand if it is connected to the vertical feeder.



Figure 4.5 – 2 m X-Quad circular pol. emphaser

4.1.4 Pre-amplifiers

In order to strengthen the signal received by the X-Quad antennas, two mast pre-amplifiers are used, the *SHF-Elektronik Mini 2* for the 2 m antenna and the *MVV 432/2* for the 70 cm antenna.

In the technical specifications in table 4.3 it is indicated that two 70 cm antennas can be connected to the *MVV 432/2* simultaneously, although only one can be amplified at a time controlled by the power supply. Since at the moment of the installation there was only one antenna for this band, this connection was left unused but prepared, in case it is required in the future. A picture of the Mini 2 pre-amplifier can be seen in figure 4.6.

	Mini 2	MVV 432/2	
Frequency	144–146	430–440	MHz
Noise factor	0.7–1.0	0.8–1.2	dB
Amplification	10–20	approx. 22, max. 26	dB
Transmission power allowed HF-VOX	75 FM / 150 SSB	350 SSB / 200 FM	W
Transmission power allowed PTT	75 FM / 150 SSB	750 SSB / 250 FM	W
Reception-Transmission shift	HF-BOX or PTT controlled	HF-BOX or PTT controlled	
Power supply	13.5 V, 50 mA approx.	13.5 V, 200 mA approx.	
Supply	Remote over coaxial cable or separate line	Remote over coaxial cable or separate line	
Insertion loss	< 0.2	< 0.5	dB
HF connection	N	N	
Others		Connectors for two antennas available	

Table 4.3 – *Pre-amplifiers technical specifications [11] [12]*



Figure 4.6 – *Mini 2 preamplifier*

4.1.5 Diamond MX-72D Diplexer

The possibility of simultaneously using the Diamond X-200N vertical antenna in VHF and UHF amateur bands is given by the Diamond MX-72D Diplexer. A diagram of its integration in the system is shown in figure 4.7 and technical specifications are given in table 4.4.

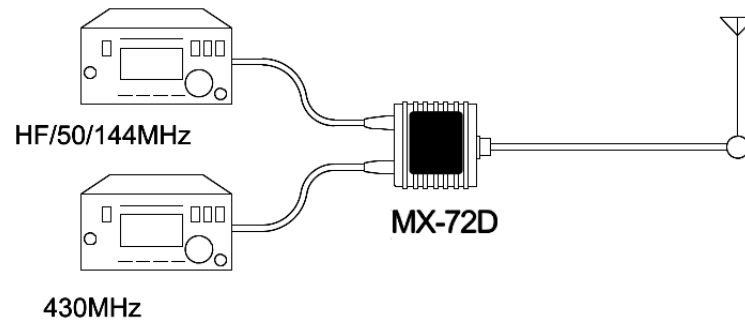


Figure 4.7 – Diagram of a diplexer operation [13]

Low pass band frequency	1.6–30 MHz	
	49–150 MHz	
High pass band frequency	400–460 MHz	
Power	1.6–30 MHz	400 W (CW) / 1 KW (PEP)
	49–150 MHz	150 W (CW) / 400 W (PEP)
	400–460 MHz	100 W (CW) / 250 W (PEP)
Insertion Loss	1.6–30 MHz	Less than 0.15
	49–150 MHz	
	400–460 MHz	Less than 0.2
Impedance	50 Ω	
V.SWR	less than 1.2	
Isolation	More than 60 dB	
Connector	MIX	SO-239
	144 & 430 MHz	PL-259
Dimensions	46 x 27 x 57 mm	
Weight	180 g	

Table 4.4 – Diamond MX-72D Diplexer technical specifications [13]

4.2 Rotor

The Yaesu G-5500 rotor provides the X-Quad antennas with the capacity to aim towards a desired direction (i.e. a satellite moving in the sky in its orbit). A controller unit is supplied with the rotor, which allows the manual operation with its switches or automatic operation with a PC via an external control interface, as shown in figure 4.9. The external control interface is described in section 4.2.1. Figure 4.8 shows the front view of the rotor controller unit and its internal circuitry.

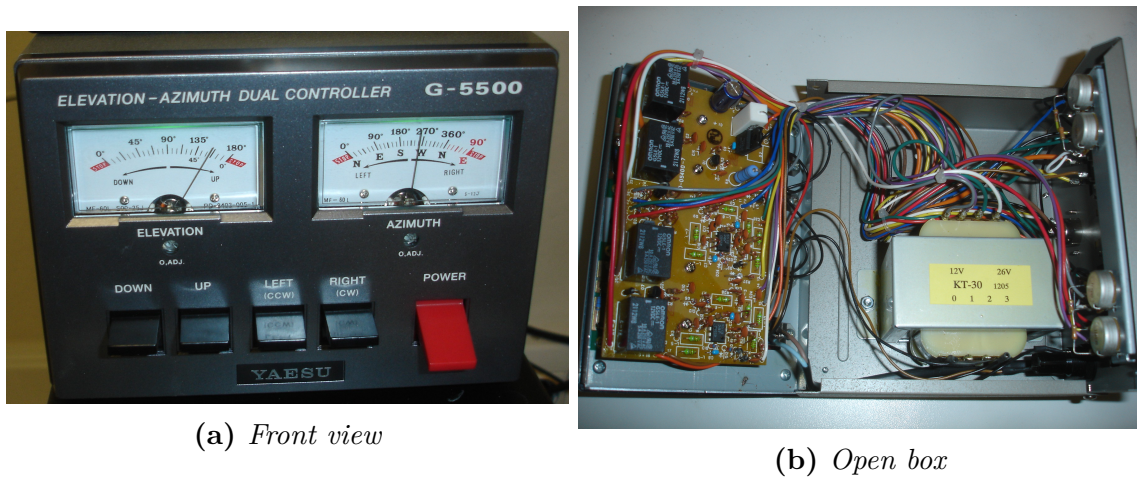


Figure 4.8 – Yaesu G-5500 rotor controller unit

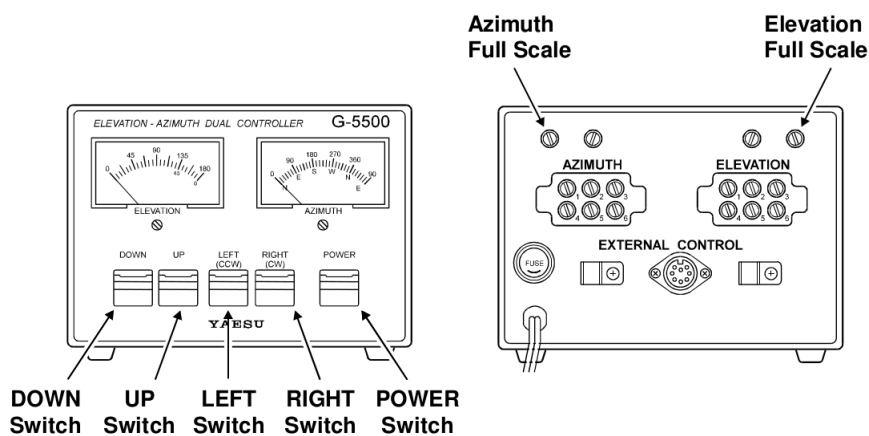


Figure 4.9 – Rotor controller unit buttons and functions [24]

Although 360° in the azimuth and 90° in the elevation axis would be sufficient to reach all the positions above the horizon, the rotor provides 450° and 180° , respectively, suppressing

therefore the necessity to perform a whole turn in the case that the tracking of a satellite requires going through one of these limits. Technical data of the Yaesu G-5500 rotor is given in table 4.5.

Voltage requirement	110–120 or 200-240 VAC
Motor voltage	24 VAC
Rotation time (approx., @60Hz)	Elevation (180°): 67 sec. Azimuth (360°): 58 sec.
Maximum continuous operation	5 minutes
Rotation torque	Elevation: 14 kg-m Azimuth: 6 kg-m
Braking torque	Elevation: 40 kg-m Azimuth: 60 kg-m
Vertical load	200 kg
Pointing accuracy	±4 percent
Wind surface area	1 m ²
Control cables	2x6 conductors
Mast diameter	38–63 mm
Boom diameter	32–43 mm
Weight	Rotors: 9 kg Controller: 3 kg

Table 4.5 – *Yaesu G-5500 technical specifications [24]*



Figure 4.10 – Rotor mounted on the mast

4

4.2.1 Rotor External Control

Apart from using them to perform tests, moving the rotor from its manual switches is in general not very useful. The usual operation is made from a PC running a satellite tracking software, which using its *Keplerian Elements*, can determine its position in real time and the azimuth and elevation angles from the ground station position.

The external control is based on the level of a DC signal on the external control port of the controller unit. Since this type of signal is not compatible with a common digital PC port (i.e. USB, RS-232, etc.), a direct connection between them is not possible, but an interface attached to this connector of the controller provides RS-232 connectivity.

The GS-232A Computer Control Interface, supplied by Yaesu as well, is the most straightforward device to operate the rotator from a PC. However, a lower cost and open source design has been chosen for the [GranaSAT-I](http://www.granasat-i.com/) project: [Las Vegas Boulevard tracker \(LVB\)](http://www.g6lvb.com/articles/lvbtracker/) (<http://www.g6lvb.com/articles/lvbtracker/>), designed by Howard Long G6LVB, and originally presented at the 2003 AMSAT-UK Colloquium [42].

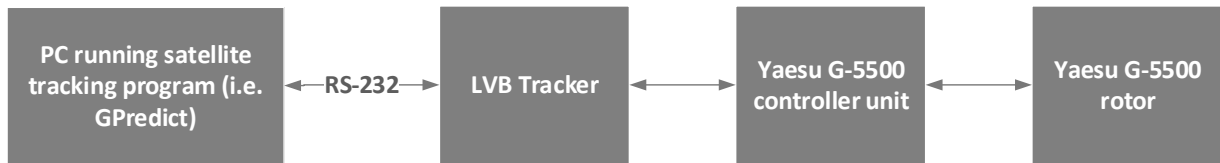


Figure 4.11 – LVB connection diagram [42]

The LVB is attached to the external control port of the rotator controller as described in figure 4.12 and table 4.6.

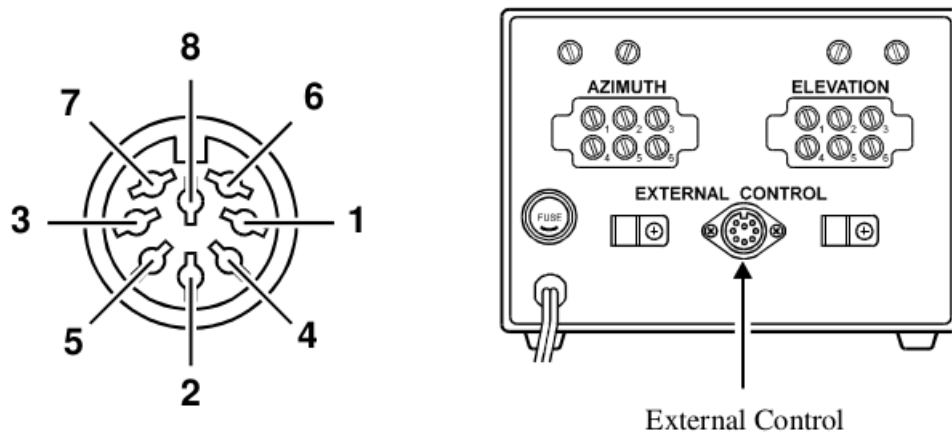


Figure 4.12 – Back view of the rotor controller unit [24]

Pin	Function
1	Provides 2 to 4.5 VDC corresponding to 0 to 180°
2	Connect to Pin 8 to rotate right (clockwise)
3	Connect to Pin 8 to rotate DOWN
4	Connect to Pin 8 to rotate left (counterclockwise)
5	Connect to Pin 8 to rotate UP
6	Provides 2 to 4.5 VDC corresponding to 0 to 450°
7	Provides DC 13 V to 6 V at up to 200 mA
8	Common ground

Table 4.6 – LVB external port pins [24]

4.3 Transceivers

4.3.1 Keenwood TM-241 and TM-441

The Keenwood TM-241 and TM-441 transceivers allow the reception and transmission of analog voice. Their technical specifications are given in tables 4.7, 4.8 and 4.9. Together with a TNC, described in section 4.4, the radio transceivers can also be used to send and receive digital data.

A photo of the Keenwood TM-241 and TM-441 transceivers used in the ground segment of GranaSAT-I can be seen in figure 4.13.



Figure 4.13 – Keenwood TM-241 and TM-441 transceivers

General	TM-241	TM-441	
Frequency range	144–148	430–440	MHz
Mode	F3E (FM)		
Antenna impedance	50		Ω
Operating temperature	-20 to 60		$^{\circ}\text{C}$
Power requirements	DC13.8 \pm 15%		V
Ground	Negative		
Current drain in transmit mode	Less than 11	Less than 10	A
Current drain in receiver mode	<0.6		A
Frequency stability	Less than \pm 10		ppm
Dimensions (W x H x D)	140 x 40 x 160		mm
Weight	1.2		kg

Table 4.7 – Keenwood TM-241 and TM-441 general technical specifications [17] [18]

Transmitter	TM-241	TM-441	
Output power HI	50	35	W
Output power MID	Approx. 10		W
Output power LOW	Approx. 5		W
Modulation	Reactance modulation		
Spurious radiation	Less than -60		dB
Maximum frequency deviation	\pm 15		kHz
Audio distortion	Less than 3% (300 to 3000 Hz)		
Microphone impedance	600		Ω

Table 4.8 – Keenwood TM-241 and TM-441 transmitter technical specifications [17] [18]

Receiver	TM-241	TM-441	
Circuitry	Double conversion superheterodyne		
Intermediate frequency (1st/2nd)	30.825MHz / 455kHz		
Sensitivity (12dB SINAD)	< 0.22	< 0.177	μV
Selectivity	-6dB: > 12 kHz ; -60dB: < 24 kHz		
Squelch sensitivity	< 0.1	< 0.177	μV
Output (0.5% distortion)	More than 2W across 8 Ω loads		
Audio distortion	Less than 3% (300 to 3000 Hz)		
External speaker impedance	8		Ω

Table 4.9 – Keenwood TM-241 and TM-441 receiver technical specifications [17] [18]

4.4 TNC

Terminal Node Controller (TNC) is a digital transmissions controller which allows the connection of a PC to an amateur **AX.25** packet network, making use of the **AX.25** packet protocol. It acts as an interface between the computer and the transceiver, converting data into **AX.25** packets and afterwards into audio tones [27].

A diagram of the the main components of a **TNC** can be seen in figure 4.14.

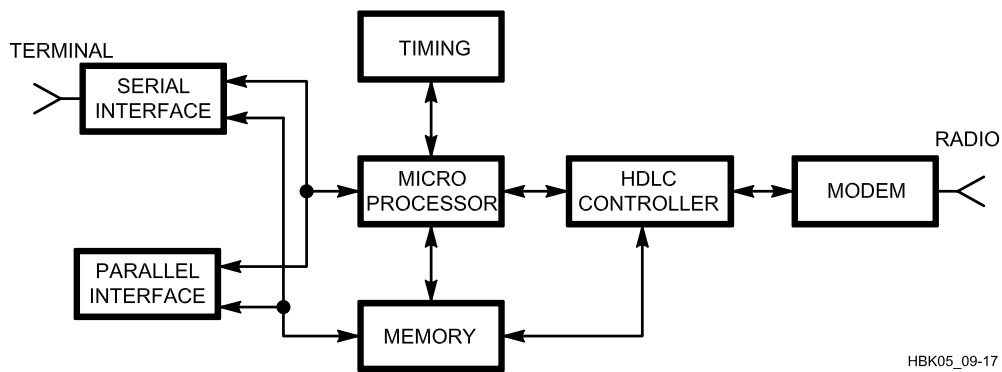


Figure 4.14 – *Functional block diagram of a typical TNC [27]*

A photo of the **TNC** used in the ground segment is shown in figure 4.15.



Figure 4.15 – TNC-URE

4.5 Antenna switcher

An antenna switcher is employed to operate in different frequency bands avoiding the need of manually changing the signal cable to the rest of the equipment. There are different models in the market which allow automatic switching. However, a manual switcher like the employed **MFJ-1704** is also adequate for small control rooms.

The switcher can be set to five different positions. In the centre one, all connectors are disconnected and grounded. The remaining four are assigned to one antenna each. Therefore, there is one connector which will remain unused but it will give the possibility to connect another antenna if a ground station expansion is considered in the future.

The MFJ-1704 switcher is shown in figure 4.16 and its technical details are given in table 4.10. In addition, another important characteristic is its replaceable lightning/surge protection pellet. Should a lightning strike occur, it will short to ground protecting the equipment. The active connector is hence automatically protected with the replaceable lightning/surge protector [10].

Power rating	2.5 KW PEP	
Impedance	50 Ω	
Connectors	SO-239 (PL)	
VSWR	30 MHz	< 1.1 : 1
	150 MHz	< 1.3 : 1
	450 MHz	< 1.4 : 1
	500 MHz	< 1.4 : 1

Table 4.10 – *MFJ-1704 antenna switcher technical specifications [10]*

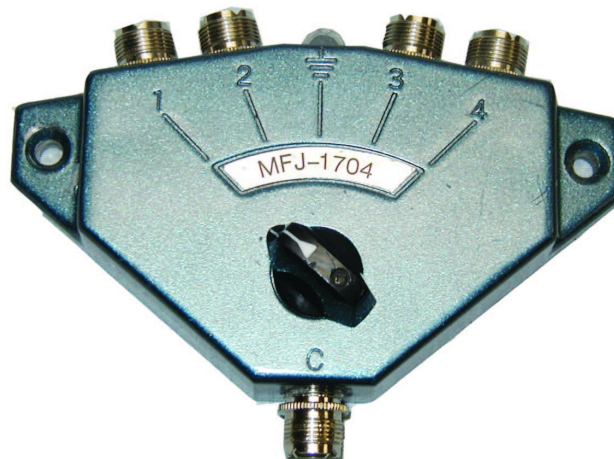


Figure 4.16 – *MFJ-1704 Antenna switcher [10]*

4.6 Diamond SX600 Dual-Band SWR/Power meter

The SX600 is an insertion type SWR/Power meter being connected between a transmitter and an antenna. This allows the easy detection of problems with the antennas or the HF network. Both bands of interest for this project can be simultaneously connected, avoiding the necessity of manually changing the cables. Technical details of the SX600 SWR/Power meter are given in table 4.10 and a photo of the device is shown in figure 6.17.

	S1	S2
Frequency range	1.8–160 MHz	140–525 MHz
Power measurement range	0 – 200 W (intermitent measurements)	
Power range	5 W / 20 W / 200 W	
Accuracy of full scale	±10%	
Minimum power at swr meter	1 W	4 W
Measurement range at swr measurement	1.0–∞	
Insertion loss	0.2 dB max.	0.3 dB max.
Impedance	50 Ω	
Connectors	SO-239 (PL)	
Dimintions	155 x 63 x 103 mm (W x H x D)	
Weight	630 g	
Acesories	Operation instructions DC power cable	

Table 4.11 – *SX600 Dual-Band SWR/Power meter technical specefications [16]*



Figure 4.17 – *SX600 Dual-Band SWR/Power Meter [16]*

4.7 USB receivers

A very interesting alternative to the Keenwood transceivers are the USB receivers. They sample the signal from the antennas and transfer it to the computer via its USB port. The PC is responsible for the rest of the tasks in the reception –demodulation, filtering, etc– as well of additional functions that can be applied to the signal, such as the Fourier Transform or digital data decoding. This is known as **Software Defined Radio (SDR)** and will be discussed in detail in section 4.8. Two different models were acquired for the GranaSAT-I ground station, the *FUNcube Dongle Pro+* and the usually known as *RTL-SDR*.

A more detailed discussion about *Software Defined Radio* as well as [SDR](#) receivers is made in chapter 5.

4.8 Software

The ground station equipment is completed with a PC running a series of useful programs. Linux Mint and Microsoft Windows 7 operating systems were simultaneously installed in order to provide two of the most common platforms on which programs are executed.

4.8.1 Satellite tracking software

A satellite tracking software is a crucial element in the ground station. Using its Keplerian Elements, it determines in real time the position of a satellite, predicts where it will be in the future and calculates its coverage circle. These features are common in most of them and, additionally, many also determine the elevation and azimuth angles from the ground station location and can control the rotor to aim it to the appropriate direction. Another very useful function that tracking software usually includes is the calculation of the [Doppler shift](#) and automatic adjustment of the frequency of the transceivers if they allow this characteristic.

There exist many tracking programs that are suitable for the [GranaSAT-I](#) project. Although a few of them are commercial software, there is also a considerable amount of quality open source and freeware programs very extended among radio amateurs and CubeSats projects, for instance WXTrack, Orbitron or WinOrbit.

The chosen tracking program was **GPredict**, which, besides including all the functions described earlier in this section, it was found to fit perfectly the [GranaSAT-I](#) ground station for the following reasons:

- It is a **multi-platform** program (for Linux, Mac OS X and Windows) and can therefore be used independently of the operating system required by other programs.
- It is licensed under the GNU General Public License (**open source**), hence giving the freedom to modify it to suit any possible need that might arise.
- It is **free of charge** and consequently meets the ground station low budget requirement.
- It supports the control of the Yaesu G-5500 rotor, allowing the real time tracking of satellites.
- It supports the control a big variety of transceivers.

The [Doppler shift](#) correction and the rotor control commands are sent via TCP protocol to the preferred host and port. In many cases, the local loop is used and the [hamlib](#) library acts as interface to communicate with other devices or programs.

An screenshot of the main screen of GPredict is shown in figure 4.18.

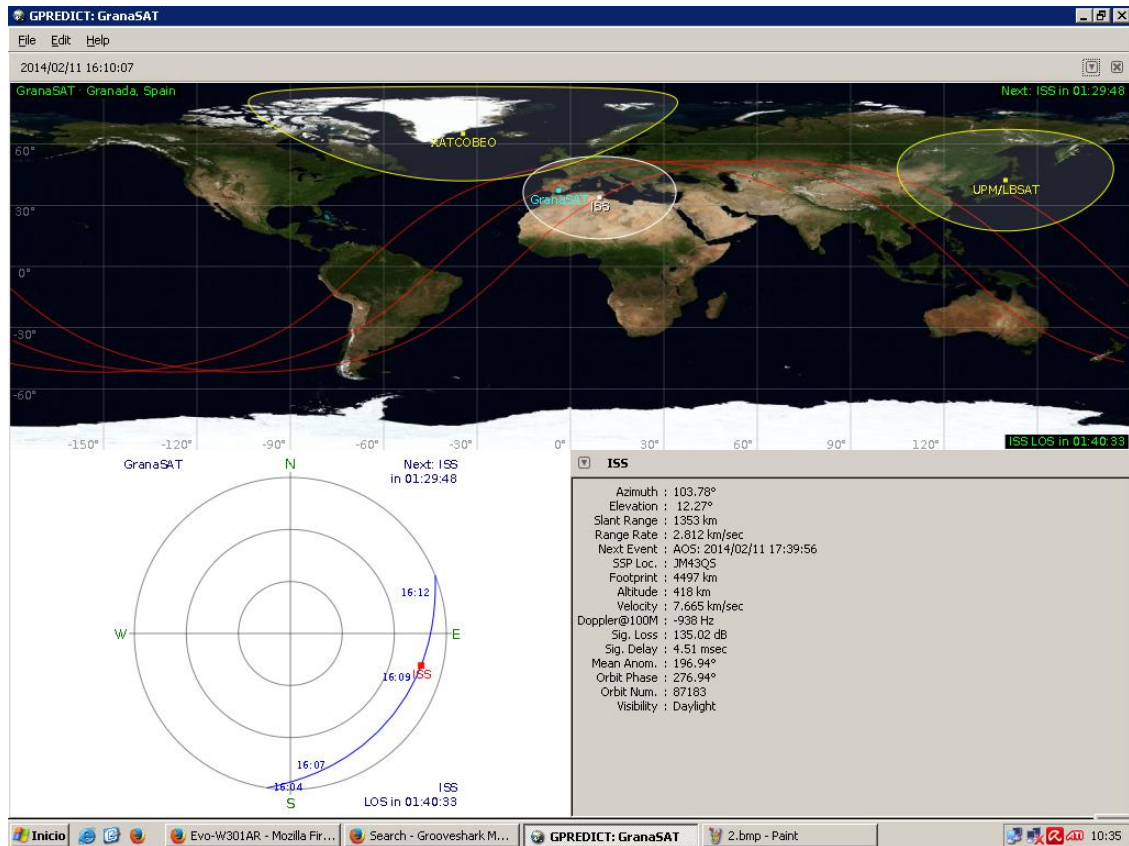


Figure 4.18 – Screenshot of the main screen of GPredict tracking program

4.8.2 SDR programs

4.8.3 Multi-functionality programs

Two of the most interesting programs to operate with sampled signals are **SDR#** and **GNURadio**, both open source and free of charge.

SDR# is a very extended open source program for Windows among radio amateurs, which offers a user-friendly graphical interface with many functions and most necessary options for satellite signal reception. One of its main features is the display real-time Fourier Transform, although a variety of functions are available by default or after installing pluggins, for instance analog demodulation or **Doppler shift** correction. An screenshot of **SDR#** is shown in figure 4.19.

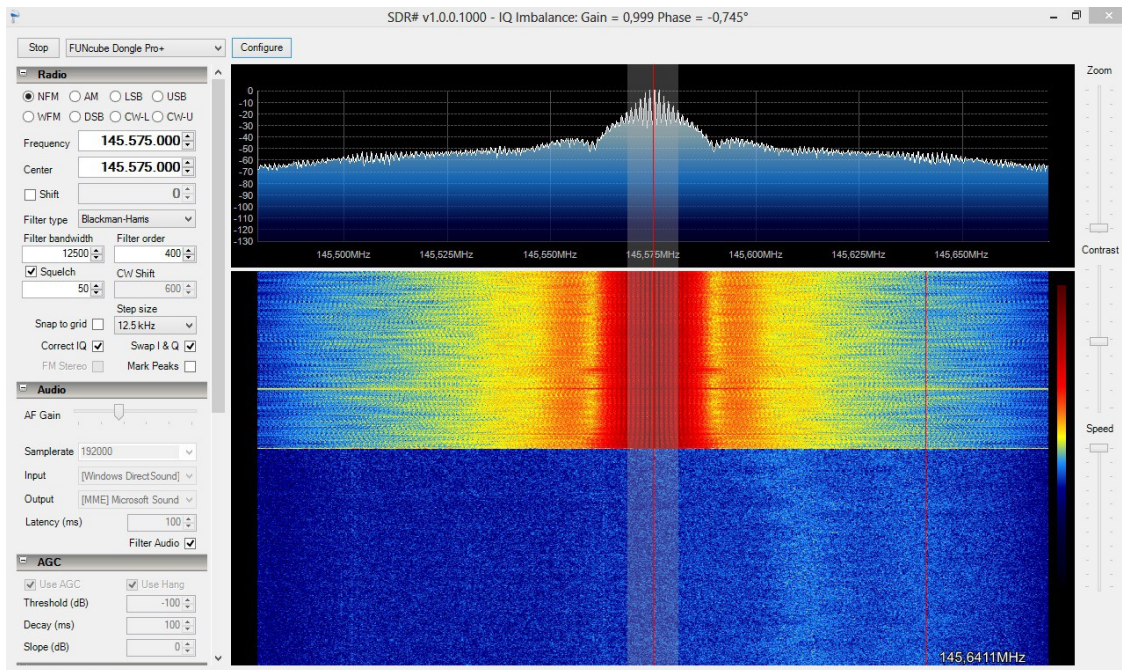


Figure 4.19 – Screenshot of the main screen of SDR#

GNURadio is an open source development toolkit for Linux that allows users to build their own software radio using blocks or programmatically. It includes a big variety of signal processing functions, so users can create a communications system that fits perfectly their needs. A higher versatility can be accounted as the immediate advantage with respect to SDR#. On the other hand, the big time investment it requires for its configuration and the poor documentation available were found to be its main drawbacks. An screenshot of GNURadio is shown in figure 4.20.

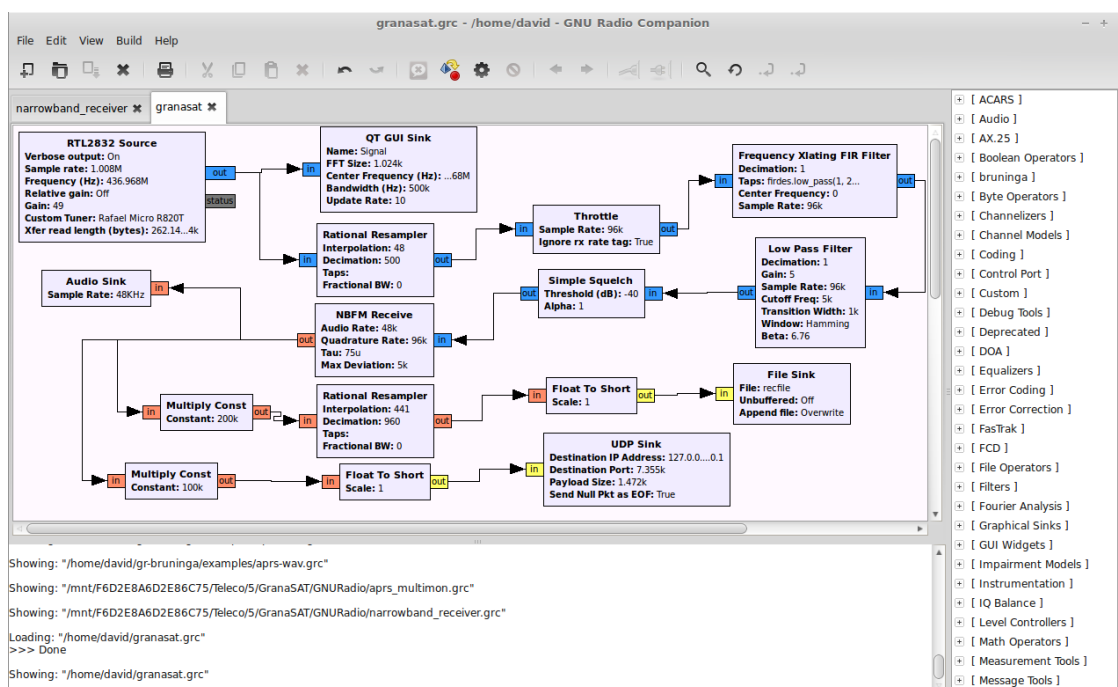


Figure 4.20 – Screenshot of the main screen of GNURadio

4.8.4 FUNcube Telemetry Dashboard

The FUNcube Dashboard is a tool developed by the [FUNcube-1](#) team which, upon the reception of signal from this satellite, decodes the [telemetry](#) data and displays it. This program is not very relevant for the project because it does not have further functionality, but it was useful for the first tests, as it automatically compensates the [Doppler shift](#) and does not require almost any configuration.

Additionally, according to its developers, it is planned to release the code so it could be useful in the future when the [telemetry](#) acquisition system is designed.

A screenshot of the FUNcube Telemetry Dashboard can be seen in figure [7.1](#)

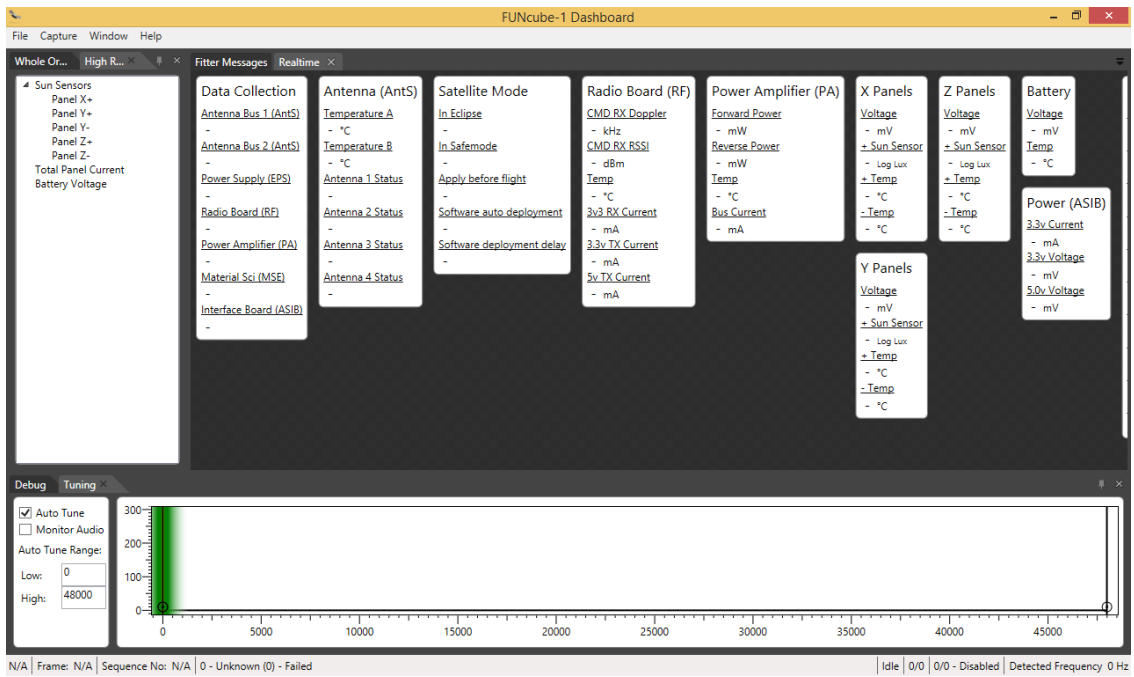


Figure 4.21 – Screenshot of FUNcube Telemetry Dashboard

CHAPTER

5

SOFTWARE DEFINED RADIO

Software Defined Radio (SDR) is a radio transmitter and/or receiver whose **RF** parameters, including frequency range, modulation type or output power are controlled by software [48]. Although this might include a wide spectrum of systems, most usually **SDR** refers to systems in which hardware is limited to an **RF** interface and an ADC (analog-to-digital converter). In this way, the next stages work with digital samples in contrast to traditional radios, which perform most of the signal processing in the hardware domain.

Usual **SDR** systems are formed by powerful embedded computers or by FPGAs using an **RF** interface. However, general purpose PCs or even simpler computers like Raspberry Pi together with an **RF** interface can function as inexpensive **SDR** systems, too. There is thus a big variety of **SDR** systems with different capabilities. As common advantages over traditional non-programmable systems it can be listed:

- **Flexibility:** as a programmable system, an upgrade in an **SDR** based transceiver does not necessarily imply the substitution of hardware elements, but often the modification of the code. This can include for instance the support of a new communication protocol or standard.
- **Scalability:** since the hardware part is limited to the conversion of the signal between the analog and digital domains, the system can be easily designed to be modular and only incorporate the functions needed at a time. The growth of the system does not require therefore a whole replacement but the substitution or addition of new modules when they are required.

- **Extended functionality:** the concept of **SDR** implies the work with digital data instead of analogic. This offers the possibility to use digital samples directly for treatment of **payload** data –for instance image reception and processing– or **satellite bus** module monitoring and control –**telemetry** and **telecommand**–.
- **Educational value:** In addition to technical advantages, in an university context **SDR** can provide students with a comprehensive and attractive learning tool for electronics and communication concepts. To name a few examples: real time Fourier Transform can be used to visualize signals and do measurements upon them (bandwidth, noise and signal level, etc); analog/digital modulation of signals or channel coding can be put into practice writing software or using GUI tools.

Although depending on the system in particular different schemes may apply, a typical **RF** stage of an **SDR** system is shown in figure 5.1.

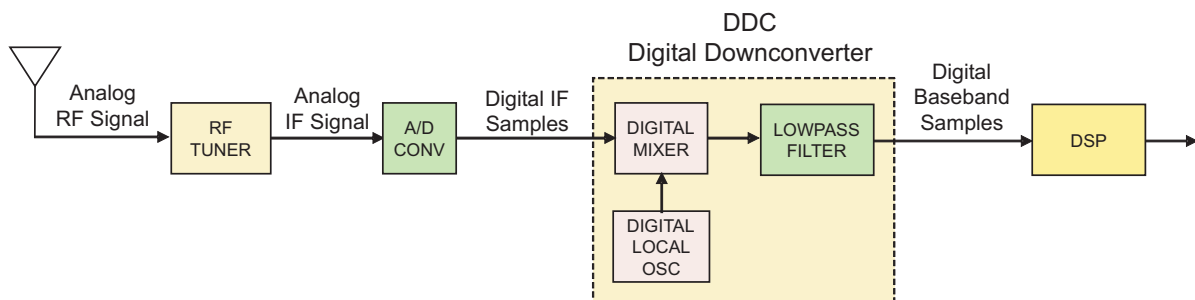


Figure 5.1 – Simple SDR receiver diagram [46]

In order to compare different **SDR** devices, a research of COTS (Commercial Off-The-Shell) hardware was carried out and is presented below. The following factors have been identified as determining for the election of the hardware components:

- **Frequency range:** The operating frequencies of the ground segment are in the 144MHz and 440MHz bands. This requirement is decisive and therefore devices which do not meet it were not included. A larger range was considered advantageous, specially covering the S-Band (2GHz – 4GHz), frequently used for space applications as well.
- **Transmit capability:** While every **SDR** device can work as receiver, not all of them are capable of transmitting. **Tx** capability allows sending **telecommands** instead of only receiving **telemetry** or **payload** data from the satellite.
- **Reception sensitivity and output power:** Given the large distances in satellite links, a big **Tx** power is necessary as well as a big sensitivity for **Rx**. For this reason power amplifiers are used in ground segments, but the interconnection between them

and the **SDR** device must be taken into account and in any case a lower sensitivity as well as a higher transmit power were considered as advantageous.

- **Sampling rate:** The first limit encountered by **Mathematical operations performed upon a certain digitalized signal (Digital Signal Processing)** techniques is the Nyquist-Shannon Sampling Theorem, which states that a signal can only be reconstructed from its discrete samples if the sampling rate is at least twice the frequency of this signal. Therefore, the sampling rate has for instance a direct effect on the bandwidth of the real time Fourier Transform, among other consequences.
- **Price:** For a reduced budget project this factor is determining. However a variety of devices with different capabilities and prices was considered in order to have a wider view of the market.
- **Frequency drift:** drifts in the frequency of the local oscillator are produced by factors like temperature or ageing, producing a drift in the tuned frequency. Therefore a low frequency drift is preferred.

Model	Frequency band [MHz]	Bandwidth [MHz]	Frequency stability [ppm]	Tx?	Noise Figure [dB]	Tx power [dBm]	Sample Rate (ADC/DAC) [MS/s]	Sample resolution (ADC/DAC) [bits]	Open hardware / software	Price
USRP1	0 – 6000		25	Yes. With extension ¹	5	15	64 / 128	12/14	Yes (SW)	€675.00
USRP B200	70 – 6000	56	2	Yes	<8	>10	61.44	12	Yes (SW)	€645.00
USRP B210	70 – 6000	56	2	Yes	<8	>10	61.44	12	Yes (SW)	€1050.00
USRP X300	0 – 6000	120	2.5	Yes. With extension ¹	8	>10	200 / 800	14/16	Yes (SW)	€3730.00
USRP X310	0 – 6000	120	2.5	Yes. With extension ¹	8	>10	200 / 800	14/16	Yes (SW)	€4590.00
USRP N200	0 – 6000		2.5	Yes. With extension ¹	5	15	100 / 400	14/16	Yes (SW)	€1450.00
USRP N210	0 – 6000		2.5	Yes. With extension ¹	5	15	100 / 400	14/16	Yes (SW)	€1640.00
USRP E310	70 – 6000	56	2	Yes	8	>10	61.44	12	Yes (SW)	€2580.00
USRP E100			2.5	Yes. With extension ¹	5	15	64 / 85	12/14	Yes (SW)	€1260.00
USRP E110			2.5	Yes. With extension ¹	5	15	64 / 85	12/14	Yes (SW)	€1450.00
UmTRX	300 – 3800	26		Yes		17 – 20			Yes (SW/HW)	\$1450.00
FUNCube Dongle	0.150–240 420–1900		1.5	No	3.5		0.192	16		£124.99
HackRF	10 – 6000			Yes		5 – 15	20	16	Yes (SW/HW)	€344.00
bladeRF x40	300 – 3800		0.040	Yes			40	12	Yes (SW)	\$420.00
bladeRF x115	300 – 3800		0.040	Yes			40	12	Yes (SW)	\$650.00
RTL2832U + R820T (DVB-RTL)	24 – 1766			No	3.5		2.4	8	No	\$12.00
PicoSDR	300 – 3800	28	2	Yes		5 – 10			No	
ZeptoSDR	300 – 3800	28		Yes		5 – 10			No	

¹RF stage both for Rx and Tx is not included. An extra extra daughterboard is needed.

Table 5.1 – SDR Sampling hardware

Though a more versatile and **Tx**-capable device like the widely extended USRP would have been very interesting for the ground segment, due to budget restrictions only the **FUNcube Dongle Pro+** and a Digital Video Broadcasting receiver based on the Realtek RTL2832U chip (usually referred to as DVB-RTL or **RTL-SDR**) could be incorporated into the equipment. These **Rx**-only devices work as **RF** interface sending samples in form of I/Q (In-Phase/Quadrature) components to a PC via a USB port, being the rest of the stages in the reception –filtering, demodulation, etc.– based on **Digital Signal Processing** techniques. In FPGA based approaches, hardware reconfiguration capabilities can be used to perform all or some of this tasks efficiently and only use a computer for storing or displaying purposes, for instance.

Among the big variety of software applications that can be categorized as **SDR**, the most relevant for this project are the receivers performing real-time Fourier Transform. They display the Fourier Transform of a certain range of the frequency spectrum, allowing a fast and easy location of a signal. This offers an intuitive possibility of identifying several relevant parameters in a certain band of the frequency spectrum, for instance signal and noise level or bandwidth of the signal.

In addition, another important function of traditional hardware systems in ground segments is sending and receiving digital packets. The standard communication protocol used in micro satellite projects is **AX.25** and the capability to code and decode messages in this protocol is also possible using **SDR**, as a substitute for a **TNC**.

5.1 FUNcube Dongle Pro+

The **FUNcube Dongle Pro+** is the second generation of an USB receiver developed in the context of the **FUNCube-1** satellite project, capable of tuning a broad frequency range, including the **VHF** and **UHF** amateur bands. Its technical characteristics are given in table 5.2 and a photo of the device can be seen in figure 5.2.

Frequency range	150 kHz–240 MHz and 420 MHz–1.9 GHz
Sensitivity	Typically 12 dB SINAD NBFM for 0.15 μ V at 145 MHz
Reference oscillator	1.5 ppm 26 MHz
Sampling rate	192 kHz
Bit depth	16 bits (32 bits used internally)
PC interface	USB 1.x Make A Full Speed (12 Mbps)
RF interface	Standard SMA female (not reverse Polarity [RP])

Table 5.2 – *FUNCube Dongle Pro+ technical specifications [34]*



Figure 5.2 – *FUNCube Dongle Pro+ [34]*

5.2 Realtek RTL2832U based DVB-T receivers

Realtek RTL2832U based digital video broadcasting – terrestrial receivers (**RTL-SDR**) are a very low price dongles, commercially sold as DVB-T TV tuner. Thanks to the inverse engineering work of Antti Palosaari, Eric Fry and Osmocom it was found that the signal in-phase and quadrature (I/Q) data could be accessed directly, which allowed the DVB-T TV tuner to be converted into an wideband **SDR** receiver [58].

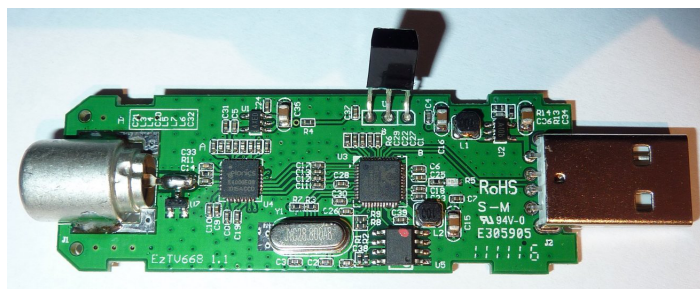
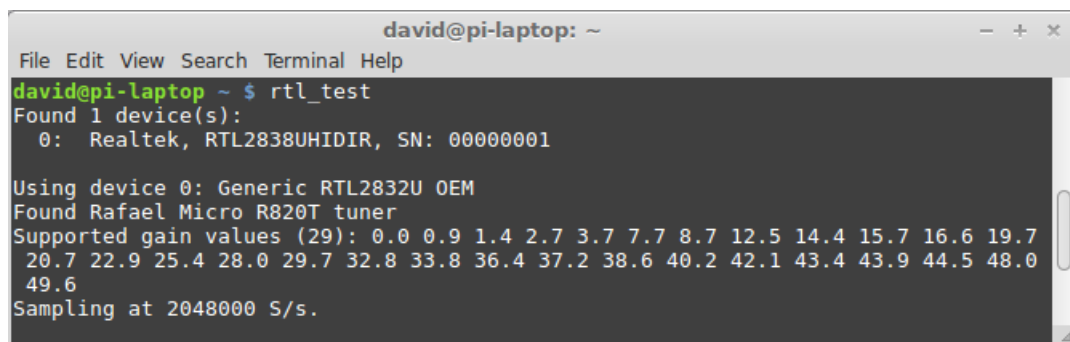


Figure 5.3 – *RTL2832U based devices: EzTV 668 [58]*

Although no technical specifications are provided by the vendor, probably because it is not intended to be used as an **SDR** receiver, it is possible to obtain a few characteristics

thanks to the Osmocom [RTL-SDR](#) library for GNU-Linux [14].



```
david@pi-laptop: ~
File Edit View Search Terminal Help
david@pi-laptop ~ $ rtl_test
Found 1 device(s):
 0: Realtek, RTL2838UHIDIR, SN: 00000001

Using device 0: Generic RTL2832U OEM
Found Rafael Micro R820T tuner
Supported gain values (29): 0.0 0.9 1.4 2.7 3.7 7.7 8.7 12.5 14.4 15.7 16.6 19.7
20.7 22.9 25.4 28.0 29.7 32.8 33.8 36.4 37.2 38.6 40.2 42.1 43.4 43.9 44.5 48.0
49.6
Sampling at 2048000 S/s.
```

Figure 5.4 – *Rtl-test command output*

According to the information provided by the Osmocom project as well, the RTL2832U outputs 8-bit I/Q-samples, and the frequency range for a *Rafael Micro R820T* tuner is 24–1766 MHz, with adjustable sample rate up to a theoretic maximum of 3.2 MS/s, although samples are dropped at rates higher than 2.4 MS/s. The adjustable gain is also displayed in figure 5.4 and goes from 0 to 49.6 dB.

Despite its smaller resolution of 8 versus 16 bits, the [RTL-SDR](#) receiver offers a better performance in comparison with the [FUNCube Dongle Pro+](#) due to its greater sample frequency, which implies a much bigger bandwidth. A brief comparison is shown in table 5.3.

	Frequency range	Sampling frequency	Host interface	Platform	Base price
FUNCube Dongle Pro+	0.15–240 MHz, 420–1.900 MHz	192 kHz	USB	Windows, Linux, Mac	\$200
Realtek RTL2832U DVB-T tuner	24–1.766 MHz (R820T tuner)	2.4 MHz	USB	Windows, Linux, Mac	\$8–10

Table 5.3 – *Comparison of FUNCube Dongle Pro+ and Realtek RTL2832U*

5.2.1 RTL-TCP

A further advantage of the RTL2832U receiver is possibility to use the library RTL-TCP in order to send the captured samples over a TCP connection to a remote host. This is done with the following command:


```
rtl_tcp.exe -a [destination host] -p [destination port]
```

SDR# allows to receive and plot the stream of samples in real time. The screenshots for this configuration are shown in figures 5.5 and 5.5.

```
C:\Windows\system32\cmd.exe - rtl_tcp.exe -a 192.168.2.102 -p 4839
Microsoft Windows [Version 6.1.7601]
Copyright (c) 2009 Microsoft Corporation. All rights reserved.

C:\Users\granasad>cd c:\Program Files\rtl-sdr-release\x32
c:\Program Files\rtl-sdr-release\x32>rtl_tcp.exe -a 192.168.2.102 -p 4839
Found 1 device(s):
  0: Realtek, RTL2838UHIDIR, SN: 00000001

Using device 0: Generic RTL2832U OEM
Found Rafael Micro R820T tuner
Tuned to 100000000 Hz.
Listening...
Use the device argument 'rtl_tcp=192.168.2.102:4839' in OsmoSDR (gr-osmosdr) source
to receive samples in GRC and control rtl_tcp parameters (frequency, gain, ...).
```

Figure 5.5 – Sample configuration of rtl-tcp

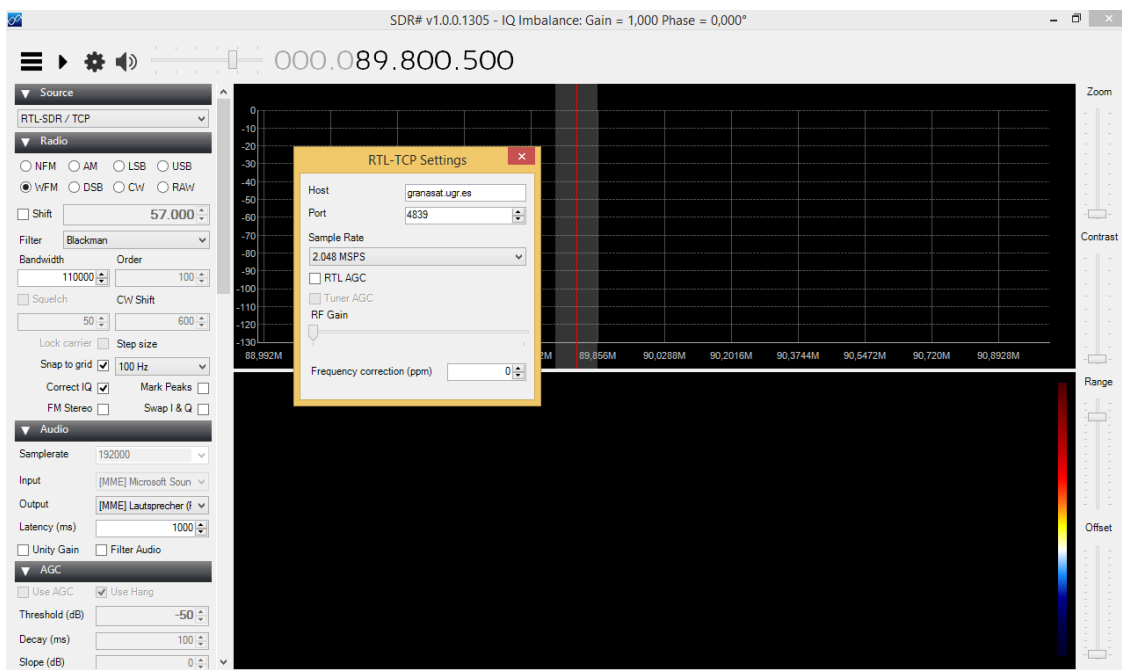


Figure 5.6 – Configuration of SDR# for rtl-tcp reception

CHAPTER

6

GROUND STATION DEPLOYMENT

Once the components of the ground station have been presented in detail, the interconnection of the equipment and deployment process will be described in this chapter.

6.1 Antennas deployment

The first elements to be placed were the signal and power supply cables from the control room, located in the basement of the Faculty of Science, to the rooftop of the building. The base of the mast supporting the [X-Quad](#) was also installed on top of the Faculty (coordinates: 37.179746,-3.609523). This work was carried out by the university technicians. Preliminary work on the project also includes the implementation of the RS-232 rotor interface [LVB](#) carried out by Telecommunications Engineering student Alejandro González. A photo of the base of the mast is shown in figure [6.1](#).

The antennas assembly was straightforward following the manufacturer's instructions. Due to its installation simplicity, in comparison with the others, the Diamond X-200N two-band vertical antenna (support antenna) was the first to be placed. Its mast was fixed with 5mm screws to a concrete air house on top of the Faculty, providing strong attachment. The Diamond X-200N after its installation is shown in figure [6.2](#).

To minimize the obstruction of direct vision with the satellite caused by buildings, trees or mountains, the two [X-Quad](#) antennas are mounted on a mast, which is a triangled galvanized steel structure composed by 3 m modules. A higher altitude of the mast has therefore a direct



Figure 6.1 – *Base of the mast*



Figure 6.2 – *Diamond X-200N two-band vertical antenna*

impact on the **total time view** of the satellite. But there are other factors to take into account as well, such as the mechanical force that a high mast has to support due to the wind, or the difficulty to maintain the connection when the satellite is close to the horizon. In this case, not only is the distance between the two end points of the communication very

big, but also the Earth atmosphere comprises the biggest part of this distance. This results in a significant signal attenuation, as discussed in chapters 2 and 3.

For the reasons mentioned above, it was determined that a satisfactory compromise would be to make use of two 3 m modules, providing the antennas with enough altitude as to avoid significant vision obstruction with the surrounding elements of the environment, while sacrificing a few degrees of elevation over the horizon where the quality of the connection would not be very satisfying either way. A photo of the mast laying on the rooftop before its uprising is shown in figure 6.3.



Figure 6.3 – Mast of the X-Quad antennas

The mast is fixed to its concrete base on the rooftop with three 5 mm steel screws and was reinforced with three 2 mm steel cords attached to solid points on the rooftop, as shown in figure 6.4.

As it was introduced in previous chapters, the X-Quad antennas must be mounted on a rotor which provides them with the mobility necessary to aim their highly directive main lobe to the satellite and track it in its trajectory. More precisely, the antennas are attached to a steel tube –referred to as *boom*–, which is introduced in the middle cavity of the rotor, as shown in figure 6.5. A special attention must be paid to the signal cables, which must have enough extension at the top as to cover the rotating movement of the antennas.

Connectors between RF signal cables and devices was one of the most time demanding tasks. N-type connectors must be soldered to the the inner conductor of the cable while the



Figure 6.4 – *Attachment of the cords to the floor*



Figure 6.5 – *X-Quad antennas mounted on the rotor*

outer conductor is directly in contact with the metallic cover of the connector. The final step is crimping the connector so that it is strongly attached to the cable. A photo demonstrating

the preparation of a coaxial cable is shown in figure 6.6.



Figure 6.6 – *N-Connector preparation*

In addition, self-amalgamating tape was employed in order to minimize the damage of the junctions that are exposed to rain and other bad weather conditions. The results on the feeders of the [UHF X-Quad](#) antenna can be seen in figure 6.7.



Figure 6.7 – *Self-amalgamating tape covering the two connectors of the 70 cm antenna*

The power supply for the pre-amplifiers and the rotor comes directly from the control room together with the RF cables. For the rotor, the connection is very straightforward, as it only requires to connect the two ends of each numbered cable to the corresponding screw in the rotor and in the rotor controller. For the case of the pre-amplifiers, one of them is powered by a DIN-type connector while the other needs a RCA one.

Both pre-amplifiers require the same voltage supply (13.5 V DC), hence a single cable for this purpose was stretched from the control room and a parallel connection was made directly between the connectors, as shown in figure 6.8. The other end of the cable in the control room was directly connected to the PC power supply unit providing 12 V DC. Although this is slightly less than the stated voltage requirement, it is enough to satisfy power demand of the amplifiers and it simplifies the operation of the ground station because the amplifiers will be automatically on when the PC on the control room is running.

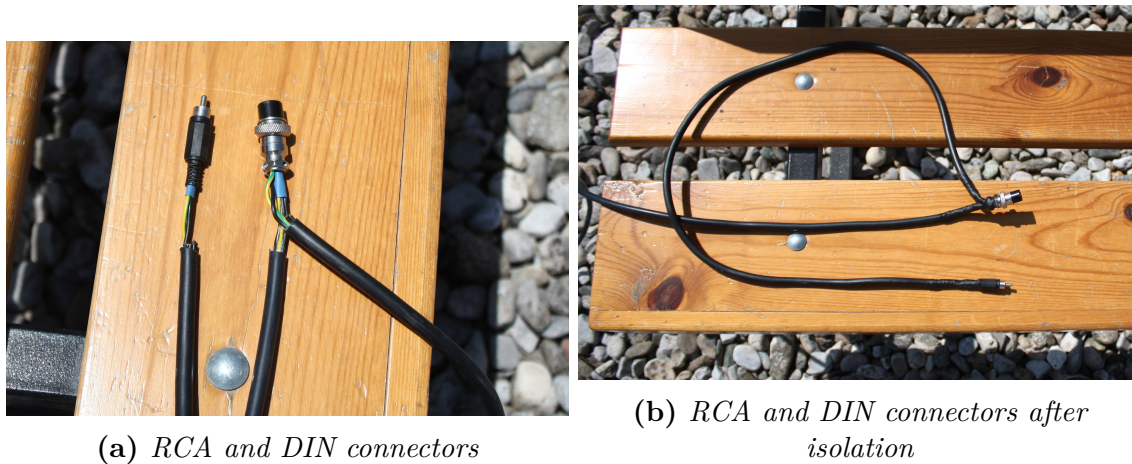


Figure 6.8 – *Parallel connection of the RCA and DIN connectors*

6

Once the rotor, the antennas and the pre-amplifiers have been placed, and all the connectors have been soldered, the signal and power supply cables can be connected. One of the signal cables originating in the control room is connected directly to the bi-band antenna. The remaining two are assigned to the 2 m band and the other to the 70 cm, respectively. The first is therefore attached to the 2 m pre-amplifier and from there to the circular polarizer of the 2 m antenna, as it can be seen in the diagram in figure 6.9. The polarizer is connected to the 2 m antenna as described in section 4.1. The process is analog for the 70 cm antenna.

The power for the rotor is supplied by six wires packed in a PVC hose. They originate in the control room as well and must be connected following the scheme in figure 6.10. The wires inside the hose are numbered and must be consistently connected to the control unit in the control room.

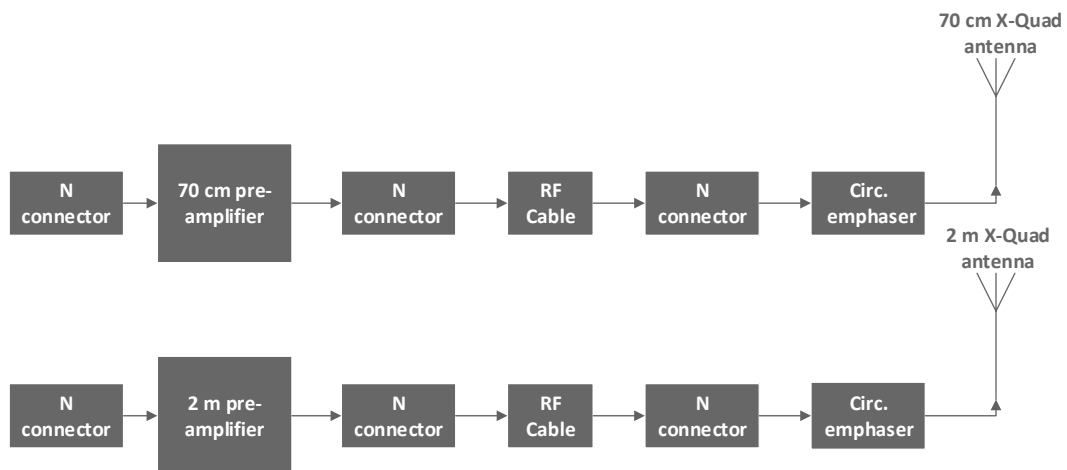


Figure 6.9 – Detailed diagram of X-Quad antennas interconnection

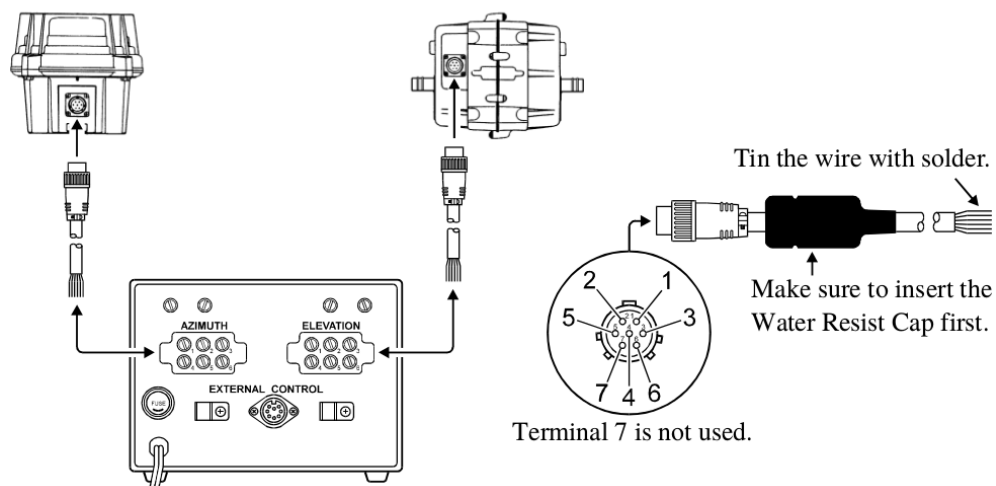


Figure 6.10 – Connection scheme of rotor supply [24]

The last task before setting the mast vertical was to calibrate the rotor. Calibration consists on setting the inferior limit of the azimuth axis to the North and superior limit to the South, as well as both the inferior and superior limit of the elevation axis parallel to a horizontal plane, in this case the rooftop of the faculty.

For the azimuth, a fine calibration would require complex instruments and hence a simple method based on a visual reference was considered more appropriate. A visible landmark in the North direction was searched for on a satellite view of the Faculty of Science. The *Virgen de las Nieves Hospital* was the most remarkable one found, as it lies exactly northwards the antennas and there is a considerable distance as to minimize the error when pointing. A satellite view of the site is shown on figure 6.11, where the maximum depointing angle used in section 3.4 is also displayed.

After pointing the antennas accordingly for the inferior limits, the rotor is set to its superior limits from the control unit. If the lecture in the control unit display does not agree with the real pointing direction, it can be adjusted using the calibration screws at the back of the control unit box.



Figure 6.11 – Satellite view of the Faculty of Science [7]

6

After executing all the tasks described above, the mast was set vertical. Six people were involved in this step in order to execute it safely. Two of them pushed directly the mast while the other four pulled a rope attached to the extreme of the mast closest to the antennas.



Figure 6.12 – Mast uprising

6.2 Control room deployment

6.2.1 Rotor control

The operation of the antennas on the rooftop is performed from the control room, which is provided with the necessary equipment to send and receive signal and to control the rotor of the [X-Quad](#) antennas.

The rotor power supply and bearing control is directly made by its controller unit. The power supply cable is connected to the back screws of the device attending to the same numbering as the one used for the rotor, as shown in [figure 6.13](#).

The controller unit allows manual operation of the rotor. However, [LEO](#) satellites typical contact time is from 8 to 12 minutes, which is translated in a fast angular rate. Hence, an automatic control of the rotor is required to perform a tracking of this kind of satellites. For this purpose, the [LVB](#) external control attached to the external control port of the rotor and to the RS-232 port of the PC is employed.

Once the [LVB](#) is attached, a warning message will appear on its LCD screen, as it can be seen in [figure 6.14](#). This indicates that a calibration must be performed before the correct elevation and azimuth values of the rotator are displayed. This can be performed directly with the front panel buttons or with a PC via RS-232 or USB connection, in case they have



Figure 6.13 – Back view of the rotor controller unit

been set up in the [LVB](#). Since the RS-232 link is the one used in this project, this was the one chosen for the calibration as well.



Figure 6.14 – Calibration warning of the rotor

To calibrate the [LVB](#) tracker via RS-232 the next steps are to be followed:

1. The connection must be established with a serial terminal with the next parameters:
 - Baud rate: 9600 bauds per second
 - Data bits: 8
 - Parity: None
 - Hand shaking: None

2. It is possible to check whether the connection has been successfully established by typing letter 'c' and then *Enter*. The azimuth coordinate should be returned.

Output example: +0344.

If no similar output is returned, there is a problem with the connection and the calibration via RS-232 cannot continue until it is solved.

3. The rotor Azimuth and Elevation have to be taken to 0 degrees using whether the controller unit switches or the [LVB](#) buttons.
4. The left-most azimuth is set by typing in sequence keys 'FAS' and then *Enter*. An offset will be returned as an output, indicating the system full scale.
5. The bottom-most elevation is set by typing in sequence 'FES' and then *Enter*. The returned offset indicates again the system full scale.
6. Next, the elevation must be set to 90 degrees and the azimuth to 360 degrees by using the controller switches or the [LVB](#) buttons.
At this step, it is also possible to set the elevation and azimuth to 180 and 450 degrees, respectively, for capable rotors such as the Yaesu G-5500. The result will be the same.
7. The right-most azimuth is set by typing in sequence keys 'FAE' and then *Enter*.
8. The top-most elevation is set by typing in sequence keys 'FEN' and the *Enter*.
9. For South Counter Clock Wise stopping rotors such us the Yaesu G-5500, keys 'FS' and *Enter* must be introduced, while for North Counter Clock Wise stopping rotors the key sequence is 'FN' and *Enter*.
10. Lastly, the calibration process is committed to the EEPROM memory by typing in sequence 'FW' and then *Enter*. After restarting the controller unit, the changes should be remembered.

A sample screenshot of the RS-232 terminal showing the response message of the [LVB](#) after its calibration can be observed in figure [6.15](#).

After the calibration, the rotor is prepared to be operated from the RS-232 terminal. The command set supported is described below.

- C: Return azimuth
- C2: Return azimuth and elevation
- Maaa: Set azimuth to <aaa> (Firmware 0.7 and above)
- S: Stop rotator

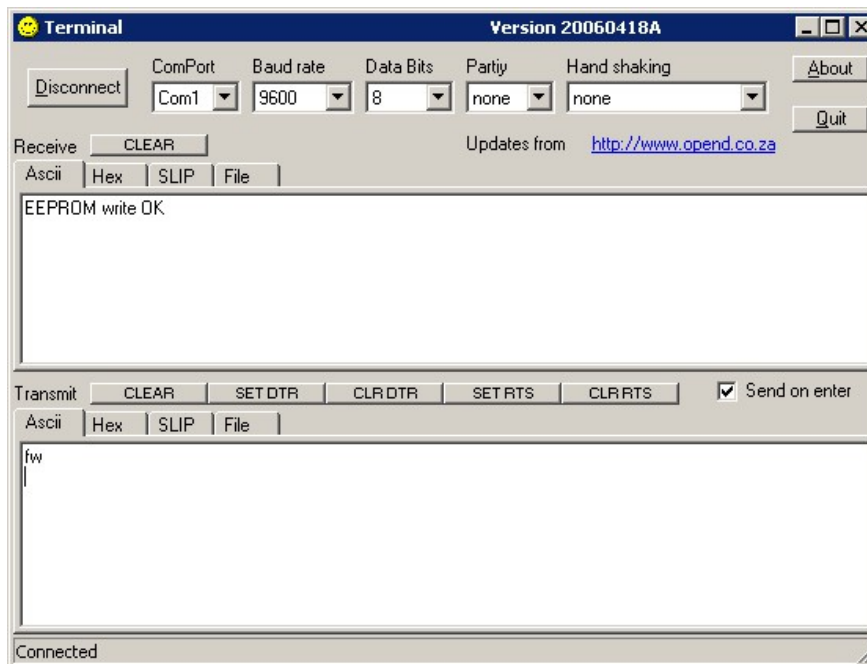


Figure 6.15 – Screenshot with the response message of LVB after calibration

- Waaa: Set azimuth to <aaa>
- Waaa eee: Set azimuth and elevation to <aaa> and <eee>

The last requirement to provide the rotor with the capability to track satellites is the interaction with GPredict, which can control rotors via a TCP port. An interface between the RS-232 port and the chosen TCP port is therefore required. The [hamlib](#) set of libraries provide low-level radio and antenna rotator drivers for applications such as GPredict. The library is available for Windows operating systems as well as for Unix/Linux.

One of the tools that the [hamlib](#) libraries include is **rotctl**, an interactive command line tool for sending command to and reading status from the rotor. To initialize it, the model of the rotor has to be specified and the physical port of the PC to which the rotor controller is connected. A complete list of the supported rotors and their assigned model number can be obtained by typing [8]:

```
rigctl -l
```

Rig #	Mfg	Model	Version	Status
1	Hamlib	Dummy	0.2	Beta
2	Hamlib	NET rotctl	0.3	Beta
201	Hamlib	EasycommI	0.3	Beta
202	Hamlib	EasycommII	0.3	Beta
301	XQ2F0D	Fodtrack	0.2	Stable
401	Idiom Press	Rotor-EZ	2010-02-14	Beta
402	Idiom Press	RotorCard	2010-02-14	Untested
403	Hy-Gain	DCU-1/DCU-1X	2010-08-23	Untested

404	DF9GR	ERC	2010-08-23b	Alpha
501	SARtek	SARtek-1	0.2	Untested
601	Yaesu	GS-232A	0.3	Beta
602	Yaesu/Kenpro	GS-232	0.1	Beta
603	Yaesu	GS-232B	0.2	Beta
604	F1TE	GS232/F1TE Tracker	0.1	Beta
701	WA6UFQ	PcRotor	0.1	Untested
801	Heathkit	HD 1780 Intellirotor	0.1	Beta
901	SPID	Rot2Prog	1.0	Stable
902	SPID	Rot1Prog	1.0	Stable
1001	M2	RC2800	0.1.1	Beta
1101	EA4TX	ARS RCI AZ&EL	0.1	Beta
1102	EA4TX	ARS RCI AZ	0.1	Beta
1201	AMSAT	IF-100	0.1	Untested
1301	LA7LKA	ts7400	0.1	Beta
1401	Celestron	NexStar	0.1	Untested

The Yaesu G-5500 rotor makes use of the GS-232A control interface. Therefore, among the three Yaesu models displayed, the rig number corresponding to the Yaesu G-5500 rotor is 601.

The physical and TCP ports must also be specified to initialize the `rotctl` tool. The serial port is usually named COM in Windows systems while in Unix/Linux systems it is assigned to `/dev/tty`. The TCP port can be freely chosen provided that no other application is making use of it. The only requirement is that it has to be in accordance with the one chosen in GPredict.

Hence, assuming that the LVB controller is connected to the the first serial port –the one with the lowest number– and the chosen TCP port is 1234, the command to be executed is:

```
rigctl -m 601 -t 4533 -r /dev/tty0
```

```
rigctl -m 601 -t 4533 -r COM1
```

After initializing `rigctl` it is possible to send commands to the rotor and read its status. The list of available commands is:

- P: `set_pos` (Azimuth, Elevation)
- p: `get_pos`
- K: `park`
- S: `stop`
- R: `reset` (Reset)
- M: `move` (Direction, Speed)
- C: `set_conf` (Token, Value)
- `_`: `get_info`

- w: send_cmd (Cmd)
- l: dump_caps
- ?: dump_state
- L: lonlat2loc (Longitude, Latitude, Loc Len [2-12])
- l: loc2lonlat (Locator)
- D: dms2dec (Degrees, Minutes, Seconds, S/W)
- d: dec2dms (Dec Degrees)
- E: dmmm2dec (Degrees, Dec Minutes, S/W)
- e: dec2dmmm (Dec Deg)
- B: qrb (Lon 1, Lat 1, Lon 2, Lat 2)
- A: a_sp2a_lp (Short Path Deg)
- a: d_sp2d_lp (Short Path km)

In order to use it together with GPredict, the *rigctl* tool must function as a server and it must therefore be initialized as a daemon. For this purpose, *hamlib* also includes the packet **rigctld**. The daemon must be active during the whole operation time and the syntax to initialize it is the same as the one described above.

```
rigctld -m 601 -t 1234 -r /dev/tty0
```

```
rigctld -m 601 -t 1234 -r COM1
```

Lastly, the rotor must be added to GPredict. The rotor configuration window can be found in **Edit**→**Preferences**→**Interfaces**→**Rotators**→**Add New**. The following parameters must be specified:

- **Name:** The desired name for this configuration
- **Host:** The host name i.e IP address of the host where the controller unit is connected. If the controller unit is connected at the same host where the GPredict the local loopback can be declared as *localhost*.

GPredict can control rotor in a remote host as well by introducing its IP or host name, which is translated using DNS. Since the connection is associated with an TCP port, the latter must be opened in the router of the remote and local host.

- **Port:** The TCP port used to communicate with the *hamlib*. It must be consistent with the one chosen in the *hamlib* daemon.
- **Az type:** Depending on rotor model, it the azimuth range can be measured between 0 and 360 degrees or between -180 and 180 degrees. In this case, the first option was selected.
- **Minimum and maximum azimuthal:** The range of degrees that the rotor is capable of in the azimuth angle. For the case of the Yaesu G-5500 this is 0 and 450 degrees, respectively.
- **Minimum and maximum elevation:** The range of degrees that the rotor is capable of in the elevation angle. For the case of the Yaesu G-5500 this is 0 and 180 degrees, respectively.

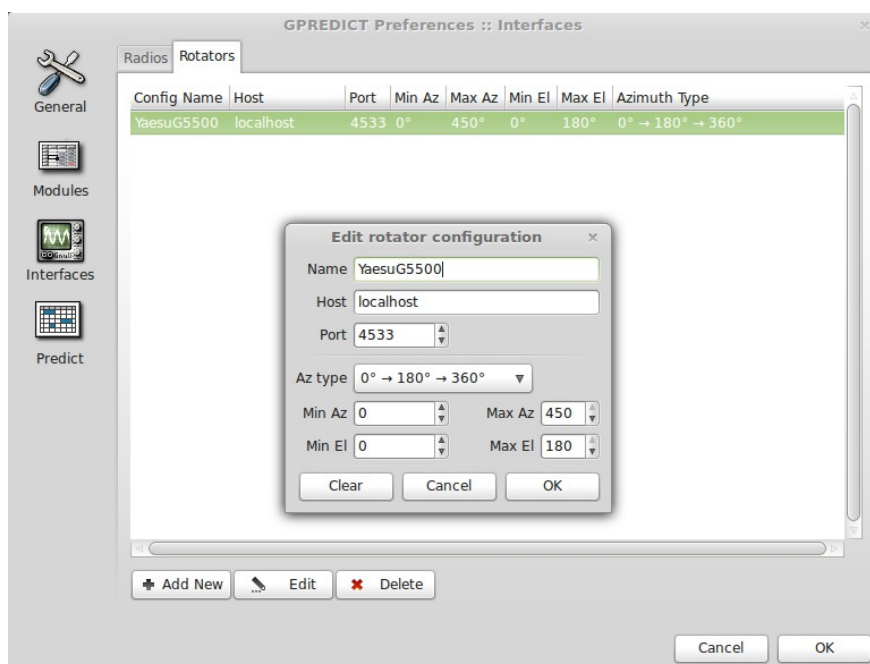


Figure 6.16 – Sample screenshot of the rotor addition in GPredict

6.2.2 Transceivers

The signal cables, ending in a N-type connector, are connected to a manual antenna switcher. This element avoids the need of changing the cable connected to the transceivers when a different frequency band is going to be used. Additionally, it performs lightning protection for the rest of the equipment. For this capability, both through-holes of its base plate must be connected to ground.

The next element in the connection flow is a SWR meter, which is used to guarantee a safe operation of the equipment. One **UHF** antenna and one **VHF** antenna can be connected simultaneously, as shown in figure 6.17.

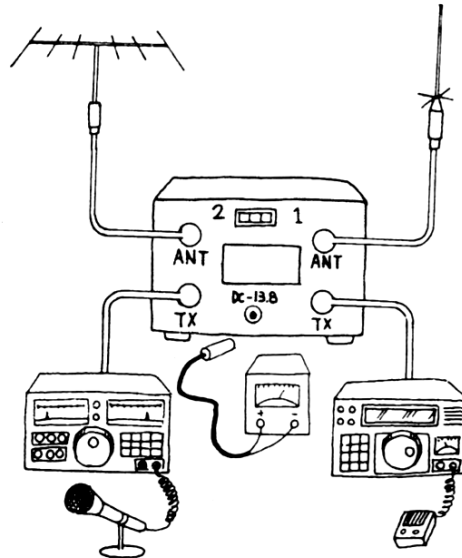


Figure 6.17 – SWR meter connection scheme

A calibration must be performed as well prior to its use:

1. First, the CAL function is selected in the middle switch.
2. The CAL knob must be turned counter clockwise to the minimum
3. Simultaneously transmitting, the CAL knob must be moved until the meter is in the full scale (denoted with symbol ∇).

After calibration, the function switch is set to SWR.

A SWR below 1.5 indicates that the reflected wave is low and therefore all the power is radiated.

The Diamond MX-72D diplexer is employed to connect a single input/output of the SWR metre to the Keenwood TM-241 and TM-441 transceivers. They operate in the **VHF** and **UHF** amateur bands, respectively.

To conclude, the coaxial cables coming from the SWR meter are directly attached to the Keenwood TM-241 and TM-441 transceivers. Although the control of the transceiver and automatic frequency tuning with **Doppler shift** correction can be performed by GPredict, the Keenwood TM-241 and TM-441 do not have an external control port.

A picture of the control room can be seen on figure 6.18.



Figure 6.18 – *Equipment on the control room*

6.3 Reparation after deployment

After the deployment was completed and the first tests were carried out in order to check the performance of the ground segment, it was noticed that the reception in **VHF** had a very poor quality and signals from satellites could not be successfully received.

This unexpected behaviour was first thought to be due to a certain misconfiguration of some device. However, after double checking all the involved elements on the control room no problem was found. It was then decided to check on the antennas as well, which would require taking the mast with the antennas down to the ground again.

The origin of this anomaly was found to be that the **RF** cable of the **VHF** antenna had been ripped by the rotor on its movement, as it can be seen in figure 6.19.

Since this breaking only affected to the 1.5 meters cable connecting the pre-amplifiers with the circular emphaser of the 2 m antenna, a new **RF** cable was prepared to substitute



Figure 6.19 – *Ripped cable on the side of the rotor*

it.

Due to its difficulty, it was desirable to avoid the need of descending the antennas again. For that reason, a measurement with the Keysight E5071C vectorial network analyzer was carried out over the circular emphasers connected to the antennas. A picture of the network analyzer is shown in figure 6.20.



Figure 6.20 – *Front view of the Keysight E5071C vectorial network analyzer[35]*

The measurements of S_{11} Scattering parameter are shown in figures 6.22 and 6.23. Although attending to the diagram shown in figure 6.21 S_{11} corresponds to the reflection coefficient, the vectorial network analyzer allows to directly display the SWR as well, shown in figures 6.22 and 6.23. For matched and non-faulty components, this value should be close to 1.

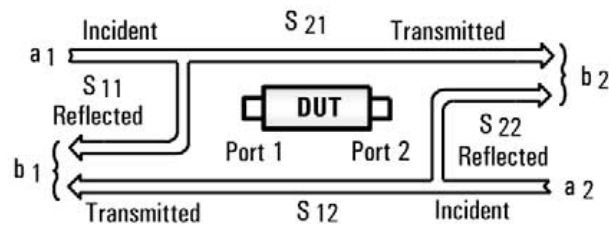


Figure 6.21 – Scattering parameters diagram [36]

As it can be observed, the SWR goes up to approximately 3.5 in both cases. Although this is a value higher than expected, no faulty element was found in this case and later tests proved a correct reception with this SWR value.

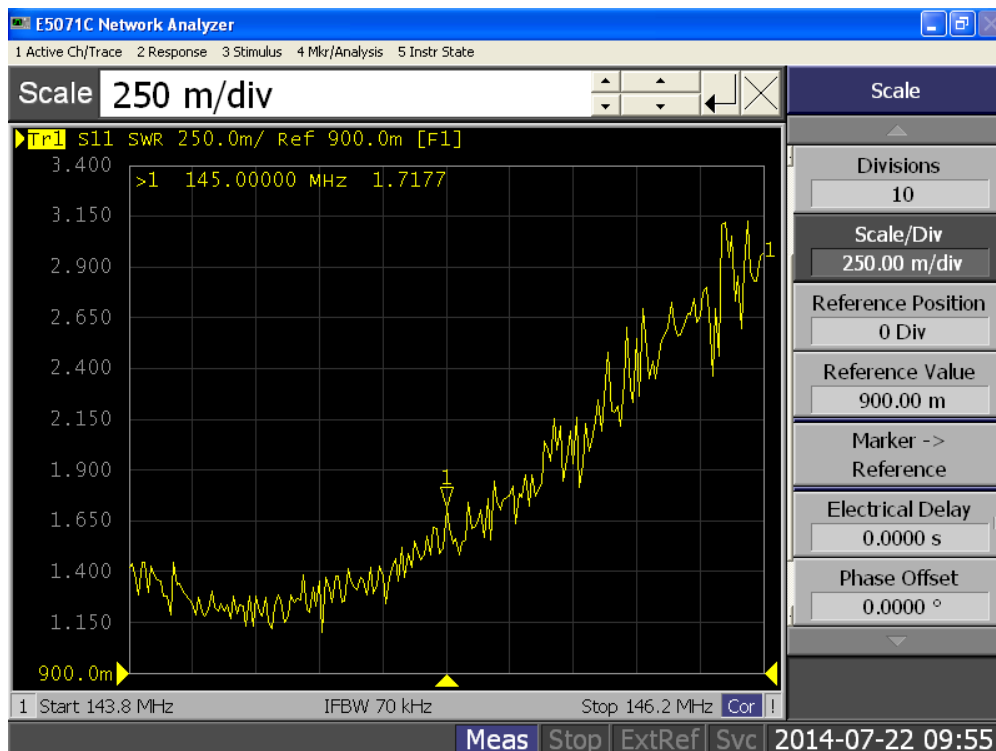


Figure 6.22 – Measurement of the S_{11} parameter over the VHF circular emphaser connected to the 2 m antenna

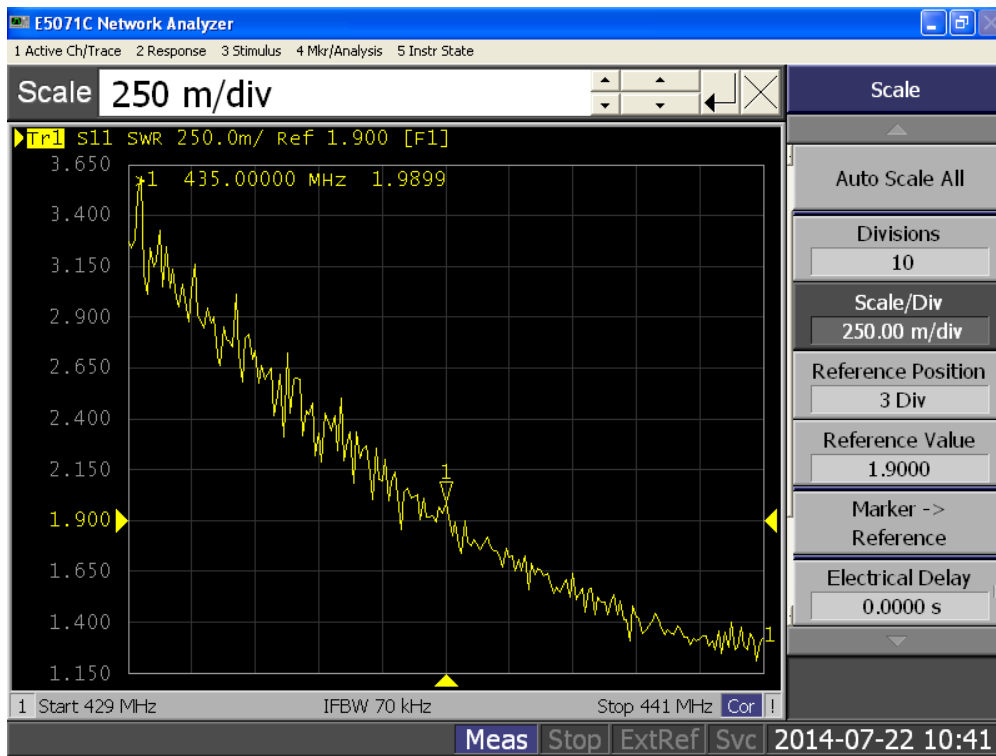


Figure 6.23 – Measurement of the S_{11} parameter over the UHF circular emphaser connected to the 70 cm antenna

CHAPTER

7

SYSTEM PERFORMANCE AND CONCLUSION

The evaluation of the system performance was made with a series of reception attempts. Since the segment did not possess capability for transmission into space, only reception tests were carried out.

It must be also remarked that, although the reception with the Keenwood TM-241 and TM-441 was successful too, the impossibility to record the results led to the constraint of the next sections to tests with [SDR](#) devices.

7.1 Evaluation of system performance

7.1.1 FUNcube

[FUNcube-1](#) (AO-73) is a [CubeSat](#) launched Nov 21st 2013, whose main purpose is the promotion of radio, space, physics and electronics among young people [6]. Its downlink transponder operates in the [VHF](#) amateur band (145.950 – 145.970 MHz, Upper Side Band), being therefore compatible with the [GranaSAT-I](#) ground segment. In addition, [FUNcube-1](#) developers have released a [telemetry](#) program for PCs, which using I/Q samples coming from the [FUNcube Dongle Pro+](#), automatically demodulates the signal and decodes the [telemetry](#) data sent their satellite.

This tool was used in the first reception attempts, which initially led to the discovery of the ripped cable in the [VHF X-Quad](#) antenna and afterwards served to prove the correct operation of the bi-band antenna in [VHF](#) as well as the 2 m [X-Quad](#) antenna after its reparation.

A screenshot of the FUNcube Dashboard after reception of [telemetry](#) from the satellite can be observed in figure 7.1.

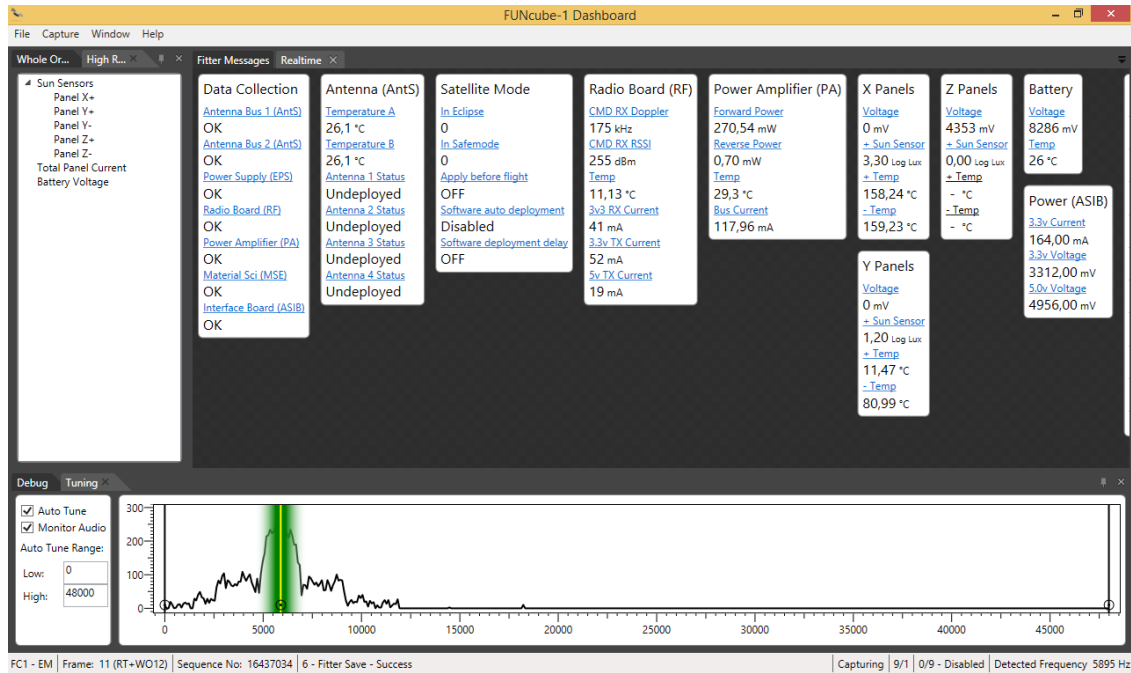


Figure 7.1 – Telemetry data from FUNcube-1 displayed in its dashboard

7.1.2 ISS contact

The capability to establish a contact with the [ISS](#) was considered as one of the objectives of the ground segment presented in this Thesis. At the moment of the writing of this report the transmission for space communications had not been implemented yet. However, the reception of a contact established with a location geographically close to Granada was a good opportunity to test the correct functioning of the system.

On June 28th 2014 at 12:08:21 UTC a direct contact from the [ARISS](#) to the German high school *Markt Indersdorf*, in Markt Indersdorf (Germany) was scheduled. The nominal downlink frequency from the [ARISS](#) was 145.800 MHz, which was not possible to receive with the 2 m [X-Quad](#) antenna due to its still unrepaired ripped [RF](#) cable. Nevertheless, the contact was successfully recorded using the bi-band antenna and an [SDR](#) sampling device and [SDR#](#).

A transcript of the the conversation can be read below, and the recording can be fully accessed in <https://youtu.be/5pD820Z9xrI>. Since only the transmissions from the ISS could be received from Granada, only the voice from ESA astronaut Alexander Gerst can be heard. Additionally, this contact was marred during the entire pass by an apparent local ham which impeded a fully successful contact between the astronaut and the pupils [2].

"Delta November Four Oscar Delta (DN4OD) from Delta Papa Zero India Sierra Sierra (DP0ISS), this is the international space station, how do you copy?"

[Continues in German] Guten Morgen Markt Indersdorf, viele Grüße von der Internationalen Raumstation, wir können es gerne auf Deutsch machen.

Delta November Four Oscar Delta, com check?"

7.1.3 NOAA APT

The **National Oceanic and Atmospheric Administration (NOAA) Automatic Picture Transmission (APT)** service is an analog broadcast transmission of an image strip that continues as long as the transmission is received at the ground station. The received image consists of two images, side by side, representing the same view of the Earth in two different spectral bands [19].

The transmission of such images by the NOAA-15, NOAA-18 and NOAA-19 satellites is made in frequencies in the range [137.6200 – 137.1000] MHz, very close to the amateur VHF band [4]. Therefore, a reception from Earth observation images from the NOAA satellites was also attempted as a system test. **WXtoImg** specialised software running on a Windows machine was used to perform the data processing. It receives the FM demodulated audio signal from another SDR program and decodes the image sent by the satellite. A diagram representing the reception process can be seen in figure 7.2.

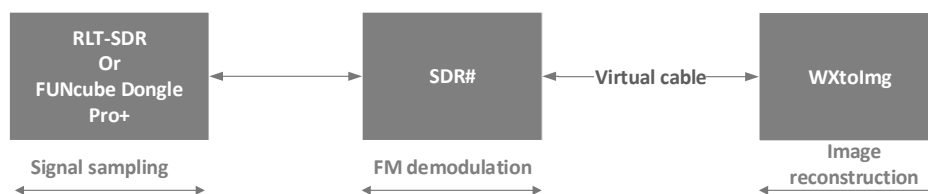


Figure 7.2 – Diagram of the NOAA APT reception process

A screenshot of **SDR#** displaying the real time FFT of the signal sampled with the **RTL-SDR** can be observed in figure 7.3.

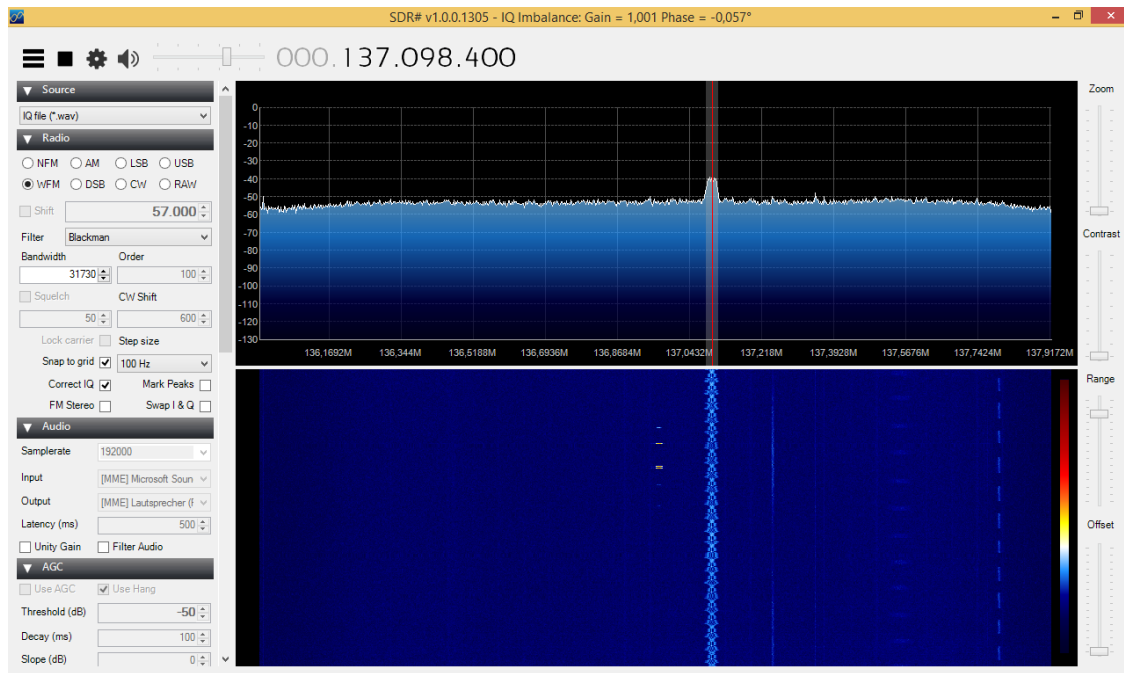


Figure 7.3 – Real time FFT of NOAA's APT signal in SDR#

An image received from NOAA-18 on January 2nd 2015 is shown in figure 7.4. This signal has no further processing than converting the audio to pixels. As it can be observed the Southwestern Europe (mainly the Iberian Peninsula), North Africa, the Atlantic Ocean and Mediterranean Sea are displayed on the left image rotated 180 degrees.

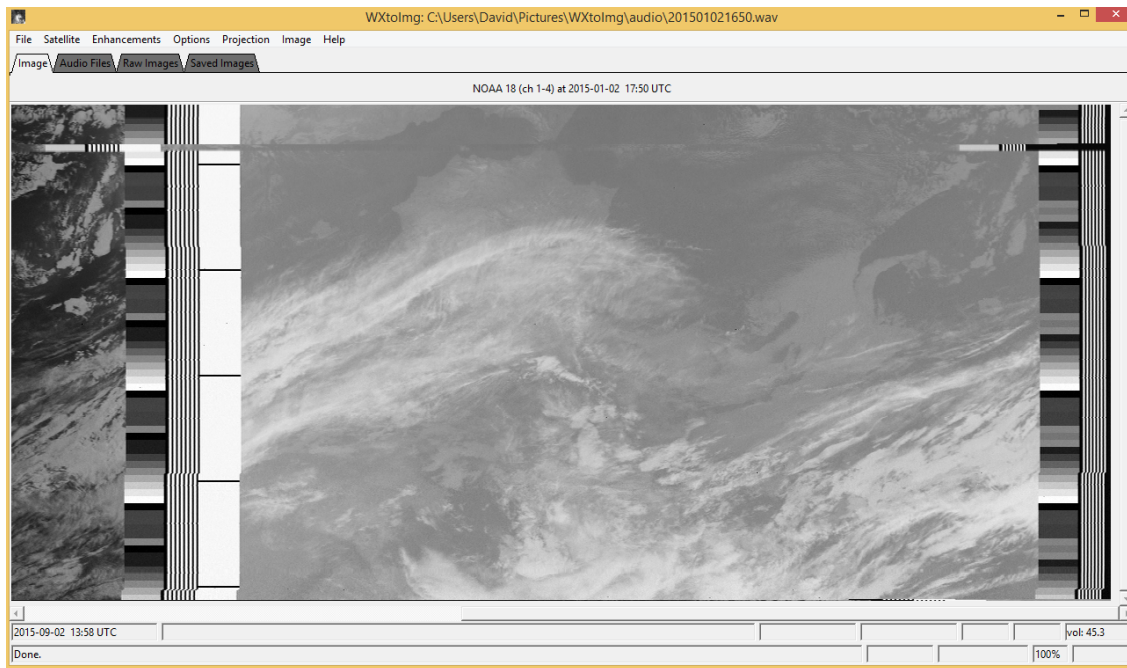


Figure 7.4 – *Image received from NOAA-18 on January 2nd 2015*

Wxtoimg can also perform additional image processing, for instance adding colour layers and applying filters to the image. This can be seen in figure 7.5, the same image as in figure 7.4 after rotating 180° and applying a *MCIR* (Motion-map Constrained Image Reconstruction) *map color IR* enhancement. In figure 7.6 a *NO colour IR* enhancement is applied.

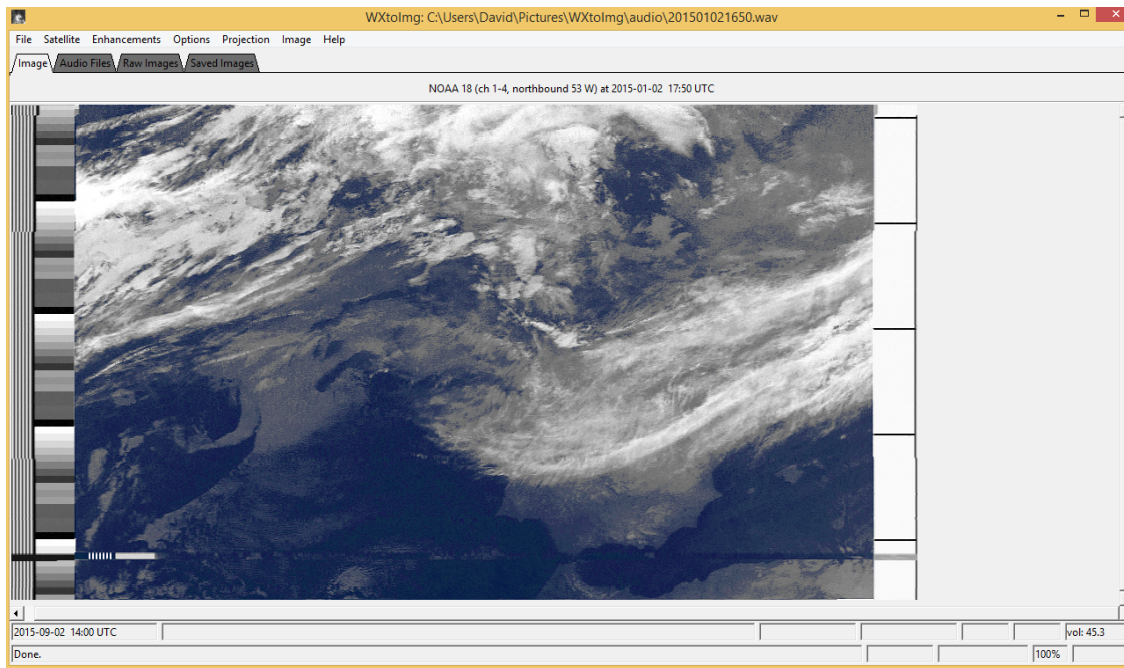


Figure 7.5 – Image received from NOAA-18 on January 2nd 2015, rotated and with MCIR map color IR enhancement

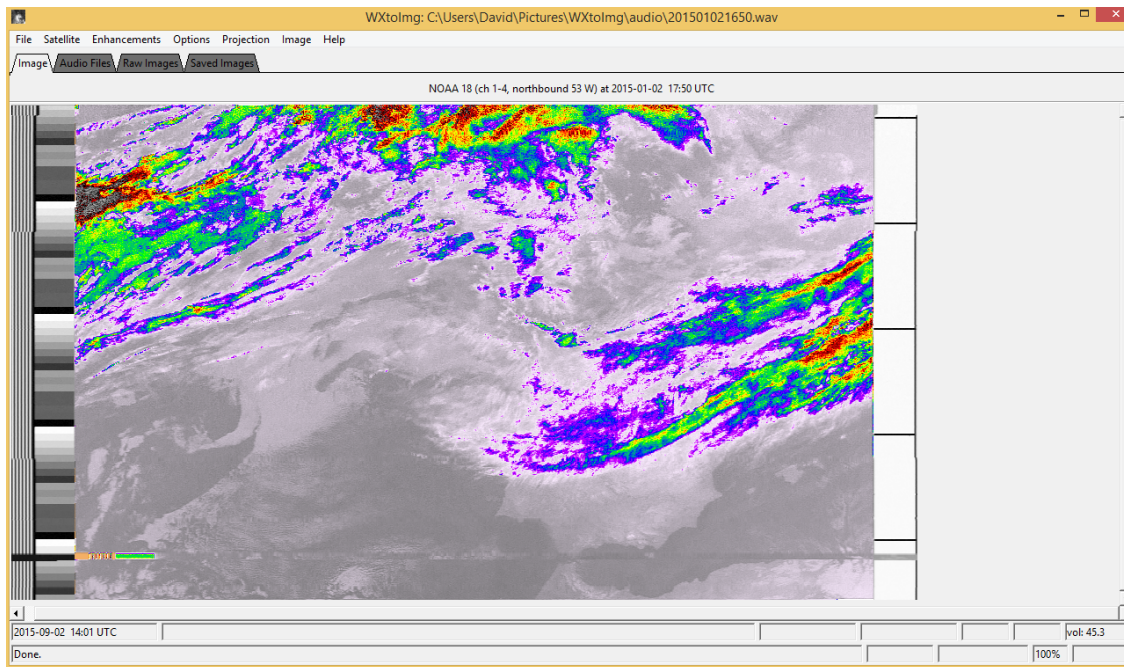


Figure 7.6 – Image received from NOAA-18 on January 2nd 2015, rotated and with NO colour IR enhancement

7

7.2 Conclusion

In this Thesis the design and deployment of the ground segment for the [GranaSAT-I CubeSat](#) have been presented. A theoretic analysis in chapters 2, concluded with a [link budget](#) in chapter 3, was carried out in order to choose the appropriate hardware and software. The employed hardware and software equipment is described in chapter 4, with a special focus on [SDR](#) technology in chapter 5.

To conclude, the deployment was executed in several phases and presented in chapter 6, finalizing with the reparation of a damaged piece. After that, different reception tests were carried out in order to check the performance. As it is presented at the beginning of 7, the results were positive and it can be therefore concluded that the proposed design is adequate for satellite communications.

A panoramic view of the rooftop of the Faculty of Sciences, where the antennas can be seen after the conclusion of the work, can be seen in figure 7.7.



Figure 7.7 – *Panoramic photo of the rooftop of the Faculty of Sciences*

7.2.1 Future work

The current design of the station will be further developed by other students and collaborators. Future improvements will be most probably focused in the following points:

- Reception of digital [AX.25](#) packets with a [TNC](#). Although the current design includes a [TNC](#), its complete integration in the system is still to be concluded.
- Transmission capability for space communications. Although at the moment of the conclusion of this Thesis that was not necessary, the launch of the [GranaSAT-I CubeSat](#) will require a fully operational ground segment with transmission capability for long distances.
- Increase of number of frequency bands. [VHF](#) and [UHF](#) amateur bands have been used in the current design. They are commonly used for [CubeSats](#), but a wider range of workable frequencies would expand the functionality of the ground segment.

In addition, the integration of the ground segment in a world network of ground stations is an objective on which other students are already working. The purpose of the network is the capability to share resources so that each participating institution will be able to establish communication with their own satellite using both their ground segment and other participants' stations.

Appendices

APPENDIX

A

PROJECT BUDGET

A.1 Project budget

A.1.1 Material cost

Some material employed in the ground segment was bought for this purpose, whereas some other parts belonged to the department or private persons who donated it. In the second case, an estimation will be calculated, which is marked as such in the budget calculations.

A.1.2 Human resources costs

The work on the project consisted primarily on the Masters Thesis of David Aguilera. Some other students and collaborators contributed in the execution of tasks which required their help. In all cases, their work was made free of charge.

Additionally, teaching assistant Dr. Andrés Roldán and the University technicians also carried out several tasks, as it was described in 6. In this case, as employees of the University of Granada, the remuneration for that work is covered by their salary.

All human resources costs will be therefore estimated, since no invoices were issued.

A.1.3 Final project budget

Description	Quantity	Estimated / Exact	Unit price (€)	Subtotal (€)
X-Quad antenna 2 m	1	Exact	102.07	102.07
X-Quad antenna 70 cm	1	Exact	105.20	105.20
Diamond X-200N antenna 144-430 MHz	1	Exact	74.38	74.38
Circular pol. Emphaser 2 m	1	Exact	39.45	39.45
Circular pol. Emphaser 70 cm	1	Exact	43.18	43.18
SHF Mini 2 pre-amplifier 2 m	1	Exact	85.98	85.98
SHF MVV 432/2 pre-amplifier 70 cm	1	Exact	179.33	179.33
Diamond MX-72D diplexer	1	Exact	37.19	37.19
Diamond SX600 Dual-Band SWR/Power meter	1	Exact	107.44	107.44
MFJ-1704 antenna switcher	1	Exact	71.90	71.90
Delivery	1	Exact	24.38	24.38
RG-11 coaxial cable	100 m	Exact	1.60	160.00
RF connector	30	Exact	2.50	75.00
Control cable 6 wires	100 m	Exact	1.30	130.00
Kenwood TM-241 transceiver	1	Estimated	150.00	150.00
Kenwood TM-441 transceiver	1	Estimated	150.00	150.00
General purpose PC	1	Estimated	500.00	500.00
MATLAB Student	1	Exact	35.00	35.00
Base total				1635.695
IVA (21%)				434.805
Material total				2070.50

Description	Estimated Number of hours	Estimated price per hour (€)	Subtotal (€)
Master Thesis work	1100	10.00	11000.00
Collaborations	100	15.00	1500.00
Base total			9875
IVA (21%)			2625
Personnel total			12500.00

Total ground segment budget

Base total	11510.695
IVA (21%)	3059.805
Project total	14570.50

Table A.1 – Project budget

APPENDIX

B

GANTT DIAGRAM

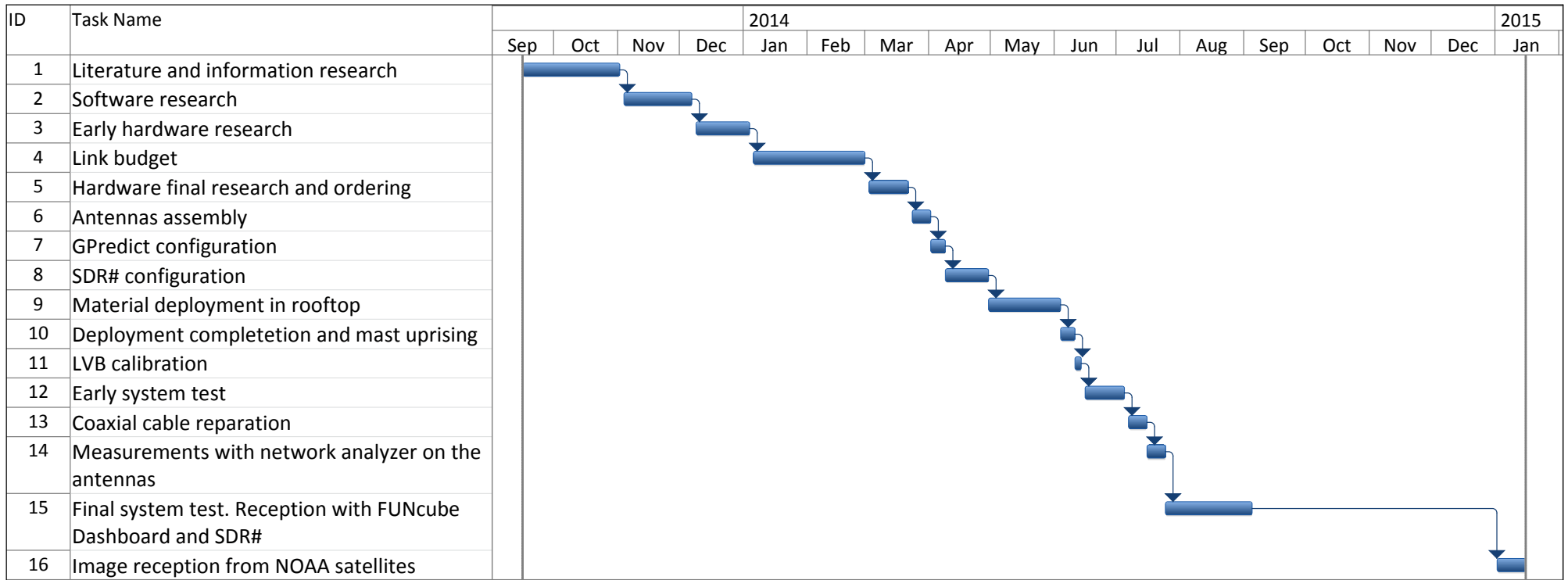


Table B.1 – Gantt diagram

ACRONYMS

APT Automatic Picture Transmission. Analog broadcast transmission system used in NOAA satellites for Earth observation images. [93](#)

ARISS Amateur Radio on the ISS. [4](#), [39](#), [92](#)

Digital Signal Processing Mathematical operations performed upon a certain digitalized signal. [65](#), [67](#)

FSL Free-Space path Loss. Ratio between the received power and the transmitted power of a signal. [17](#), [28](#), [30](#), [31](#)

IARU International Amateur Radio Union. [3](#)

ISS International Space Station. [4](#), [39](#), [92](#), [93](#)

ITU International Telecommunication Union. [3](#)

ITU-R ITU Radiocommunication Sector. [20](#)

LEO Low Earth Orbit. Defined as an orbit with an altitude between 160 and 1600 km. [29–31](#), [36](#), [79](#)

LVB Las Vegas Boulevard. Interface used in order to controll the Yaesu G-5500 rotor controller unit from a PC RS-232 port. [50](#), [51](#), [71](#), [79–81](#), [83](#)

NOAA National Oceanic and Atmospheric Administration. [93](#), [94](#)

RF Radio Frequency. Range of frequencies used for radio communications. [5](#), [28](#), [63](#), [64](#), [67](#), [73](#), [76](#), [87](#), [92](#)

SDR Software Defined Radio. Radio transmitter and/or receiver whose RF parameters are controlled by software. [57](#), [58](#), [63–65](#), [67](#), [68](#), [91–93](#), [97](#), [107](#)

SSP Sub-Satellite Point. Closest point on the surface of the Earth to a satellite. [11](#), [13](#), [29](#), [30](#)

TLE Two-Line Element. File which contains the Keplerian elements and data of a certain satellite. [9](#)

TNC Terminal Node Controller. Digital transmissions controller for the amateur AX.25 packet network. [26](#), [52](#), [54](#), [67](#), [97](#)

UHF Ultra High Frequency. Defined as the frequency band between 300 MHz and 3 GHz. [3](#), [14](#), [22](#), [23](#), [30](#), [31](#), [35](#), [36](#), [41](#), [47](#), [67](#), [75](#), [86](#), [97](#)

VHF Very High Frequency. Defined as the frequency band between 30 MHz and 300 MHz. [3](#), [14](#), [22](#), [23](#), [30](#), [31](#), [35](#), [36](#), [41](#), [47](#), [67](#), [86](#), [87](#), [91–93](#), [97](#)

GLOSSARY

Antenna pointing loss Offset between the direction of the main lobes of the transmitting and receiving antennas. [32](#), [33](#)

AX.25 Amateur digital link-layer transmission protocol [[27](#)]. [26](#), [54](#), [67](#), [97](#)

Bus Part of a satellite providing infrastructure to the payload, including communications system, thermal protection, etc.. [64](#)

CubeSat Standard for reduced cost and fast design of pico-satellites. [2](#), [4](#), [16](#), [26](#), [27](#), [29](#), [35](#), [36](#), [91](#), [97](#), [107](#)

Doppler shift Offset between the transmitted frequency and received frequency due to relative motion between transmitter and receiver. [13](#), [23](#), [24](#), [58](#), [59](#), [61](#), [86](#)

FUNcube Dongle Pro+ Signal sampling interface for [SDR](#) applications developed by the [FUNCube-1](#) team. [57](#), [67](#), [69](#), [91](#)

FUNCube-1 British educational [CubeSat](#), also known as AO-73. [61](#), [67](#), [91](#), [107](#)

GranaSAT-I Cubesat currently in development process at the University of Granada. [1](#), [3](#), [4](#), [16](#), [29](#), [35](#), [50](#), [52](#), [57](#), [58](#), [91](#), [97](#)

Ham Amateur radio operator. [2](#), [93](#)

Ham radio Amateur radio. [2](#)

- Hamlib** set of libraries provide low-level radio and antenna rotator drivers for applications such as GPredict. [58](#), [82](#), [84](#), [85](#)
- Line-of-sight** Imaginary straight line between the end points of a radio link. [11](#), [13](#)
- Link budget** Analysis carried out in order to calculate the level of a signal upon its arrival to a receiver. [1](#), [27](#), [32](#), [35](#), [36](#), [97](#)
- Payload** Instruments and parts of a satellite responsible for executing the satellite mission. [64](#)
- RTL-SDR** Digital Video Broadcasting receiver based on the Realtek RTL2832U chip, used as signal sampling interface for SDR applications. [57](#), [67–69](#), [93](#)
- Rx** Abbreviation for "receiver" or "reception". [23](#), [64](#), [67](#)
- SDR#** Computer program which performs several digital signal processing functions, like analog demodulation or Fourier transform. [59](#), [60](#), [70](#), [92](#), [93](#)
- Slant range** Line-of-sight distance between two points. [13](#), [29–31](#)
- Telecommand** Referred to the set of instructions sent to a satellite in order to operate it remotely. [1](#), [26](#), [64](#)
- Telemetry** Information sent by a satellite including payload data, satellite health reports, etc.. [1](#), [26](#), [61](#), [64](#), [91](#), [92](#)
- Tx** Abbreviation for "transmitter" or "transmission". [23](#), [35](#), [64](#), [67](#)
- X-Quad** Commercial name of an directive antenna sold by the company Wimo GmbH. [41–43](#), [45](#), [48](#), [71](#), [73](#), [75](#), [79](#), [92](#)

BIBLIOGRAPHY

- [1] Ariss ground station recommendation. http://www.ariss.org/uploads/1/9/6/8/19681527/ariss_ground_station.pdf. [Online; accessed 19-August-2014].
- [2] Ariss news june 29th 2014. <http://www.ariss.org/news-archive/archives/06-2014>. [Online; accessed 12-July-2015].
- [3] Cubesat design specification v13. Cal Poly SLO.
- [4] Currently active satellites noaa satellites. <http://www.wxtoimg.com/support/>. [Online; accessed 20-July-2015].
- [5] Definition of two-line element set coordinate system. http://spaceflight.nasa.gov/realdata/sightings/SSapplications/Post/JavaSSOP/SSOP_Help/tle_def.html. [Online; accessed 10-August-2014].
- [6] Funcube website. <http://funcube.org.uk/>. [Online; accessed 27-June-2015].
- [7] Google maps. <http://maps.google.com>.
- [8] Gpredict user manual. <http://gpredict.oz9aec.net/>. [Online; accessed 10-June-2015].
- [9] Itu zones and regions. <http://www.iau.org/regions.html>. [Online; accessed 12-May-2015].
- [10] Mfj-1704 instruction manual.
- [11] Mini 2 instruction manual. SHF Elektronik.

Bibliography

- [12] Mv 432/2 instruction manual. SHF Elektronik.
- [13] Mx-72d diplexer instruction manual. Diamond Antenna.
- [14] Osmocom rtl-sdr library. <http://cgit.osmocom.org/rtl-sdr/>. [Online; accessed 24-August-2014].
- [15] Scintillation indices. <http://swaciweb.dlr.de/data-and-products/public/scintillation-index/?L=1>. [Online; accessed 02-April-2015].
- [16] Sx600 instruction manual.
- [17] Tm-241 instruction manual. Kenwood.
- [18] Tm-441 instruction manual. Kenwood.
- [19] User's guide for building and operating environmental satellite receiving stations. http://noaasis.noaa.gov/NOAASIS/pubs/Users_Guide-Building_Receive_Stations_March_2009.pdf. [Online; accessed 29-July-2015].
- [20] What is ham radio. <http://www.arrl.org/what-is-ham-radio/>. [Online; accessed 06-August-2014].
- [21] World conference on international communications. ITU. Year 2012.
- [22] X200n instruction manual. Diamond Antenna.
- [23] Xquad instruction manual.
- [24] Yaesu 5500 instruction manual. Yaesu.
- [25] *Telecommunications: Glossary of Telecommunications Terms. Federal Standard 1037C*. General Services Administration. Information Technology Service, 1996.
- [26] Guidelines for evaluation of radio transmission technologies for imt-2000. Tech. rep., ITU-R, 1997. RECOMMENDATION ITU-R M.1225.
- [27] *The ARRL handbook for radio communications, 2005*. American Radio Relay League, Newington, CT, 2004.
- [28] Effects of tropospheric refraction on radiowave propagation. Tech. rep., ITU-R, 2005. RECOMMENDATION ITU-R P.834-4.
- [29] *AU-18 Space Primer*. Maxwell Air Force Base, Alabama: Air University Press, 2009.
- [30] Attenuation by atmospheric gases. Tech. rep., ITU-R, 2013. Recommendation ITU-R P.676-10.
- [31] Ionospheric propagation data and prediction methods required for the design of satellite services and systems. Tech. rep., ITU-R, 2013. Recommendation ITU-R P.531-12.

- [32] Propagation data and prediction methods required for the design of earth-space telecommunication systems. Tech. rep., ITU-R, 2013. Recommendation ITU-R P.618-11.
- [33] Tub small satellite database. https://www.raumfahrttechnik.tu-berlin.de/menue/publikationen/small_satellite_database/parameter/en/, August 2014. [Online; accessed 07-August-2015].
- [34] Funcube dongle pro+ user manual (v4). <http://www.funcubedongle.com/MyImages/FCD2ManualV4.pdf>, February 2013. [Online; accessed 24-August-2015].
- [35] AGILENT. Keysight e5071c datasheet. <http://cp.literature.agilent.com/litweb/pdf/5989-5479EN.pdf>. [Online; accessed 1-September-2015].
- [36] AGILENT. Network analyzer basics. <http://cp.literature.agilent.com/litweb/pdf/5965-7917E.pdf>. [Online; accessed 1-September-2015].
- [37] BALANIS, C. A. *Antenna Theory*. Arizona State University, 1997.
- [38] BESANT, W. H. *Conic Sections*. 1985.
- [39] CAPDEROU, M. *Handbook of Satellite Orbits. From Kepler to GPS*. Springer, 2014.
- [40] CARDAMA AZNAR, A. *Antenas*. UPC, Barcelona, 2002.
- [41] DAVIDOFF, M. *The Radio Amateur's Satellite Handbook*. ARRL, 1998.
- [42] G6LVB, H. L. Las vegas boulevard tracker. <http://www.g6lvb.com/articles/lvbtracker/>. [Online; accessed 21-August-2014].
- [43] GAGLIARDI, R. *Satellite communications*. Van Nostrand Reinhold, New York, 1991.
- [44] GHASEMI, A. *Propagation engineering in radio links design*. Springer, New York, NY, 2013.
- [45] GUOCHANG. *Orbits 2nd order singularity-free solutions*. Springer, Berlin New York, 2013.
- [46] HOSKING, R. H. *Software defined radio handbook*. Pentek Inc., January 2010.
- [47] IPPOLITO, L. *Radiowave Propagation in Satellite Communications*. Springer Netherlands, Dordrecht, 1986.
- [48] ITU-R. *Definitions of Software Defined Radio (SDR) and Cognitive Radio System (CRS)* (2009). Report ITU-R SM.2152.
- [49] KASTELIC, M. *VHF MANAGERS HANDBOOK*. IARU Region 1, 2013.
- [50] MARAL, G. *VSAT networks*. J. Wiley, West Sussex, England Hoboken, NJ, 2003.

Bibliography

- [51] MARCO SCHMIDT, K. S. *Distributed space missions for earth system monitoring*. Springer Microcosm Press, New York, NY El Segundo, Calif, 2013.
- [52] The concept of transmission loss for radio links. Tech. rep., ITU-R, 1999.
- [53] ROGER R. BATE, DONALD D. MUELLER, J. E. W. *Fundamentals of Astrodynamics*. New York: Dover Publications, 1971.
- [54] SADIKU, M. *Elements of electromagnetics*. Oxford University Press, New York, 2015.
- [55] SCHMIDT, M. *Ground Station Networks for Efficient Operation of Distributed Small Satellite Systems*. PhD thesis, Lehrstuhl Informatik VII: Robotik und Telematik. Universität Würzburg, 2011.
- [56] SWARTWOUT, M. The first one hundred cubesats: A statistical look. *Journal of Small Satellites* (2013).
- [57] TIPLER, P. *Fisica para la ciencia y la tecnologia*. Editorial Reverte, Barcelona.
- [58] WELTE, H. Turning usd 20 realtek dvb-t receiver into a sdr. <http://sdr.osmocom.org/trac/raw-attachment/wiki/rtl-sdr/rtl-sdr.2.pdf>, June 2012. [Online; accessed 24-August-2015].
- [59] WILLIAM H. HAYT JR., J. A. B. *Engineering electromagnetics*. McGraw-Hill, New York, NY, 2012.